

# **Numerical Modeling of Storm Surge for the Coastal Region of Bangladesh**

By

Samara Chaudhury  
15305022

A thesis submitted to the Department of Mathematics and Natural Sciences in partial fulfillment of the requirements for the degree of  
B.Sc. in Mathematics

Department of Mathematics and Natural Sciences  
Brac University  
Fall 2022

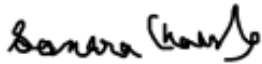
© 2022. Brac University  
All rights reserved.

## Declaration

It is hereby declared that

1. The thesis submitted is my/our own original work while completing degree at Brac University.
2. The thesis does not contain material previously published or written by a third party, except where this is appropriately cited through full and accurate referencing.
3. The thesis does not contain material which has been accepted, or submitted, for any other degree or diploma at a university or other institution.
4. I have acknowledged all main sources of help.

**Student's Full Name & Signature:**



---

**Samara Chaudhury**

15305022

## Approval

The thesis/project titled “ Numerical Modeling of Storm Surge for the Coastal Region of Bangladesh” submitted by

Samara Chaudhury (15305022)

of Fall, 2022 has been accepted as satisfactory in partial fulfillment of the requirement for the degree of B.Sc. in Mathematics on October, 2022.

### Examining Committee:

Supervisor:

(Dr. Hasibun Naher)

---

Dr. Hasibun Naher  
Associate Professor  
Department of Mathematics and Natural Sciences  
Brac University

Program Coordinator:

(Dr. Syed Hasibul Hassan  
Chowdhury)

---

Dr. Syed Hasibul Hassan Chowdhury  
Professor  
Department of Mathematics and Natural Sciences  
Brac University

Departmental Head:

(Dr. A F M Yusuf Haider)

---

Dr. A F M Yusuf Haider  
Professor  
Department of Mathematics and Natural Sciences  
Brac University

## **Abstract**

This study investigates the estimated water levels during a cyclonic storm due to the interaction of tide and surge which also includes air bubble entrainment along the coastal areas of Bangladesh. Thus, a two-dimensional, vertically integrated hydrodynamic model in Cartesian coordinates has been developed. The model equations are solved using finite difference schemes implementing a staggered C-grid. Nested scheme methods are used to incorporate the complexity of the coast in order to not waste central processing unit time. Along the northeast corner of the innermost scheme or the very fine mesh scheme (VFMS), the Meghna river discharge is considered and the coastal and island boundaries are approximated via proper stair steps. A stable tidal condition over the area of interest is produced by making the sea level oscillate with the major tidal constituent  $M_2$  through the southern open boundary of the parent scheme or the coarse mesh scheme (CMS). The model is used to compute the water levels due to tide-surge interaction including the air bubble effect for the April 1991 cyclone. The model results are found to compare well with the observations from Bangladesh Inland Water Transport Authority. Therefore, the model is found to adequately simulate water levels which is in the presence of air bubbles. Additionally, it can also be observed that water levels are affected by factors such as river discharge and inverse barometer among others.

## **Acknowledgements**

The completion of this thesis would not have been possible without the support, help and encouragement of several people. First of all, I would like to express my sincere gratitude to Dr. Hasibun Naher, my supervisor, for her continuous support and guidance. She has been a constant source of encouragement and enthusiasm throughout the time of this project.

I want to express my sincere gratitude to Dr. Gour Chandra Paul, Professor, Department of Mathematics, Rajshahi University. He is one of the leading experts on storm surge in Bangladesh and his extensive research works were invaluable for my thesis. I am wholeheartedly grateful to him for offering me some valuable data resources and his correspondence during my thesis.

I am also very grateful to Dr. Mahbubul Alam Majumdar, Professor and Dean, School of Data and Sciences, Brac University. His classes as well as his support for all his students' work is a source of inspiration for me and everyone else in the department.

I would also like to thank all my esteemed teachers at Brac University for their guidance and teaching that helped me to reach at this stage.

Finally, my deepest gratitude goes to my parents and my sister, for all their sacrifices, love and support throughout my life.

# Table of Contents

<b>Topic</b>	<b>Page No.</b>
<b>Declaration</b>	<b>ii</b>
<b>Approval</b>	<b>iii</b>
<b>Abstract</b>	<b>iv</b>
<b>Acknowledgements</b>	<b>v</b>
<b>Table of Contents</b>	<b>vi</b>
<b>List of Tables</b>	<b>vii</b>
<b>List of Figures</b>	<b>viii</b>
<b>Chapter One: Introduction</b>	<b>1</b>
1.1 Background of the study	1
1.2 Objectives of the study	5
1.3 Outline of the Thesis	5
<b>Chapter Two: Literature Review</b>	<b>7</b>
2.1 General	7
2.2 Storm surge and its causes	8
2.3 Principal factors influencing storm surge development	13
2.3.1 Oceanographic and hydrographic factors	13
2.3.2 Meteorological factors	14
2.3.3 Hydrological factors	16
2.3.4 Geographical factors	17
2.3.5 Surface and bottom stress	17
2.3.6 The effect of the rotation of the earth	18
2.3.7 The effect of resonance	18
2.4 Coastal Zone of Bangladesh	18
2.4.1 Western coastal zone	22
2.4.2 Central coastal zone	24
2.4.3 Eastern coastal zone	24
2.5 Overview of Storm Surge Forecasting	24
2.6 The Cyclone 1991	36
2.6.1 Wind Speed and Surge Height	42
<b>Chapter Three: Theory and Methodology</b>	<b>44</b>
3.1 Introduction	44
3.2 Mathematical Formulation of the Storm Surge Equations	44
3.2.1 Shallow water equations	44
3.2.2 Water level rise due to air bubble entrainment	50
3.2.3 Vertically integrated equations	53
3.2.4 Wind Stress Generation	60
3.2.5 Boundary and initial conditions	63

<b>Chapter Four: Numerical Procedure</b>	<b>66</b>
4.1 General	66
4.2 Set up of nested schemes	67
4.3 Numerical Procedure	71
4.3.1 Grid Generation and Stair Step Representation	71
4.3.2 Computational Procedure: Discretization of the governing equations	74
4.3.3 The Data Sources and Numerical Values	77
4.3.4 Tide Generation for the Study Domain	79
4.3.5 The Numerical Experiment	80
<b>Chapter Five: Data Analysis and Conclusion</b>	<b>82</b>
5.1 Summary	82
5.2 Discussion of results and model validation	82
5.3 Conclusion and future recommendations	91
<b>References</b>	<b>93</b>

## List of Tables

<b>Table No.</b>	<b>Title</b>	<b>Page No.</b>
Table 1.1	Location and deaths from storm surges in the Bay of Bengal region	3
Table 1.2	A brief overview of major cyclones near the coast of Bangladesh	4
Table 2.1	Storm surge inundation features in Bangladesh	30
Table 2.2	Classification of low-pressure systems for the Bay of Bengal region	37
Table 2.3	Location of the cyclonic storm of April 1991 with central pressures and its nature	40
Table 2.4	Maximum wind speed observed at different locations in April 1991 cyclone	42
Table 2.5	Estimated surge heights of April 1991 cyclone	43



## List of Figures

<b>Figure No.</b>	<b>Title</b>	<b>Page No.</b>
Figure 2.1	Broad overview of the Bay of Bengal regions vulnerable to storm surge	<b>8</b>
Figure 2.2	Difference between storm surge and storm tide	<b>9</b>
Figure 2.3	Ocean wave spectrum	<b>10</b>
Figure 2.4	November 1970 cyclone	<b>11</b>
Figure 2.5	Stages of a storm surge	<b>12</b>
Figure 2.6	Coastal zone map of Bangladesh	<b>19</b>
Figure 2.7	Coastal zones of Bangladesh	<b>23</b>
Figure 2.8	Cyclone tracks in the Bay of Bengal from 25 April to 29 April 1991	<b>41</b>
Figure 3.1	Storm surge coordinate system	<b>54</b>
Figure 4.1	Domains of the different schemes (CMS, FMS, VFMS) with the positions of some coastal areas and their water levels	<b>70</b>
Figure 4.2(a)	A structured grid system	<b>72</b>
Figure 4.2(b)	Example of a coastal boundary and its numerical representation	<b>73</b>
Figure 4.3	Input data for depth collected from the displayed diagram	<b>81</b>
Figure 5.1	Estimated water levels due to tide in April 1991 Cyclone	<b>85</b>
Figure 5.2(a)	Maximum water level elevation without air bubbles caused by surge	<b>86</b>
Figure 5.2(b)	Maximum water level elevation with air bubbles caused by surge	<b>86</b>

Figure 5.2(c)	Simulated water level elevation due to tide, surge and the interaction between the two at $C_0 = 0$	<b>87</b>
Figure 5.2(d)	Simulated water level elevation due to tide, surge and the interaction between the two at $C_0 = 0.5$	<b>87</b>
Figure 5.2(e,f)	Simulated water level elevations caused by tide, surge and the interaction of the two at $C_0 = 0.2$	<b>88</b>
Figure 5.3	Comparison of simulated overall water levels with observed data	<b>89</b>

# **Chapter 1**

## **Introduction**

### **1.1 Background of the study**

Among all the natural hazards, tropical cyclones (TCs) along with storm surges are the most catastrophic in nature along the coastal regions of Bangladesh as they cause immense loss of lives and damage. Notably, an estimated 300,000 deaths occurred in one of the most devastating cyclones that hit Bangladesh in November 1970. Following the findings of Frank (1971), approximately 65% of total annual fishing capacity of coastal areas was destroyed and about 90% of marine fishermen incurred big losses in the Great Killer Cyclone of November 1970. During tropical cyclones, there is storm surge which is the abnormal rise in sea level due to strong circulatory winds. The surges tend to have the form of long waves which push the water into shore and cause inundation. In particular, flooding caused by cyclone-induced storm surges leads to tremendous negative impact on livelihood (Gönnert et al. 2001; Karim et al. 2008; Lewis et al., 2013; Condon et al., 2012) and also causes long-term damage to coastal ecosystems and landscapes (Dietrich et al., 2013). Furthermore, it is important to highlight that the major reason of damage is due to the associated surges instead of tropical cyclones. Statistics reveal that 5% of the global tropical storms and 80% of the global casualties happen in the Bay of Bengal. The severity of the impact of these cyclone-induced surges has been shown as well in Table 1.1 and Table 1.2. From 1877 to 1995 about 154 cyclones, consisting of 43 cyclonic storms, 43 severe cyclonic storms, and 68 tropical depressions affected Bangladesh (Dasgupta et al. 2010) and more than 70 of them were the reason for major hazards (WARPO, 2004). On average, a severe cyclone hits Bangladesh every three years (GOB, 2009) and has been rising at the rate of 1.18

cyclones per year from 1950-2000 (Islam and Peterson, 2009). No less than 14 severe cyclonic storms form over the Bay of Bengal in every ten years (IWM, 2002).

The frequency of major cyclonic storms and significant disproportional negative impacts are due to the geographical location of Bangladesh which is located at the northern tip of the Bay of Bengal. More specifically, the coastal belt of the country is very vulnerable owing to the complex coastal geometry, thickly populated offshore islands of different shapes, shallow bathymetry, long continental shelf, huge discharge through Meghna and other rivers, high tidal range between east and west coasts of Bangladesh, etc (Ali, 1999; Dube et al., 1997; Murty et al., 1986; Paul and Ismail, 2013). The country has three prominent coastal plains, among which the Meghna Deltaic Plain which is at the confluence of the Ganges-Brahmaputra-Meghna river system is most vulnerable to storm surges. The triangular shape of the coast in the northeastern edge of the Meghna Estuary greatly amplifies the surge wave (Flierl and Robinson, 1972; As-Salek, 1998; Haider et al., 1991) and leads to more flooding along the coast. Additionally, the funneling shape of the coast (Das, 1972) and the wide and shallow continental shelf (Murty et al., 1986) contributes to substantial surge amplification which also causes severe flooding in the low-lying regions. High tidal range (Miyan, M.A. 2005; SMRC 2000) and tide-surge interaction during a high tide period further augments the inundation in the coastal regions (Debsarma, 2009). These inundations can persist for many years and may create huge economic losses and damages in both the short and the long run.

Taking into consideration the prevalence of the effects of tropical cyclones over time, it is critical to investigate how the surge water encroach coastal areas in order to have better understanding of timely detection of storm surges. More importantly, this requires the development of an effective model that will help reduce the cyclone induced surge deaths and the resulting inundation in the

coastal regions. Thus, with an accurate prediction of water level along the coastal belt of Bangladesh, a proper warning system can be developed which can lead to accurate estimation of coastal flooding hazards (Lewis et al., 2014) to abate the loss of life and damages to property. There have been numerous studies done for the Bay of Bengal on tide, surge generated by tropical cyclones and their interaction (Das, 1972; Das et al., 1974; Flierl and Robinson, 1972; Johns and Ali, 1980; Paul and Ismail, 2012a; Roy, 1995; Soloviev and Lukas, 2010). Despite a large volume of works done on the coastal zone of Bangladesh, there have been limited studies that include the air bubble effects in the modeling of storm surge. Existing literature show that air bubbles can lead to increasing water levels during surge. The development of a forecasting model for storm surge hazard which includes the effects of air bubbles for a more accurate prediction of peak water levels can be vital in advancing an early warning system for the different coastal regions of Bangladesh. One of the aims of this study is to explore the development of a feasible surge forecasting model which takes into consideration the air bubble effects throughout the employment of a two-dimensional, vertically integrated hydrodynamic model.

**Table 1.1***Location and deaths from storm surges in the Bay of Bengal region*

Year	Location	Death toll
1970	Bangladesh	500,000
1897	Bangladesh	175,000
1991	Bangladesh	140,000
1876	Bangladesh	100,000
1822	Bangladesh	40,000
1965	Bangladesh	19,279
1963	Bangladesh	11,520
1961	Bangladesh	11,468
1977	India	10,000
1960	Bangladesh	5,149
2007	Bangladesh	3,379
2009	India	275
2016	Bangladesh	24

*Note.* From “Simulations of storm surges in the Bay of Bengal,” by S. K. Debsarma, 2009, *Marine Geodesy*, 32(2), 178-198. Copyright 2009 by Taylor & Francis Group

**Table 1.2***A brief overview of major cyclones near the coast of Bangladesh*

Landfall date	Location of landfall	Maximum wind speed (km/h)	Maximum surge height	Death
30 Oct	Chittagong-Cox's Bazar	208	6.1	5179
09 May 1961	Bhola, Noakhali	160	3.0	11.468
28 May 1963	North of Chittagong	203	3.7	11520
11 May 1965	Barisal, Noakhali	162	4.0	19279
15 Dec 1965	Cox's Bazar	210	3.7	873
23 Oct 1996	Noakhali, Chittagong	145	6.7	850
12 Nov 1970	Chittagong	222	10.6	300000
25 May 1985	Chittagong	154	4.3	4264
29 Nov 1988	Khulna	160	4.4	1498
29 Apr 1991	Chittagong	225	6.1	138000
02 May 1994	Cox's Bazar	215	3.3	188
19 May 1997	Chittagong, Feni	225	4.6	126
26 Sept 1997	Chittagong	150	3.0	155
16 May 1998	Chittagong, Cox's Bazar	165	2.5	12
15 Nov 2007	Barguna, Patuakhali	220-250	6.0	3500

*Note.* Major cyclones refer to ones with wind speeds above 15 km/h that have made landfall near the coast of Bangladesh. From “Impacts of climate change and sea-level rise on cyclonic storm surge floods in Bangladesh,” by M. F. Karim & N. Mimura, 2008, *Global environmental change*, 18(3), 490-500. Copyright 2008 by Elsevier Ltd.

## **1.2 Objectives of the study**

This research work focuses on the development of a cyclone-induced storm surge with the inclusion of the air bubble effects during storm surge for the coastal region of Bangladesh. Taking this into account, the model attempts to simulate water levels along the coastline and offshore islands as a result of the interaction of tide and surge caused by the tropical cyclone of April 1991 by applying a vertically integrated, hydrodynamic model. The model simulated results are checked against the observed data for the April 1991 cyclone in order to verify if they are in close agreement and to evaluate the overall strength of the model. Thus, the main objectives of the study are:

- i) To determine the the factors causing storm surges and to elucidate the reasoning behind the disproportional large impacts of the surge associated with tropical cyclones on the Bangladesh coast.
- ii) To investigate the tide-surge interaction associated with the April 1991 cyclone for the coastal regions of Bangladesh.
- iii) To investigate the effect of entrained air bubbles on water levels during storm surges along the coast of bangladesh
- iv) To apply a numerical hydrodynamic model in order to simulate the water levels with the addition of the presence of air bubbles.

## **1.3 Outline of the Thesis**

The thesis has been organized into five chapters. The first chapter includes some relevant background information which describes the general information about the study, the context of

this research along with its objectives and the rationale of the study. The second chapter presents the pertinent literature and reports such as an outline of the cyclone induced storm surge processes, the factors governing storm surge, a brief narrative of the coastal zone of Bangladesh as well as an overview of the relevant existing models for storm surge forecasting. Chapter 3 deals with the theory and methodology of the study including the governing equation for storm surge and the cyclone model. It presents the vertically integrated shallow water equations as well as the boundary conditions. This section also discusses surge amplification along the coast of Bangladesh along with a brief overview of the data sources and utilized numerical values. In Chapter 4, we see the numerical procedure for the solutions of the shallow water equations. The last chapter provides the detailed results, the concluding remarks and future recommendations of the study. Finally, the references required to carry out this study are appended.



## **Chapter 2**

### **Literature Review**

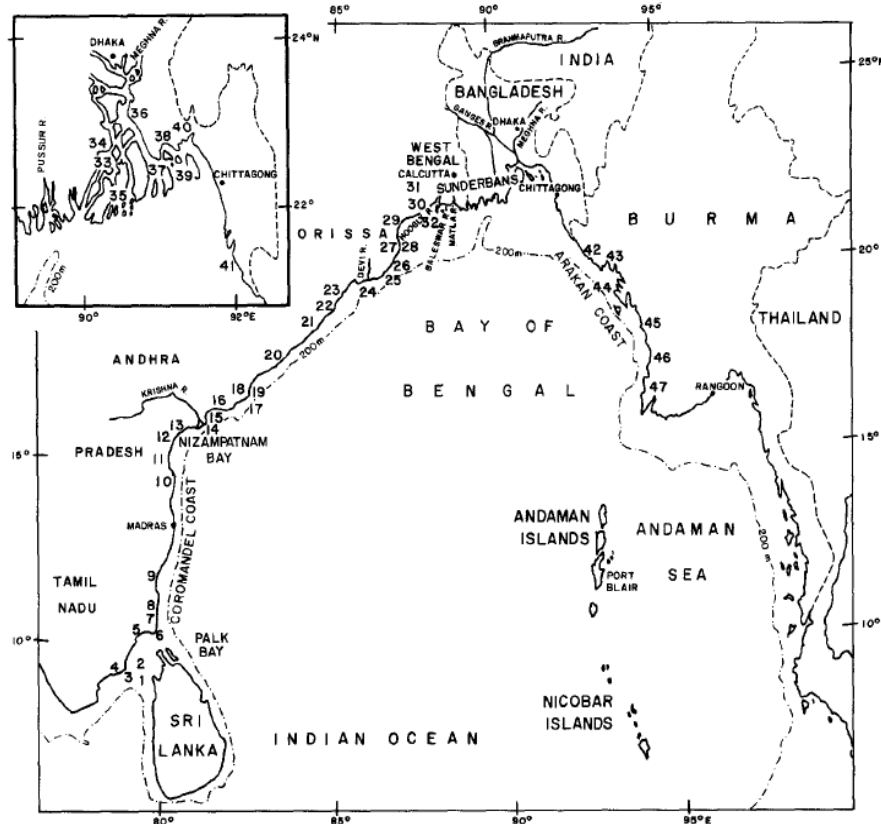
#### **2.1 General**

The destruction due to storm surge flooding has far-reaching consequences for the coastal areas of the countries along the funnel-shaped Bay of Bengal (Figure 2.1). The northern part of the Bay of Bengal along the coast of Bangladesh is particularly vulnerable to storm surges and cyclone-induced coastal flooding. This is mainly due to some of the factors stated by Ali (1979) such as: (a) shallow coastal water, (b) convergence of the bay, (c) high astronomical tide, (d) thickly populated low-lying islands, (e) favorable cyclone track, and (f) an innumerable number of inlets including the world's largest river system (Ganges-Brahmaputra-Meghna) and they are some of the key focuses in this study. Furthermore, scientific literature was studied for knowledge regarding the coastal zone of Bangladesh along with the cyclonic history and surge height during the April 1991 cyclone. Although the frequency of tropical cyclones in the Bay of Bengal is not high compared to the northwest Pacific, the coastal regions of Bangladesh, India, Myanmar, and Pakistan experience the most devastation. Approximately 60% of all deaths caused by storm surges took place in the low-lying arable coastal regions of the country at the confluence of the Bay and the adjacent Andaman Sea, with Bangladesh accounting for around 40% of loss of life (Murty, 1984). In April 1991, a severe cyclonic storm in terms of surge height, inundation, and loss of life hit the coast of Bangladesh. The surge height of the cyclone was more than 6m along a coastal stretch of 240km, causing flooding across large spans of coastal zones and offshore islands (SMRC, 1998). It was estimated that about 140,000 deaths occurred. The cyclone was tracked in the Bay early on and several warnings were issued which were ignored by a vast majority of the population. This demonstrates the crucial role of storm surge

and flood forecasting in developing an effective flood warning system to mitigate the suffering of people. Several storm surge models have also been developed for the northern Bay of Bengal and they have been reviewed in order to understand the relevant theory for our storm surge model for Cyclone 1991.

**Figure 2.1**

*Broad overview of the Bay of Bengal regions vulnerable to storm surges*



*Note.* From “The storm surge problem in the Bay of Bengal,” by T. S. Murty, R. A. Flather, 1986, *Progress in Oceanography*, 16(4), 195-233. Copyright 1986 by Elsevier Ltd.

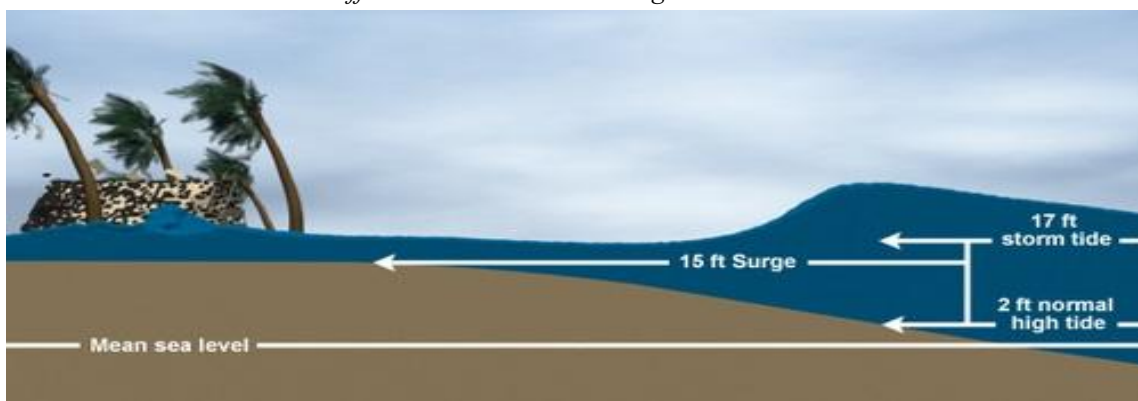
## 2.2 Storm Surge and its causes

One of the biggest hazards associated with tropical cyclones in the Bay of Bengal is a phenomenon called storm surge. National Oceanic and Atmospheric Administration (NOAA) defines storm surge as the abnormal rise in water level generated by a tropical storm, measured as the height of the water above the normal predicted astronomical tide and this hazard is the

greatest threat to both lives and property in comparison to the actual cyclone itself. Moreover, it should also be noted that there lies a significant difference between storm surge and storm tide where the latter is the water level rise caused by both storm surge, astronomical tide, and breaking wave set-up (Figure 2.2). While storm surges can take place over short periods on the order of a few minutes, they can also last for at least three days. On top of all this, storm surges can also push water tens of miles inland, leading to inundation where the water level can rise by 30 feet or more. This water level rise contributes to flooding in coastal regions, specifically when storm surge coincides with normal high tide. While the storm intensity can be a factor of surge height, there are other variables such as central pressure, high winds, and wave action associated with the storm before it makes landfall. The high winds push water towards the coast and the piling up leads to most of the coastal inundation. The central pressure of a storm also gets very low which means that the relative lack of atmospheric weight above the eye and eyewall causes a bulge in the ocean surface level. Additionally, the ocean waves also give rise to surge as the waves which are about a couple of meters out at sea grow as the ocean depth decreases to several meters near the coast.

**Figure 2.2**

*Difference between storm surge and storm tide*

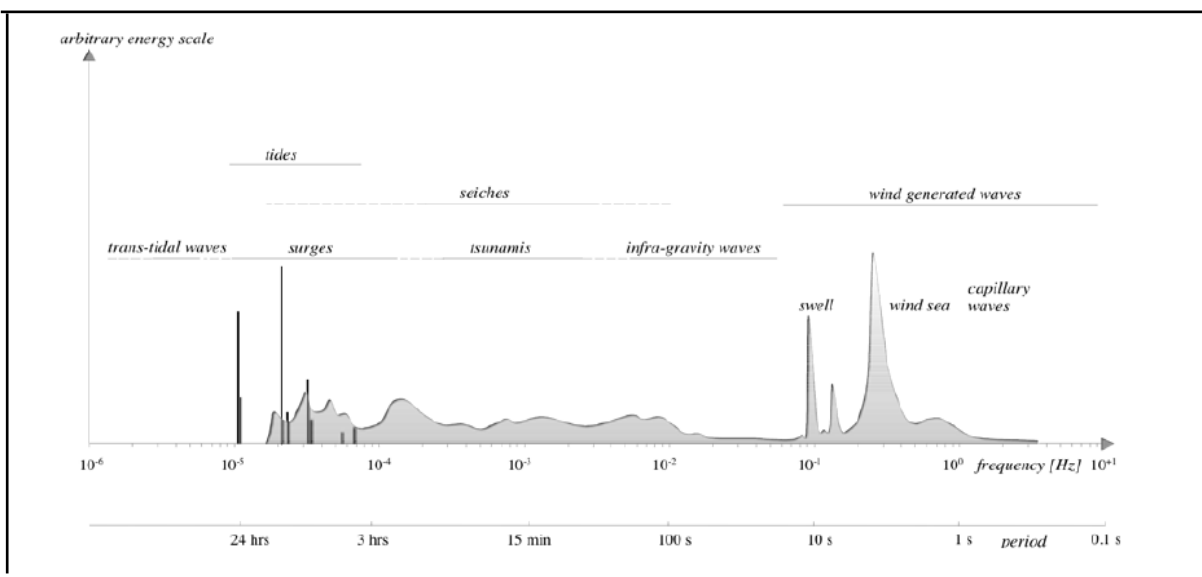


*Note.* From “Storm Surge Overview,” by National Oceanographic and Atmospheric Administration.

Gönnert et al. (2001) mention that tide, storm surges, and surges fall in the class of long gravity waves (Figure 2.3). Storm surges are centered at about  $10^{-4}$  cycles per second (cps or Hz) which yields a period of about 3 hours whereas the periods in oscillations of water level can vary considerably. This relies mostly on the topography of the water body and also somewhat, on other parameters like the direction of the storm, its strength, the stratification of the water body, the presence or absence of ice cover, and the nature of tidal motion in the water body.

**Figure 2.3**

*Ocean wave spectrum*



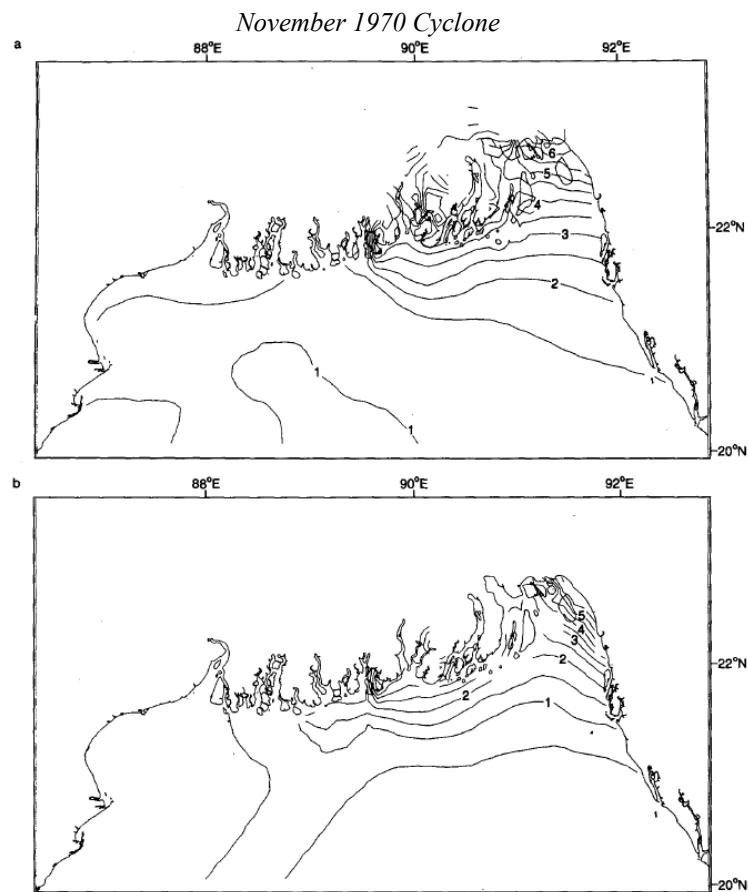
*Note.* From “Waves in Oceanic and Coastal waters,” by L. H. Holthuijsen, 2010. Copyright 2010 by Cambridge University Press.

The notable feature of a long gravity wave is that its wavelength is relatively bigger than the depth of the water over which it is traveling. In addition, even though storm surges, astronomical tides, and tsunamis are all long waves, there are two significant differences between the former and the latter two types. The first one is that tides and tsunamis happen on the oceanic scale while on the contrary, storm surges are mainly a coastal phenomenon. The second one is that tsunamis and tides cannot take place in a small, enclosed region like a small coastal or inland

body of water. However, storm surges can happen in enclosed lakes, rivers, and canals.

Figure 2.3 also shows that the amplitude of the storm surge was zero towards the deeper regions of the bay. This is due to the fact that over deep water, the storm surge spreads much faster than the speed at which the weather system travels in the atmosphere. Nevertheless, the long waves slow down in the shallowing waters of the head of the bay. Eventually, its speed corresponds with the weather system's speed of movement. At that moment, resonance coupling occurs and energy is transferred from the weather system to the ocean's surface which leads to the development of a storm surge.

**Figure 2.4**

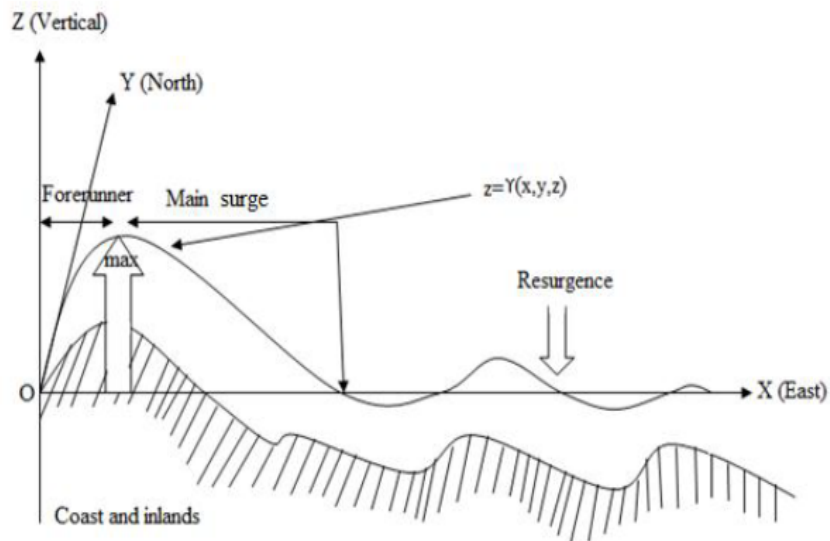


*Note.* (a) maximum estimated water level (m) caused by tide-surge interaction, and (b) peak surge elevation (m) for November 1970 cyclone. From “The storm surge problem and possible effects of sea level changes on coastal flooding in the Bay of Bengal,” by R. A. Flather and H. Khandker, 1993, *Climate and Sea Level Change: Observations, Projections and Implications*, 229-245. Copyright 1993 by Cambridge University Press.

Storm surges can be divided into three stages: forerunner, main surge, and resurgence. A forerunner is the gradual rise of sea level preceding the cyclone. In spite of the cyclone being far from the coast, it can be observed that there are some broad-scale disturbances generating variations in the coastal sea level. Therefore, the forerunner stage of the cyclone is a sign of the incoming tropical cyclone. The main surge takes place after the storm surge reaches its peak. The period of the main surge at a place varies from a few hours to more than two days and it is determined by the speed of the cyclone as well as other factors. Finally, resurgence follows the main surge where the sea level gradually goes back to its regular state. This stage has many different oscillations as a result of topographic and other effects. The period of resurgence can be around two to three days making it a destructive event for marine and inland shipping.

**Figure 2.5**

*Stages of a storm surge*



## **2.3 Principal factors influencing storm surge development**

Storm surges are complex atmospheric phenomena that have oceanographic, hydrographic, meteorological, hydrological, and geographical factors among others influencing its development. It is important to have an understanding of these factors for the implementation of a storm surge model. There is a brief explanation of each of these factors below.

### **2.3.1 Oceanographic and hydrographic factors**

Oceanographic components influencing storm surge include:

- a) bathymetry,
- b) the effect of waves,
- c) astronomical tides and
- d) inshore currents

Joseph et al. (2011) explain that storm surge is very sensitive to near-coastal bathymetry and coastal geometry in a shallow water region. The northern region of the Bay of Bengal is extremely shallow and the shallowness of water can significantly affect surge heights in this area (Johns et al. 1983a). It is also notable for the sharp changes in seabed contours.

When waves enter shallow water in the same order of depth as their own height, they will break. After breaking occurs, the water runs up the beach or river and creates a wave setup. Waves can increase the maximum surge heights greatly through this setup. To be more specific their influence varies according to the storm characteristics. Besides direct wave forcing, the wave-enhanced bottom stress in the surfzone can also create a higher wave setup and thus greater surge generation. Waves also play a role in the maximum inland flooding distance. Nonetheless, waves do not always cause as much flooding as expected.

While inshore currents have an effect on surges in the coastal areas, the more predominant factor is the astronomical tide which also contributes to the storm surge in the Bay of Bengal due to periodical movements of the celestial bodies relative to the earth. The tide can lead to a water level rise of 5m above the mean sea level in parts of the Bay of Bengal region. There can be widespread destruction in case of the surge arrival coinciding with the time of the high tide. The biggest instance of such an event was the 1970 Bhola cyclone in Bangladesh when the peak surge and high tide coincided and it led to a huge death toll. Whereas the storm surge of May 1990 took place close to the low tide, the water level rise was relatively low and there were fewer losses in terms of property and life. Additionally, the eastern part of the head of the Bay of Bengal is a large tidal range area. Furthermore, surge interacts nonlinearly with the tide in the shallow waters ( Ali et al., 1997; Flather, 1994; Henry et al., 1997; Johns et al., 1985; Sinha et al., 1996, 2008). According to Roy et al. (1995), the surge amplification due to nonlinear tide-surge interaction increases in shallow water. Debsarma (2009) also highlights that the disastrous floods is due this nonlinear interaction. The tidal range in Bangladesh displays a gradual increase from west to east to reach a maximum at the Meghna estuary and then it decreases in a south-easterly direction. Tidal amplitude also differs in different seasons along the coastal regions. During the monsoon season, there is a rise in tidal height between 60-100 cm above the normal height (Pattalo et al., 1989). In the months of October and November, if the high tide coincides with the storm surge then the consequences can be devastating. Therefore, it is important to be able to forecast tide elevations accurately under all conditions.

### **2.3.2 Meteorological factors**

Storm surges arise from an interaction between air and sea where the high winds associated with tropical storms are one of the biggest contributing factors for storm surge. The major



meteorological parameters along with the wind influencing storm surge are:

- a) pressure drop
- b) the radius of the maximum sustained wind
- c) vector motion of the storm
- d) location of landfall
- e) duration of the storm

Pressure drop is the difference between the surrounding pressure and the central pressure of the cyclone. Even though the low pressure at the center of the storm pulls the water level up, this factor contributes to the surge to a lesser degree. According to hydrostatic considerations, the water level rises by about 1 cm for every 1 hPa fall in pressure. This is known as the inverse barometer effect and it is comparable to the analogy of drinking through a straw. Wind in the tropical storm is highly dependent on the pressure drop and it is the biggest factor behind storm surge. The maximum sustained wind occupies the eyewall at a distance known as the radius of maximum wind (R). The latter is the distance between the storm center and its band of strongest winds. The heaviest rainfall takes place in the region of R of tropical storms. A composite average of 47 km for R is taken as the mean of all hurricanes with the lower central atmospheric pressure between a pressure of 909 hPa and 993 hPa. Furthermore, the R can determine the degree of storm surge and its highest potential intensity. When tropical storms gain intensity, the R decreases as the maximum sustained winds increase. The wind during a tropical storm employs both tangential and normal stresses on the water underneath, the former being the predominant one. This reinforces the importance of proper computation of surface winds in tropical storms for accurately forecasting storm surges. There is a body of research available that covers several empirically-based formulae for calculating surface winds in storm surge

forecasting models (Das et al., 1974; Holland, 1980; Jelesnianski, 1965, 1972; Jelesnianski & Taylor, 1973).

The position and magnitude of the peak surge near the coast rely on the speed and direction of the storm relative to the coast. Hence, for the proper prediction of peak surge in a specific area, it is important to know the vector motion of the storm along with the location of the landfall point. In addition, it is vital to know the duration of the storm for storm surge modeling purposes. Rao et al. (2007) emphasized that tropical storms which dwell over the sea for a considerable time period tend to produce bigger sea surface elevations in comparison to cyclones which last for a shorter time period.

### **2.3.3 Hydrological factors**

The following are the major hydrological influences on storm surge:

- a) river discharge in the sea, and
- b) rainfall distribution

Analysis from river-ocean coupled mathematical models reveals that the discharge of freshwater brought about by the rivers can alter the surge heights, chiefly in the head of the Bay of Bengal where the largest transboundary river system Ganges-Brahmaputra-Meghna (GBM) enters the sea (Dube et al., 1986, 2005, Ali et al., 1997). The riverine characteristic of this region means that there is possible deep inland penetration by surges emanating from the sea. This leads to inundation in the coastal regions and damage to coastal infrastructure. Besides storm surge, sustained heavy rainfall can cause flooding. When both precipitation and high water levels take place together, the consequences are far worse as they combine to cause compound flooding to have a multiplier effect. Water level rise can impede stormwater draining into the sea, thus leading to inland inundation, or heavy precipitation can add even more water to an existing tidal

flood.

#### **2.3.4 Geographical features**

The geographical features listed below should also be taken into consideration for affecting surge generation:

- a) coastal geometry
- b) effect of the shape of shorelines
- c) offshore islands

In simple terms, a coastline that is normal to the incoming surge wave will face the most devastation. Research by Dube et al. (1982) and Johns et al. (1981) propose that the bending coastline modifies both the position and the height of the surge. Coastal features affect wave movement through ways such as breaking, diffraction, and refraction. The position of the head of a bay in a downwind direction means that it is not blocking the wind. This causes piling up of water through wind stress and produces more powerful surges. The semi-enclosed nature of the basin of the Bay of Bengal together with its funnel shape allows the storm heading towards it channels the water towards the north. According to Proudman (1955), the convergence can cause piling up of a strong surge in the location and lead to changes in the sea surface elevation. Besides these factors, Paul and Ismail (2013) have also shown in their research how low-lying islands of different sizes can affect surge.

#### **2.3.5 Surface and bottom stress**

The atmosphere transfers energy to the ocean by means of normal and tangential stresses on the sea surface, which are generated by pressure gradients and a vertical wind profile. Some of the flow of energy in the beginning disappears because of the tangential stress at the sea-bottom. It is applied on the sea bed by the current over it. The surface stress at work in this scenario can be

represented by the quadratic law. Sea bed friction is also represented by the quadratic law. An underlying problem is that there is a lack of data for the drag coefficient values. Existing research shows that this coefficient changes very frequently as it is dependent on the state of the sea.

### **2.3.6 The effect of the rotation of the earth**

While considering the scenario of no rotation of the earth, the water motion is parallel to the direction of the wind. The Coriolis force effect causes the current orientation to move in a rightwards direction in the northern hemisphere and in a leftwards direction in the southern hemisphere.

### **2.3.7 The effect of resonance**

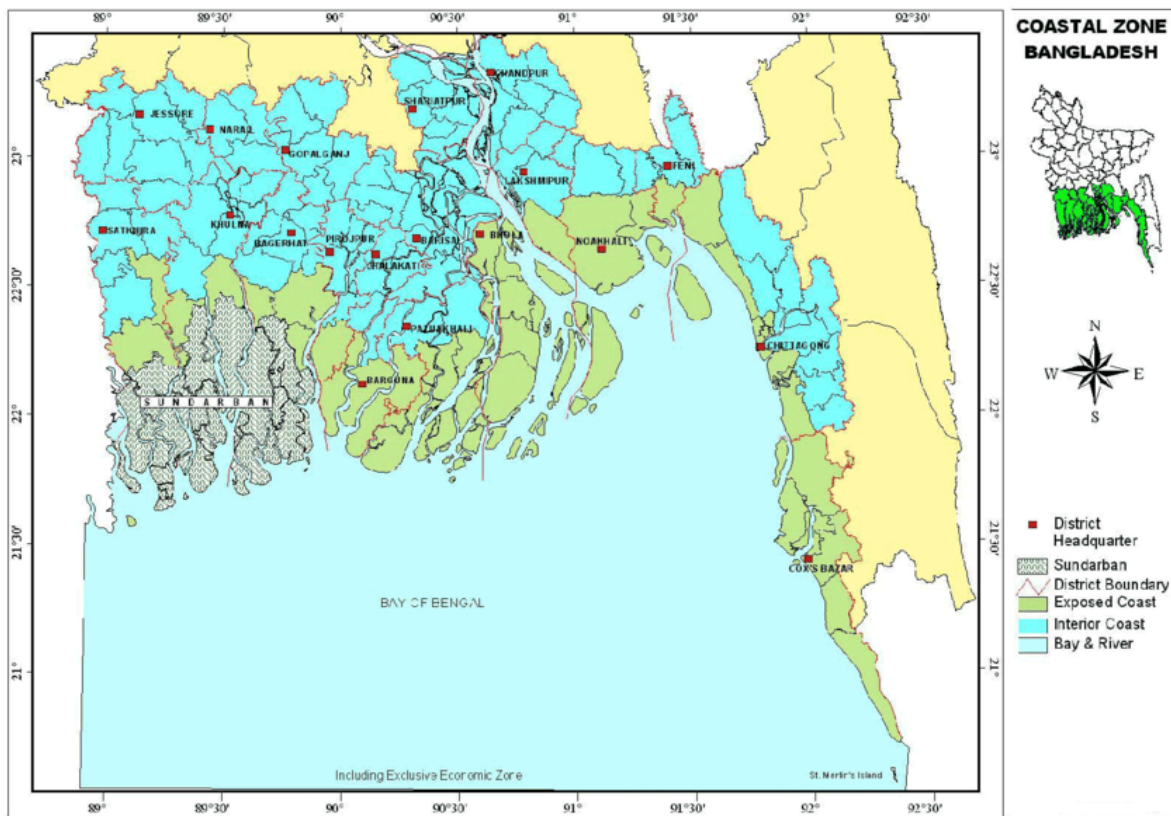
Water inlets are known for the characteristic of having its period of free oscillation. Both the surge wave impulse and the low-pressure environment causes the body of water to resonate, producing high amplitudes which are also known as seiches. This effect can be observed in seas, bays, estuaries, creeks and harbors as well.

## **2.4 Coastal Zone of Bangladesh**

The destruction due to storm surge associated with land-falling severe TCs is a serious concern along the coastal regions of the countries along the Bay of Bengal. According to Murty (1984), around 60% of deaths caused by surges have happened in the fertile, low-lying coastal areas of the countries bordering the Bay and the adjoining Andaman Sea. Bangladesh is one of the countries most vulnerable to cyclone-induced surges as it accounts for nearly 40% of all fatalities. Its susceptibility to storm surges is attributable to the country's peculiar geographical position where it lies at the juncture of the Himalayas and Khasi-Jaintia hills to the north and the

Bay of the Bengal and the North Indian Ocean to the south. Thus, it is important to describe the coastal zone in order to understand the destruction and vulnerabilities produced by storm surges in these regions. Moreover, a study of the coastal zones can contribute to the assessment of the extent of coastal flooding as a result of surges generated by tropical storms.

**Figure 2.6**  
*Coastal zone map of Bangladesh*



*Note.* From “Successful Integrated Coastal Zone Management (ICZM) Program Model of a Developing Country (Xiamen, China)–Implementation in Bangladesh Perspective,” by K.S.Islam, X.Z. Xue, and M.M. Rahman, 2009, *Journal of Wetlands Ecology*, 35-41.

The term "coastal zone" means the coastal waters (including the lands surrounding these waters) and the adjacent shorelands (including the waters these areas), strongly influenced by each other and in proximity to the shorelines of the several coastal states which includes islands, transitional and intertidal areas, salt marshes, wetlands, and beaches (Congress, 1972). In

addition, following the Mediterranean ICZM Protocol it can be defined as the geomorphologic region on either side of the seashore in which interaction between the marine and land parts happen in the form of complex ecological and resource systems made up of biotic and abiotic components coexisting and interacting with human communities and relevant socioeconomic activities (UNEP, 2008). In more simple terms, a coastal zone can be described as the area where the land, atmosphere, and water interact with each other making it dynamic and diverse in nature (National Geographic Society, 2012; Nelson, 2018). According to Nelson (2018), the energy reaching the coast can become high during storms, and such high energies make coastal zones areas which are highly vulnerable to natural hazards. The latter work highlights that the coastal zone is always undergoing change due to the dynamic interaction between the ocean and the lands.

In Bangladesh, the coastal zone has been characterized in a number of ways by different agencies for various purposes based on widely used criteria such as social aspects, natural system processes, economic opportunities, and erosion-prone areas. According to the GoB policy note on ICZM (MoWR, 1999), the coastal zone was explained as being difficult to define precisely according to spatial boundaries and was delineated in line with recognized administrative boundaries in Bangladesh to suit management purposes. Later, this concept for delineating the coastal zone underwent changes to represent the typical coastal vulnerabilities and opportunities by including the three basic natural processes: tidal fluctuations; salinities (soil, surface water, or groundwater), and cyclone and storm surge risk. Based on the aforementioned three criteria, the coastal zone of Bangladesh is composed of 133 upazilas of 19 districts (total 147 upazilas), specifically Bagerhat, Barisal, Bhola, Barguna, Chittagong, Cox's Bazar, Chandpur, Feni, Gopalganj, Jessore, Jhalakathi, Khulna, Lakshmipur, Noakhali, Narail, Pirojpur, Patuakhali,

Satkhira, and Shariatpur (Uddin & Kaudstall, 2003). The upazilas have been labeled as “coastal” and the 19 districts are considered as “coastal districts”. Among all the different zones, Exclusive Economic Zone (EEZ) is also included in the coastal zone of Bangladesh. It comprises of a sea zone over which a coastal state has sovereign rights for the use and exploration of marine resources, including oil and gas. This zone generally stretches from the seaward edge of the state's 12 nautical miles territorial sea out to 200 nautical miles from its coast (Treves, 1982). Besides, there lies a difference between upazilas facing the coast or the estuary and the upazilas located behind them. A total number of 48 upazilas in 12 districts are defined as the exposed coast as these areas are directly exposed to the sea and or lower estuaries, where the interaction with the marine environment is most intensive. While the remaining 99 upazilas of the coastal districts are defined as the interior coast.

Given a coastline of 700 km, the coastal areas of Bangladesh have an area of 47201 km<sup>2</sup> which accounts for 32% of the total area of the country (Islam, 2004; Khan & Awal, 2009). Bangladesh Bureau of Statistics (2003) states that the population of the coastal zone is about 35 million. This whole region is greatly exposed to surges and coastal flooding. Its predominant feature would be its extensive network of rivers, a dynamic Ganges-Brahmaputra-Meghna river system shared with India, Bhutan, Nepal, and China, and the fact that it is the third-largest freshwater outlet to the world's oceans (Milliman, 1991). The delta plain of the Ganges (Padma), Brahmaputra (Jamuna), and Meghna rivers and their tributaries occupy 79% of the country. All the coastal zones are characterized as arable land with wide river networks and are labeled as char land with the exclusion of the Chittagong-Cox's Bazar. The country has three significant coastal plains, viz; (i) the Ganges Tidal Plain, otherwise, the Western Region; (ii) the Chittagong plain or the Eastern Region; and (iii) the Meghna Delta Plain, also known as the Central Region which lies

between the other two. Among the plains, the Meghna Plain is the most prone to storm surges in the world as it lies at the interface of the Ganges, Brahmaputra, and Meghna rivers. The causes for this vulnerability can be due to the long continental shelf, excessive bending of the coastline, densely populated small and big offshore islands, shallowness of the water, discharge through Meghna and other rivers, favorable cyclone track, and complex tidal phenomenon (Ali, 1979; Debsarma, 2009; Paul & Ismail, 2012a). Moreover, the head of the Bay of Bengal is a huge tidal range area where the tidal constituents,  $M_2$  and  $S_2$  are particularly dominant due to the attractions of the sun and the moon. As the tide and surge phenomena are long-wave phenomena, there is a tremendous increase in the amplitude of the waves when they intrude into the shallow coastal zone of Bangladesh. Besides, given the low-lying nature of the offshore islands and the coastal regions and the small inland upward slope, surge water can pervade onshore and cause coastal inundation. The different coastal zones have distinctive riverine, geographical, and topographical characteristics that contribute to coastal inundation in varied forms. Despite the exposure of the coastal zone to tropical storms and being the hub of the most global casualties, the coastal region of Bangladesh has not been adequately investigated and it further emphasizes the importance of more research required for the correct prediction of water levels because of tide-surge interaction in order to reduce the impact of storm surge induced destruction. As mentioned above, from a geomorphological point of view the coastal zone of Bangladesh has been divided into three regions (MCSP, 1993; ESCAP, 1987; PDO-ICZMP, 2001), known as the western, central, and eastern zone which have been explained in the following sections.

#### **2.4.1 Western coastal zone**

The western coastal zone is known for being the flood plain of the Ganges river. In particular, this region surrounds the southwest part of the country as it can be seen in Figure 2.7 where it



covers greater Khulna and part of Patuakhali district. It has a semi-active delta so land erosion, accretion, and sediment flow are comparatively low in this part of the zone. According to Islam (2003), the mangroves of this region have soil formation of alluvium which arrives from the Himalayas. The coastal zone is marked by an extensive network of rivers, namely the Bishkhaki-Buriswar river, the Sibsa river, the Tetulia river, and the Passur river. The most well-known aspect would be the Sundarbans, otherwise, the largest mangrove forest which explains the little to no soil erosion in this region. It is widely interspersed with mangrove swamps, tidal creeks, natural levees, and tidal flats. The mangrove forest facilitates feeding and provides breeding grounds for fish and shrimp species while simultaneously boosting the ecosystem. Most importantly, it works as a strong barrier against tropical storms and their associated surges (Ali, 1999).

**Figure 2.7**

*Coastal Zones of Bangladesh*



*Note.* From “Soil Health and Food Security: Perspective from Southwestern Coastal Region of Bangladesh,” by A.Z.M.Moslehuddin, M.A.Abedin, M.A.R.Hossain, and U.Habiba, 2015, *Food Security and Risk Reduction in Bangladesh*, 187-212. Copyright 2015 by Springer Japan.

### **2.4.2 Central coastal zone**

The central coastal zone lies at the interface of the Ganges-Brahmaputra-Meghna (GBM) rivers. Its morphology is the most dynamic out of all the other zones due to the powerful current and heavy sediment discharge carried from the GBM river system to the Bay of Bengal, thus leading to high erosion and accretion rates. At least 70% of the sediment deposition is silt along with an added 10% volume of sand (Allison et al., 2003; Coleman, 1969). This zone has a large number of islands, many of which have formed within the last few years through the land accretion process and have also vanished or eroded (Pramanik, 1988; Rahman et al. 1993; SDNP, 2004). The central zone stretches all the way from the Feni river to the eastern section of the Sundarbans which consists of Noakhali, Bhola (the only island district of Bangladesh), Barisal, and Patuakhali districts.

### **2.4.3 Eastern coastal zone**

The eastern coastal zone is a narrow region extending from Bodormokam at the southern edge of the mainland to the Feni river estuary. This coastal zone is the most stable relative to the others which has the Karnaphuli, Mahatmuhury, and Sangu rivers flowing into the Bay of Bengal and the Naf river forming a barrier between Bangladesh and Myanmar. The soil formation is predominantly submerged sands and mudflats in this region (Islam, 2001) and the submerged sand has led to the formation of the eastern coast's most famous tourist destination - the 145 km sandy beach extending from Cox's Bazar to Teknaf.

## **2.5 Overview of Storm Surge Forecasting**

There have been numerous modelling efforts for storm surge forecasting throughout the years. The application of storm surge models largely improve the forecasting of real-time storm surge

or even the interaction of tide-surge in order to prevent the devastation caused by surge-related hazards. These models can estimate the water levels and possible flooding induced by storm surge. Moreover, they can be used to hindcast the flooding due to tropical storms, evaluate future flood risks and make flooding maps for future purposes. According to the literature for storm surge models, there are two types of commonly used models for analyzing tides and surges: the vertically integrated (depth averaged) model and the three dimensional model. The majority of the models are two dimensional as they are more than adequate for researchers to get an accurate estimate of the peak water level caused by storms whereas 3D modeling can give rise to difficulty in numerical coding (Sinha et al., 1986). The primary difference between 2D and 3D models is that a 2D model simplifies the vertical structure by neglecting the vertical velocities through vertical integration whereas a 3D model can generate more realistic and complex vertical velocities. In addition, while every storm surge model have their differences, they share a common set of required data for storm surge forecasts. For example, some general input required for a storm surge model are generally bathymetry data for the area, tidal information, atmospheric pressure and cyclone information (storm track, wind strength), and computational mesh for the study area.

Some of the earlier research by Reid and Bodine (1968), Sielecki and Wurtele (1970), and Flather and Heaps (1975) developed numerical systems which could only simulate the degree of inundation without the actual processes of wave propagation. Sometime later, crucial advancements had been made in formulating a numerical algorithm for analyzing storm surges by Hibberd & Peregrine (1979), Hebenstreit et al. (1985), and Kowalik and Bang (1987). A few of the most widely used storm surge models are the SLOSH model (the Sea, Lake, and Overland Surges from Hurricanes) developed by the National Weather Service in the 1990s (Jelesnianski

et al. 1992, Glahn et al. 2009 ), the ADvanced CIRCulation (ADCIRC) coastal circulation and storm surge model, and (CH3D)-SMSS which is the Storm Surge Modeling System with Curvilinear-grid Hydrodynamics in 3D. They are implemented throughout the US with the SLOSH model being primarily used to this day due to its computational efficiency. This model divides the coastline into 32 basins which include the US Atlantic and the Gulf of Mexico along with Hawaii, Puerto Rico, Bahamas, and the Virgin Islands. The SLOSH model has the capability of computing real-time cyclone-induced flooding and predicting the landfall with the maximum possible impact by storm surge for a region using inputs such as the storm track, intensity, and estimates of its size as given by experts at the National Hurricane Center. On the other hand, the ADCIRC model is more intricate and efficient but it has a longer run-time in comparison to the SLOSH model. ADCIRC uses a flexible mesh technique to produce surge, the model is able to simulate much better when it concerns tides forming in the ocean and it can easily ascertain the complex bathymetry as well.

A few models in other countries are the Delft3D model and also the Dutch Continental Shelf Model version 6 (DCSMv6) in the Netherlands which predict the water levels at stations along the Dutch coast every 6 hours with a 48-hour lead time. Australia runs 3 Tropical Cyclone Warning Centres (TCWCs) situated in Perth (Western Region), Darwin (Northern Region), and Brisbane (Eastern Region). The methods followed to predict storm surge produced by tropical cyclones vary somewhat in each of the three locations. In the Australian Eastern Region, the primary method for predicting surges is founded on nomograms such as the Jelesnianski-Taylor nomogram. However, it is known that nomograms of this sort are not very effective with strongly curved coasts (i.e., if the curvature of the coastal radius is smaller than the radius of the most strong winds). In Darwin (Northern Region) the principal technique for

computing storm surges associated with tropical cyclones has been derived from Jelesnianski (1972). In recent times, a system founded on the SEAtide model and a database of possible scenarios have been applied. This system was evaluated during the 2004–2005 period for Tropical Cyclone Ingrid and was formally applied in the 2005–2006 period when Tropical Cyclone Monica took place. This system has been proposed as the main storm-tide prediction tool used in Darwin TCWC. The system uses data input such as cyclone intensity, size, speed, and track to forecast the possible size, location, and duration of the total abnormal water level (storm plus tide) after many trials of the numerical model. These models have been used in 7 locations, starting from the Queensland border and covering areas westwards to the Kimberley coast of Western Australia. Furthermore, the Danish storm surge model, Mike21, was developed by the Danish Hydraulic Institute (DHI). Tide-gauge data are collected from the Danish Meteorological Institute (DMI) database, where all Danish tide-gauge data are maintained online. Storm surge forecasting or the RTSM (Regional Tide/Storm Surge Model) by the Korean Meteorological Administration (KMA) implement the operational model using atmospheric input data, the Regional Data Assimilation and Prediction System (RDAPS). Wind stress and mean sea-level pressure-fields from this model are used as input in a two-dimensional barotropic surge and tide edition of the Princeton Ocean Model. This storm surge model of medium resolution (based on a grid of approximately 8 km) covers certain parts of the East China Sea and the East Sea/Sea of Japan. Other noteworthy research for storm surge modeling were by Overland (1975) and Thacker (1977, 1979). The latter studies included the bending coastline and island boundaries by using the irregular finite difference method in place of the finite element methods. The advantage of using such a technique was less time consumption. There has also been a large volume of research for the North Sea and the North-West European

Continental Shelf. The North Sea is largely surrounded by six highly developed countries: the United Kingdom, Belgium, the Netherlands, Germany, Denmark, and Norway. Many of these low-lying areas are vulnerable to extreme storm surges. The North Sea is also one of the most crowded seas in the world. Storm surge predictions are provided by either the National Meteorological Services (the United Kingdom, the Netherlands, Denmark, Norway) or the National Maritime Services (Belgium, the Netherlands, Germany) of the countries surrounding the North Sea. The United Kingdom operational warning system that was developed is known currently as the United Kingdom Coastal Monitoring and Forecasting (UKCMF).

### **Storm Surge Forecasting Model for the Bay of Bengal Region**

There have been a large volume of research done for the Bay of Bengal region on the analysis and prediction of the tide, surge, and their interaction. Das (1972) pioneered the prediction model for surges along the coast of Bangladesh using a linear stair-step model. The model simulated the surge generated by the November 1970 storm. In a stair-step model the coastal and island boundaries are approximated along the nearest finite-difference gridlines of the numerical scheme. If the grid size is not small, the representation of the coastal boundaries along the grid lines is not accurate in the stair-step representation. Flierl and Robinson (1972) also developed the linear stair-step model but their study did not take friction coefficient into consideration. The Multi-purpose Cyclone Shelter Project (MCSP, 1993) modeled the storm surge phenomenon in the coastal region of Bangladesh with the aid of GIS and the outcome of the modeling effort included a table outlining surge inundation features for cyclones of differing strength in Bangladesh (shown in Table 1). There continued to be further developments of the forecasting of storm surge and tide along with their interaction in the head of the Bay of Bengal region by Das et al. (1974) where a stair-step model was developed and was used to simulate the tide and surge

interaction along the south coast of Bangladesh and east coast of India. Moreover, Ali (1979, 1986) also examined storm surges and sea-level rise in the Bay of Bengal. Later on, Ali et al. (1997a, 1997b) investigated river discharge, storm surges, and tidal interaction in the Meghna river mouth in Bangladesh, as well as the backwater effect of tides and storm surges on freshwater discharge through the Meghna estuary. Then Johns and Ali (1980) used the first non-linear stair-step model for simulating the tide and surge interaction along the coast of Bangladesh by including the major rivers (Ganges-Brahmaputra-Meghna) and off-shore islands. The model analyzed the effects of the cyclone tracks and islands on surge levels along the coastal boundary measured the magnitude of inland inundation. The model was also approximated along the nearest finite-difference grid lines for accuracy. It should be taken into account that in a stair-step model, coastal and island boundaries are approximated along the nearest finite grid difference lines. Thus, to represent the facts accurately via such a model, its grid resolution has to be very high. However, the model by Johns and Ali (1980) did not have a high grid resolution which meant that the model lacked accuracy as the representation of coastal and island boundaries in the study differed in part from reality. Notably, Johns et al. (1981) developed the first transformed coordinate model for the Bay of Bengal region consisting of the east coast of India by the natural shoreline. The model was used to simulate the surges generated by the Andra Cyclone of 1977. Roy (1995) improved the model of Johns and Ali (1980) with a stair-step one consisting of a nested numerical scheme. The model inserted a fine grid model for the Meghna estuarine area into a parental coarse grid model extended up to 15° N lat and assessed the sensitivity of wind velocity and surge route on water levels due to the nonlinear interaction of tide surge. Simulated flood level was found to be highly sensitive to wind speed and cyclone landfall (see Johns & Ali, 1980). This result was in agreement with the outcome of the

simulation done by Lewis et al.(2014). In the fine mesh scheme, major islands were incorporated through proper stair step representation as the region between Barisal and Cox’s Bazar contains islands of many sizes and offshore islands may influence surge levels. Even though the coastal zone of Bangladesh has many islands of various sizes (Paul & Ismail, 2012a), Roy(1995) included only two offshore islands, Sandwip and Hatiya (Char Chenga). Subsequently, Roy (1999) examined the influence of coastal geometry, ocean bathymetry, offshore islands, storm intensity, and tracks on the surge levels along the coastal belt. Taking these previous works into account, Paul and Ismail (2013) incorporated all offshore islands to examine the rise in water level for the area of interest.

**Table 2.1**

*Storm surge inundation features in Bangladesh*

Wind velocity (km/h)	Storm surge height (m)	Limit to inundation (km) from the coastline
85	1.5	1.0
115	2.5	1.0
135	3.0	1.5
165	3.5	2.0
195	4.8	4.0
225	6.0	4.5
235	6.5	5.0
260	7.8	5.5

*Note.* From “ Multipurpose cyclone shelter programme: Final report,” by Bangladesh University of Engineering and Technology & Bangladesh Institute of Development Studies, 1993. Copyright 1993 by Bangladesh University of Engineering & Technology.

Some further noteworthy storm surge forecasting works done in the past century are the numerical models by Murty and Henry (1983) and Dube et al. (1985, 1986) which view the dynamic effect of factors like curving coasts and the direction of the motion of the storm relative to the coast at the location of the peak surge. The works exhibit the natural shoreline of the Bangladesh coast by actual curvilinear boundary. A similar study was carried out by Johns et al. (1981) for the east coast of India. Roy (1985) used the model of Dube et al. (1985) to investigate the sensitivity of surge levels caused by meteorological and oceanographic factors. The work of



Johns et al. (1981, 1985), Dube et al. (1986), and Sinha et al. (1986) were also based on representing the shorelines by actual curvilinear boundaries. But none of them incorporated any offshore islands. The main difficulty with including islands in the modeling process is that the position of the boundaries of an island is undetectable in the transformed domain. As previously stated, Roy (1999a) developed a mathematical method to incorporate two islands of unique shapes in order to ensure that the boundaries were known in the transformed domain. This model was tested for some previous storms and the computed results were acceptable. However, given that the coastal belt of Bangladesh is populated throughout with many islands of different sizes, the coastal boundaries can get very complex. This highlights the importance of taking all factors into consideration for the accurate prediction of water levels. More advancements took place as Roy et al. (1999) developed a cylindrical polar coordinate model with the help of a single numerical scheme that produces fine resolution near the coast and coarse resolution away from the coast. Rahman et al. (2012) made further improvements to the polar coordinate model by Roy et al. (1999) by applying the nested grid technique. In addition, Sinha et al. (1984, 1997) formulated a numerical model to simulate storm surge and sea-level rise for the Indian coasts surrounding the Bay of Bengal and the Arabian Sea. Besides the aforementioned studies, numerical models by Ghosh et al. (1983), Qayyum (1983), Dube et al. (1985, 2004), Abrol (1987), Flather and Khandaker (1987), Katsura et al. (1992), Flather (1993), Flather et al. (1994), Henry et al. (1997), Roy et al. (2001), As-Salek and Yasuda (2001), Unnikrishnan et al., (2004), Paul et al. (2012a, b, 2013), Antony et al.(2014), Debsharma et al. (2014), Kay et al. (2015), and Rahman et al. (2015) are notable for simulating surges caused by severe tropical storms in the coastal region of Bangladesh. In particular, Flather (1994) introduced a numerical model for simulating and predicting tides and storm surges in regions that can have areas of the open sea along with estuarine channels and intertidal banks for the purpose of the model. It was implemented along

the northern shelf of the Bay of Bengal and the Ganges Delta which consists of the coast of Bangladesh ravaged by a cyclone-induced surge in April 1991. The events were reproduced by using forcing derived from a semi-analytical cyclone model with data supplied by the Joint Typhoon Warning Center (JTWC). The results revealed that the timing of cyclone landfall and its occurrence with high tide ascertain the area worst affected by inundation. The forecasting was based on a standard JTWC warning issued 12–18 hours ahead of the event. The predicted landfall was located accurately but its timing was about 5 hours late. As a result, the area with the highest water levels shifted north. Lastly, the model results for April 1991 cyclone were compared with those from a simulation of the November 1970 cyclone. Peak surges and water levels were similar in magnitude in the two events, but differences in track and tidal conditions are again shown to be important, producing flooding in a large area of the southern delta in 1970 but along the mainland coast south of Chittagong in 1991.

Ali (1997a) contributed to the discourse on tropical cyclones as being the most catastrophic disaster for countries along the rim of the Bay of Bengal with Bangladesh particularly suffering the most out of all the other countries. The study included the extent of devastation and the risk-prone aspects of Bangladesh as well as discussions on causes of natural disasters extending from strong winds, storm surge, rainfall, socioeconomic factor, etc. More importantly, Ali (1997b) studied the interaction among river discharge, storm surges, and tides in the Meghna river estuary in Bangladesh using a two-dimensional vertically integrated numerical model in the northern Bay of Bengal. River discharge and tidal flow across the river mouth have both positive and negative effects depending on the tidal phase, positively during tide and negatively during low tide. This is also true for the combination of all three forces. On the other hand, in most cases, river discharge acts in opposition to the storm surges. Under certain conditions and on rare

occasions, they act positively. The interactions between river discharge and storm surges, however, depend on their relative magnitudes with respect to total elevation in the estuarial region, river discharge tends to increase the surge level. However, away from the estuary, the effect of river discharge is hardly discernible. Some more studies on the tide and surge and their interaction include As-Salek (1997) delineating that negative surges destroyed coastal aquaculture installations and hindered rescue–evacuation operations during cyclones and storm surges in the Meghna estuary in Bangladesh. The impact of the cyclone characteristics hitting the Noakhali–Chittagong–Cox’s Bazar coast on the negative surges in the Meghna estuary was investigated. The negative surges in the Meghna estuary were found to have a duration of 4–6 h, occurring before the main surge. The study revealed that the negative surges in the region showed high sensitivity to the astronomical tides and to the propagation path of a cyclone. Based on the findings of the previous study As-Salek (1998) analyzed that depending on the characteristics of the atmospheric cyclone and the astronomical tide, storm surges can be trapped in the Meghna estuary and propagate like edge waves along the coastline causing widespread destruction. The literature found that the funneling effect of the narrowing estuary acts strongly on the pressure response and most strongly in the region north of Sandwip Island. The merging of both the coastal trapping and the funneling effect leads to the far-reaching nature of the surges in the Meghna estuary. The widespread nature of the surges is directly proportional to the wind inflow angle and to the radius of maximum cyclonic wind, however, it is inversely proportional to the angle of the crossing of the cyclone made with the coastline. The results showed that the cyclone hitting the Noakhali–Chittagong coast generates more widespread surges in comparison to a cyclone striking the Chittagong–Cox’s Bazar coast. A rapidly moving cyclone drives the surges toward the northern coast. If a cyclone strikes during the ebb tide phase, then nonlinear

tide–surge interaction also generates separate surges far to the west in the Khepupara region. Later in 2001, As-Salek used a numerical model of  $(1/120)^\circ$  resolution to show that overall the tide–surge interaction in the Meghna estuary has a progressive wave nature of the local tide. The study illustrated that as the peak of the maximum surge coincides with the tidal peak close to landfall, the surge propagates toward the north faster than when the surge peak coincides with the tidal trough. The study also showed that cyclones that make landfall before the arrival of the tidal peak generate higher but shorter duration surges than those that make landfall after the arrival of the tidal peak. On the other hand, if the landfall time of the cyclone is kept fixed, the surge peaks are found to arrive earlier with the increase in the propagation speed of the cyclone and with the decrease of the radius of the maximum cyclonic wind.

Some of the more recent significant studies on storm surge forecasting include Debsarma (2009) which used IIT Kharagpur Model (2002) for the simulations of storm surges in the Bay of Bengal region. In this work, three or six hourly positional data of numerous severe storms that hit the Orissa, West Bengal, and Bangladesh coasts have been used for creating gradual changes in the storm surge scenario. A Generic Mapping Tool (GMT) has been employed with a view to capture the image of surges and then there were calculations of the time series of storm surges due to the cyclone of April 29, 1991, at Chittagong; the cyclone of September 19, 1997, at Sandwip; and the Orissa super cyclone of October 29, 1999, at Paradeep. Lastly, a 3D view of the peak surges during landfall was done by including geo-referenced peak surge data into Windsurfer. The results obtained from the model were in close agreement with the reported data. Another notable modeling approach is IWM (2009) which examined 18 severe cyclones from the past 47 years (1960- 2007) that have affected the coastal region of Bangladesh. IWM used its storm surge model for hindcasting storm surge events and determined the surge level and the

likelihood of flooding in the areas of interest. The study succeeded in making an inundation risk map based on the maximum inundation depths of the past 18 cyclones and the results showed that the eastern coast sustains the most flooding within the range of 4-6 m and the western coast sustains flooding between 3-5 m. Only a few years prior to this work, Jakobsen (2006) simulated and examined 17 severe cyclones that have hit the coasts of Bangladesh in the last 40 years. The research compared simulated cyclone-induced storm surges with the observations and the results were found to be satisfactory. Jakobsen also carried out a statistical evaluation of the return period based surge level determined from simulated surge levels by considering the frequency distribution of the events that were accounted for in the study. Lastly, the analysis found that a storm surge of 10.6 m (PWD) has a return period of 652 years in the Northern Meghna Estuary. The simulated maximum surge level for the 1876 cyclone in Bangladesh was 12.5 m (PWD) which is in strong agreement with the observations. Likewise, the surge generated by the Bakerganj cyclone in 1876 was simulated by Shahadat (2000) and the model's maximum surge residual is in accordance with the information of BMD (Bangladesh Meteorological Department). The work's sensitivity analyses for 4 different conditions show that factors like wind speed and cyclonic time determine the surge level in comparison to cyclonic pressure which is deemed to be significantly less important. On top of such modeling efforts and analyses, other factors that contribute to the storm surge problem were also investigated in studies such as the work of Paul and Ismail (2012a) which explored the contributing factors of surge levels such as air bubbles on the coastal belt of Bangladesh. Afterward, based on these findings, Paul and Ismail (2012b) improved their previous model by interacting astronomical tide with surge nonlinearly. It is important to note that two important factors, namely river dynamics and inverse barometer were not part of the model, and only major islands were taken into account through a

stair-step representation. However, the Bangladeshi coast is populated with low lying small and big islands (Paul & Ismail, 2012a), and these islands along with Meghna river discharge can affect surge levels in this region, particularly along the Meghna estuarine area (Paul & Ismail, 2013; Paul et al. 2014), wherein the inverse barometer can have a significant contribution. Thus, as Lewis et al. (2014) states, it is essential to incorporate all factors that influence surge levels for accurate prediction of maximum water levels and therefore, for accurate estimation of coastal inundation disasters.

There have also been several 3D modeling works for studying storm surge forecasting such as research by Sinha et al. (1986) which compare the surge response via both the vertically integrated 2D model and the 3D model for the Bangladeshi coast. The results showed that the response was the same on both the models given that the bottom friction coefficient on vertically integrated 2D model is selected properly. This also leads to the conclusion that a vertically integrated 2D model is more than sufficient for estimating water levels of cyclonic surges due to simpler computation techniques.

## **2.6 The Cyclone 1991**

Cyclones in the Bay of Bengal region tend to occur in the April-May and October-December monsoon seasons. These cyclonic storms develop in the southern area of the bay or in the Andaman Sea and follow tracks towards north- northwest. Few of these storms head west and make landfall along the eastern part of the Indian coast (Andra Pradesh and Orisa regions). Many others head into the northeast part of the bay and strike the coastal region of Bangladesh. From 1900 onwards, 70 cyclones categorized as cyclonic storms or higher had landfalls along the coast of Bangladesh (SMRC, 1998). The classifications of storms are shown in more detail in Table

2.2. In the last century, four super cyclonic storms having wind speeds greater than 222 km/h have struck the country (May 1963, November 1970, April 1991, and May 1997) wherein the November 1970 and April 1991 cyclones have caused most losses in terms of casualties and economic damages. The time history of the April 1991 cyclone, also known as BOB 01, and some of its impacts have been further explored in this section for the purpose of this research.

**Table 2.2**

*Classification of low pressure systems for the Bay of Bengal region*

Class	Cyclonic disturbance	Maximum wind speed (km/h)	Radius (km)
D	Depression	31-51	26
DD	Deep depression	52-61	29
CS	Cyclonic storm	62-88	32
SCS	Severe cyclonic storm	89-118	38
SCSH	Severe cyclonic storm with hurricane intensity	119-221	44
SSCS	Super cyclonic storm	>222	44

*Note.* The table includes information about the different phases of a cyclonic storm, its associated radius to the maximum wind found in this project. Adapted from “Operational plan for the Bay of Bengal and the Arabian Sea,” by World Meteorological Organization, 2001, *World Meteorological Organization Progress Report TCP-21*. Copyright 2001 by WMO.

On 29 April 1991, a severe cyclone with wind speeds of over 24 km/h hit the coast of Bangladesh. The path of the eye reportedly raised a storm surge greater than 9 m above the mean sea level which caused massive destruction in offshore islands and along the coastal belt. The loss of lives and damage to property due to the cyclonic surge made it one of the world’s biggest natural hazards of the century. The cyclone caused almost 139,000 deaths which left almost equal number of people injured. The government has estimated the degree of damage due to the cyclone-induced surge at US\$ 1390 million. According to Khalil (1993), the cyclone was detected for the first time as a depression on 23rd April with wind speed not being more than 62 km/h in the satellite picture taken at the Space Research and Remote Sensing Organisation (SPARRSO) from NOAA-11 and GMS-4 satellites. At 0300 UTC (universal time coordinated) of 25th April, the depression was detected at 10.0°N latitude and 89.0°E longitude. On the same

day at 1200 UTC, it intensified into a deep depression near 11.5°N and 88.5°E, and later at 1800 UTC, the deep depression became a cyclonic storm. It was recorded to have maximum sustained wind speed between 65-87 km/h and a central pressure of 996 mb. This intensity continued till 0900 UTC of 27 April after which it developed into a severe cyclonic storm having wind velocity of 90-115 km/h and a central pressure of 990 mb. At 1800 UTC, the severe cyclonic storm was located at 14.5°N and 87.5°E. On 28th April at 0300 UTC, it became a storm with a hurricane core with wind speeds of more than 130 km/h near 15.5°N and 87.5°E. On this day, it headed in a north-easterly direction and traversed the coast north of Chittagong port at approximately 2000 UTC of 29 April, otherwise at around 0200 Bangladesh standard time on 30th April. According to observations, the maximum wind speed at Sandwip was 234 km/h and according to measurements by the Chittagong port authority of Bangladesh, the central pressure of the cyclone was about 938 mb. Talukder et al. (1992) estimated the maximum pressure drop as about 60 mb. Table 2.3 outlines the April 1991 cyclonic time history and Figure 1 depicts the cyclonic storm path in the Bay of Bengal.

On 29 April 1991, a severe cyclone with wind speeds of over 24 km/h hit the coast of Bangladesh. The path of the eye reportedly raised a storm surge greater than 9 m above the mean sea level which caused massive destruction in offshore islands and along the coastal belt. The loss of lives and damage to property due to the cyclonic surge made it one of the world's biggest natural hazards of the century. The cyclone caused almost 139,000 deaths which left almost equal number of people injured. The government has estimated the degree of damage due to the cyclone-induced surge at US\$ 1390 million. According to Khalil (1993), the cyclone was detected for the first time as a depression on 23rd April with wind speed not being more than 62 km/h in the satellite picture taken at the Space Research and Remote Sensing Organisation



(SPARRSO) from NOAA-11 and GMS-4 satellites. At 0300 UTC (universal time coordinated) of 25th April, the depression was detected at 10.0°N latitude and 89.0°E longitude. On the same day at 1200 UTC, it intensified into a deep depression near 11.5°N and 88.5°E, and later at 1800 UTC, the deep depression became a cyclonic storm. It was recorded to have maximum sustained wind speed between 65-87 km/h and a central pressure of 996 mb. This intensity continued till 0900 UTC of 27 April after which it developed into a severe cyclonic storm having wind velocity of 90-115 km/h and a central pressure of 990 mb. At 1800 UTC, the severe cyclonic storm was located at 14.5°N and 87.5°E. On 28th April at 0300 UTC, it became a storm with a hurricane core with wind speeds of more than 130 km/h near 15.5°N and 87.5°E. On this day, it headed in a north-easterly direction and traversed the coast north of Chittagong port at approximately 2000 UTC of 29th April, otherwise at around 0200 Bangladesh standard time on 30th April. According to observations, the maximum wind speed at Sandwip was 234 km/h and according to measurements by the Chittagong port authority of Bangladesh, the central pressure of the cyclone was about 938 mb. Talukder et al. (1992) estimated the maximum pressure drop of about 60 mb. Table 2 outlines the April 1991 cyclonic time history and Figure 1 depicts the cyclonic storm path in the Bay of Bengal.

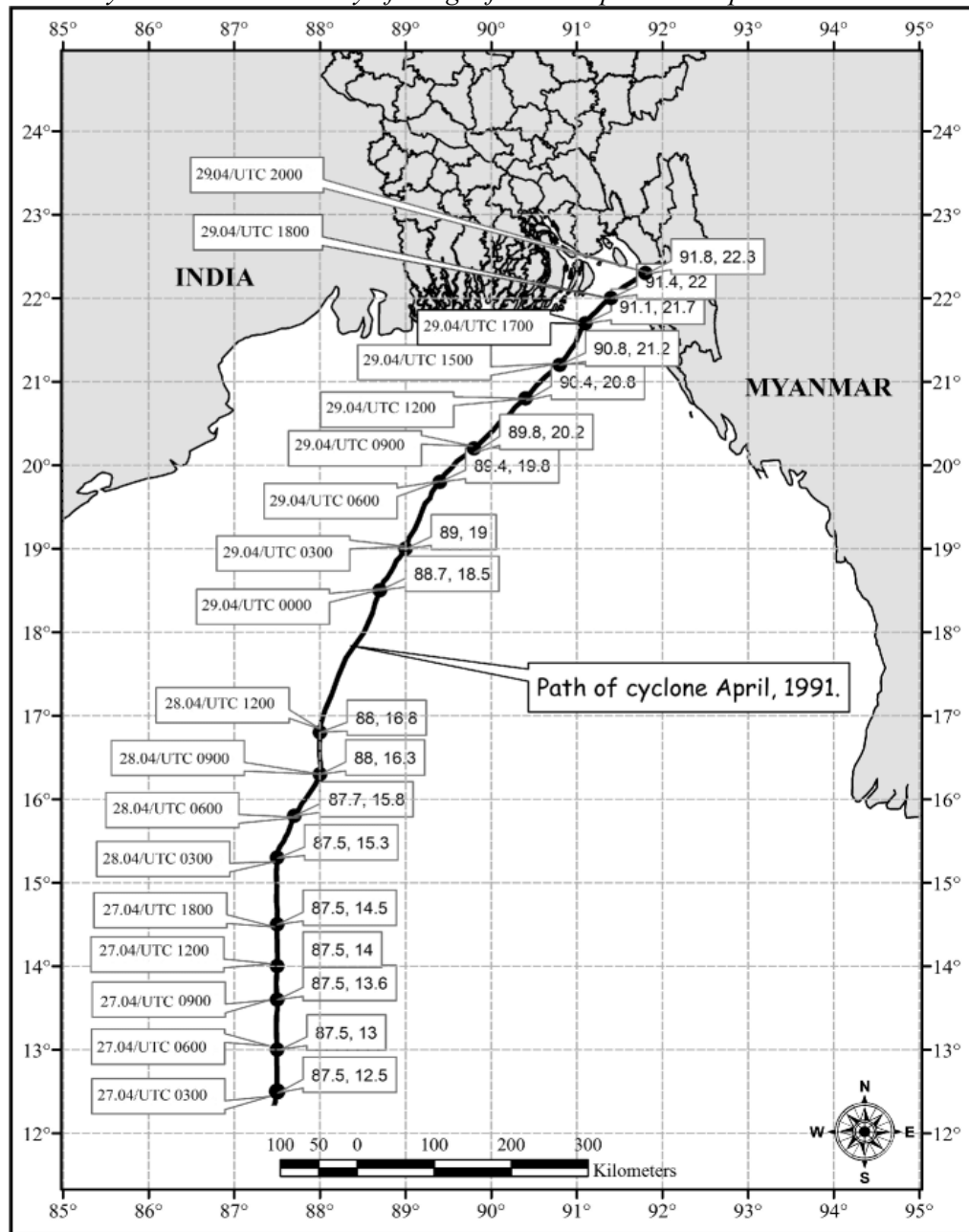
**Table 2.3.***Location of the cyclonic storm of April 1991 with central pressures and its nature*

Date (1991)	Hour (UTC)	Latitude (°N)	Longitude(°E)	Central pressure (mb)	Nature of the storm
25 April	0300	10.00	89.00		Depression
25 April	1200	11.50	88.50		Deep depression
25 April	1800	11.80	88.50	996.00	Cyclonic storm
26 April	1800	11.80	88.50	996.00	Cyclonic storm
27 April	0300	12.50	87.50	996.00	Cyclonic storm
27 April	0600	13.00	87.50	996.00	Cyclonic storm
27 April	0900	13.60	87.50	990.00	Severe cyclonic storm
27 April	1800	14.50	87.50	938.00	Severe cyclonic storm with hurricane core
28 April	0600	15.80	87.50	938.00	Severe cyclonic storm with hurricane core
28 April	0800	16.50	88.00	938.00	Severe cyclonic storm with hurricane core
28 April	1800	17.60	88.30	938.00	Severe cyclonic storm with hurricane core
29 April	0600	19.80	89.40	938.00	Severe cyclonic storm with hurricane core
29 April	1200	20.80	90.40	938.00	Severe cyclonic storm with hurricane core
29 April	1800	22.00	91.40	938.00	Severe cyclonic storm with hurricane core
29 April	2000	22.30	91.80	-	Severe cyclonic storm with hurricane core
				-	
30 April	Crossing the coast near Chittagong 0000	23.00	92.40		
				-	
	Crossed the Coast				
30 April	0200	23.50	92.80		

*Note.* From “Living with cyclone: Study on storm surge prediction and disaster preparedness,” by J.Talukder, 1992. Copyright 1992 by Community Development Library.

Figure 2.8

*Cyclone track in the Bay of Bengal from 25 April to 29 April 1991*



(Bangladesh Meteorological Department, n.d.)

### 2.6.1 Wind Speed and Surge Height

The winds observed in the 1991 cyclone were much stronger in comparison to winds from the November 1970 cyclone. According to Frank (1971), the maximum wind speed of the 1970 cyclone was about 185 km/h whereas the wind speed recorded for the 1991 cyclone exceeded even that. At Sandwip, the wind speed was measured to be around 225 km/h but due to the wind measuring device getting lost in the event, the maximum wind speed was significantly higher. The various wind speeds measured at different locations have been listed in Table 2.4.

Sevenhuysen (1991) reported that measurements by ships anchored outside the port of Chittagong showed that the central pressure of the 1991 cyclone was about 938 mb. Thus, a low pressure along with the full moon increased tidal levels to the highest of the normal range. This led to surge levels within the 4-9 m range at various locations, submerging areas in the districts of Noakhali, Bhola, Cox's Bazar, and Chittagong. The Chittagong Airport was submerged in at least 2m of water. The surge induced flood levels in different areas have been shown in Table 2.5.

**Table 2.4.**

*Maximum wind speed observed at different locations in the April 1991 cyclone*

Place	Maximum wind speed (km/h)
Sandwip	< 225
Chittagong	210
Khepupara	180
Kutubdia	180
Cox's Bazar	185
Bhola	178
Teknaf	157

*Note.* From "Cyclone '91: An Environmental and Perceptual Study," by R. Haider, A. A. Rahman, and S. Huq (Eds.), 1991. Copyright 1991 by Bangladesh Centre for Advanced Studies.

**Table 2.5***Estimated surge heights of April 1991 cyclone*

Upazila	Surge height (meters)
Anowara	6.06
Banshkhali	9.10
Bandar	6.06
Sanwip	6.00
Cox's Bazar	7.58
Moheshkhali	6.06
Kutubdia	6.06
Manpura	4.85
Hatiya	6.00

*Note.* From "The April disaster: Study on cyclone affected region in Bangladesh," by Community Development Library, 1992.

Given the aforementioned information, it can be seen that the cyclone was tracked in the Bay of Bengal for a number of days and warnings had been issued. Haque (1991) carried out a study based on a post-cyclone survey in two coastal communities of Bangladesh and found that a significant proportion of participants failed to take cyclone warnings seriously and thus, they did not try to take shelter. Even though BMD gave cyclone warnings for maritime ports, there was widespread confusion among the coastal population about the actual signal number of their respective localities. The vast majority of the coastal population are not well educated and lack awareness of the meaning of cyclone signals. Further inquiry revealed that most of the poverty-stricken coastal population do not also own a radio which happened to be one of the sources of information. Bangladesh Centre for Advanced Studies (1991) also emphasized that cyclone warnings were ignored as previously there had been analogous warnings issued and they were associated with almost normal water levels. The immense loss of life could have been reduced considerably if there had been accurate storm surge and flood forecasting and an effective warning procedure.

## **Chapter 3**

### **Theory and Methodology**

#### **3.1 Introduction**

This chapter examines the water level estimation due to the tide-surge interaction which includes the air bubble effects as well during a storm along the coastline of Bangladesh. To carry out this research, we look at storm surge equations such as vertically integrated shallow water equations (SWEs) in Cartesian coordinate system which are commonly applied in 2D modelling and are effective for accomplishing this study's objectives. The shallow water equations are solved using nested finite difference schemes. Furthermore, Chapter 2 explores the relevant bottom and surface conditions along with the generation of the wind field and the necessary boundary conditions. The radiation type of boundary condition is considered here for the open-sea boundary in the Bay of Bengal region as it allows the disturbance produced within the model domain to go out through the open boundary.

#### **3.2 Mathematical Formulation of the Storm Surge Equations**

##### **3.2.1 Shallow water equations**

There have been extensive implementation of depth-integrated hydrodynamic models in simulating sea level heights and currents on continental shelves because of astronomical forcing and storm surges. One of the more commonly used numerical methods in depth-integrated hydrodynamic models is based on the shallow water equations (SWEs). These equations are a set of parabolic/hyperbolic partial differential equations (PDEs) which can help to model the fluid flow in the oceans, rivers, estuaries, and coastal areas. They are derived from the Navier Stokes

equations which describe the motion of fluids. The Navier Stokes equations are derived from the physical conservation laws for mass and linear momentum. They also work for problems where shallow water flow in the vertical dimension is comparatively smaller than the horizontal scale; in these problems they work by carrying out depth averaging to get rid of the vertical dimension (Bresch and Nobel, 2007; Falconer, 1993). Despite shallow water flows being 3D in nature, the aforementioned assumptions enable simplifications to be carried out through integration of the horizontal velocity over the vertical direction to get a representative depth-averaged velocity flow field. The 2D shallow water equations includes the depth-averaged continuity equation and the x- and y-momentum equations which will be described in this section as well. The shallow water equations have been used in tsunami forecasting, atmospheric flows, storm surges and even planetary flows.

As previously mentioned, the primary assumption of shallow water theory is that horizontal scales (wavelength) are much larger than vertical scales (water depth) so it has also been established that the  $z$  component of the momentum equation can be approximated by the hydrostatic equation given below.

$$\frac{\partial \rho}{\partial z} = -\rho(1 - C(z))g \quad (3.1)$$

In addition, if the variation of density is negligible everywhere then the continuity equation reduces to the nondivergence of velocity. Considering these approximations and neglecting the molecular velocity, the basic shallow water equations for fluid motion in the sea in a right-handed Cartesian coordinate system can be stated as (Paul and Ismail, 2012a):

$$\frac{\partial u}{\partial t} + u \frac{\partial u}{\partial x} + v \frac{\partial u}{\partial y} + w \frac{\partial u}{\partial z} - fv = -\frac{1}{\rho} \frac{\partial p}{\partial x}, \quad (3.2)$$

$$\frac{\partial v}{\partial t} + u \frac{\partial v}{\partial x} + v \frac{\partial v}{\partial y} + w \frac{\partial v}{\partial z} + fu = -\frac{1}{\rho} \frac{\partial p}{\partial y}, \quad (3.3)$$

$$\frac{\partial p}{\partial z} = -\rho g, \quad (3.4)$$

$$\frac{\partial u}{\partial x} + \frac{\partial v}{\partial y} + \frac{\partial w}{\partial z} = 0, \quad (3.5)$$

In these set of equations,  $u$  and  $v$  are the Reynolds averaged components of velocity in the directions of  $x$  and  $y$ ,  $f=2\Omega \sin \phi$  is the Coriolis parameter with  $\Omega$  being the angular speed of the earth rotation and  $\phi$  being the latitude of the area of interest,  $g$  is the acceleration due to gravity,  $\rho$  is the density of the sea water which is taken to be homogenous and incompressible. Equation (3.5) is the continuity equation and it can be used to express (3.3) and (3.4), respectively, in the following manner:

$$\frac{\partial u}{\partial t} + u \frac{\partial u}{\partial x} + v \frac{\partial u}{\partial y} + w \frac{\partial u}{\partial z} - fv = -\frac{1}{\rho} \frac{\partial p}{\partial x}$$

$$\text{or, } \frac{\partial u}{\partial t} + \frac{\partial}{\partial x}(uu) + \frac{\partial}{\partial y}(uv) + \frac{\partial}{\partial z}(uw) - u \frac{\partial u}{\partial x} - u \frac{\partial v}{\partial y} - u \frac{\partial w}{\partial z} - fv = -\frac{1}{\rho} \frac{\partial p}{\partial x}$$

$$\text{or, } \frac{\partial u}{\partial t} + \frac{\partial}{\partial x}(uu) + \frac{\partial}{\partial y}(uv) + \frac{\partial}{\partial z}(uw) - u \left( \frac{\partial u}{\partial x} + \frac{\partial v}{\partial y} + \frac{\partial w}{\partial z} \right) - fv = -\frac{1}{\rho} \frac{\partial p}{\partial x}$$

$$\text{or, } \frac{\partial u}{\partial t} + \frac{\partial}{\partial x}(uu) + \frac{\partial}{\partial y}(uv) + \frac{\partial}{\partial z}(uw) - fv = -\frac{1}{\rho} \frac{\partial p}{\partial x}. \quad (3.6)$$



Likewise,

$$\frac{\partial u}{\partial t} + \frac{\partial}{\partial x}(vu) + \frac{\partial}{\partial y}(v'v) + \frac{\partial}{\partial z}(v'w) + fu = -\frac{1}{\rho} \frac{\partial p}{\partial y} . \quad (3.7)$$

The instantaneous velocity component also undergoes the following substitutions:

$$u = \langle u \rangle + u'$$

$$v = \langle v \rangle + v'$$

$$w = \langle w \rangle + w'$$

where  $\langle u \rangle$  is the mean velocity and is the average in time at a given point. Meanwhile,  $u'$  is for deviation from the mean velocity at any given time. It should also be taken into account that  $\langle u' \rangle = \langle v' \rangle = \langle w' \rangle = 0$ . If we leave out the minor variations in density in regards to turbulence then the equations can be averaged in time to get a simple partition of the flow between the mean flow and turbulent fields. For instance, the average of  $uw$  can be expressed as:

$$\langle uw \rangle = \langle (\langle u \rangle + u')(\langle w \rangle + w') \rangle = \langle u \rangle \langle w \rangle + \langle u'w' \rangle , \quad (3.8)$$

It can be observed that terms like  $\langle \langle u \rangle w' \rangle$  and  $\langle u' \langle w \rangle \rangle$  disappear as  $\langle u \rangle$  and  $\langle w \rangle$  are constants over the averaging interval. If Equation (3.5) undergoes this averaging process then the resultant equation is:

$$\frac{\partial \langle u \rangle}{\partial x} + \frac{\partial \langle v \rangle}{\partial y} + \frac{\partial \langle w \rangle}{\partial z} = 0 . \quad (3.9)$$

Similarly, if this averaging process is applied to Equation (3.6), then the results are:

$$\begin{aligned}
& \frac{\partial \langle u \rangle}{\partial t} + \frac{\partial}{\partial x} \langle (uu) \rangle + \frac{\partial}{\partial y} \langle (uv) \rangle + \frac{\partial}{\partial z} \langle (uw) \rangle - f \langle v \rangle = -\frac{1}{\rho} \frac{\partial \langle p \rangle}{\partial x} \\
\text{or, } & \frac{\partial \langle u \rangle}{\partial t} + \frac{\partial}{\partial x} \langle ((u+u')(u+u')) \rangle + \frac{\partial}{\partial y} \langle ((u+u')(v+v')) \rangle \\
& + \frac{\partial}{\partial z} \langle ((u+u')(w+w')) \rangle = f \langle v \rangle - \frac{1}{\rho} \frac{\partial \langle p \rangle}{\partial x} \\
\text{or, } & \frac{\partial \langle u \rangle}{\partial t} + \frac{\partial}{\partial x} (\langle u \rangle \langle u \rangle + \langle u' \rangle \langle u' \rangle) + \frac{\partial}{\partial y} (\langle u \rangle \langle v \rangle + \langle u' \rangle \langle v' \rangle) + \frac{\partial}{\partial z} (\langle u \rangle \langle w \rangle + \langle u' \rangle \langle w' \rangle) \\
& = f \langle v \rangle - \frac{1}{\rho} \frac{\partial \langle p \rangle}{\partial x} \\
\text{or, } & \frac{\partial \langle u \rangle}{\partial t} + 2 \langle u \rangle \frac{\partial \langle u \rangle}{\partial x} + \langle u \rangle \frac{\partial \langle v \rangle}{\partial y} + \langle v \rangle \frac{\partial \langle u \rangle}{\partial y} + \langle u \rangle \frac{\partial \langle w \rangle}{\partial z} + \langle w \rangle \frac{\partial \langle u \rangle}{\partial z} + \frac{\partial}{\partial x} (\langle u' u' \rangle) \\
& + \frac{\partial}{\partial y} (\langle u' v' \rangle) + \frac{\partial}{\partial z} (\langle u' w' \rangle) = f \langle v \rangle - \frac{1}{\rho} \frac{\partial \langle p \rangle}{\partial x} \\
\text{or, } & \frac{\partial \langle u \rangle}{\partial t} + \langle u \rangle \frac{\partial \langle u \rangle}{\partial x} + \langle v \rangle \frac{\partial \langle u \rangle}{\partial y} + \langle w \rangle \frac{\partial \langle u \rangle}{\partial z} = f \langle v \rangle - \frac{1}{\rho} \frac{\partial \langle p \rangle}{\partial x} \\
& - \left( \frac{\partial}{\partial x} \langle u' u' \rangle + \frac{\partial}{\partial y} \langle u' v' \rangle + \frac{\partial}{\partial z} \langle u' w' \rangle \right) - \langle u \rangle \left( \frac{\partial \langle u \rangle}{\partial x} + \frac{\partial \langle v \rangle}{\partial y} + \frac{\partial \langle w \rangle}{\partial z} \right).
\end{aligned}$$

Then Equation (3.9) is applied to give:

$$\begin{aligned}
& \frac{\partial \langle u \rangle}{\partial t} + \langle u \rangle \frac{\partial \langle u \rangle}{\partial x} + \langle v \rangle \frac{\partial \langle u \rangle}{\partial y} + \langle w \rangle \frac{\partial \langle u \rangle}{\partial z} = f \langle v \rangle - \frac{1}{\rho} \frac{\partial \langle p \rangle}{\partial x} \\
& - \left( \frac{\partial}{\partial x} \langle u' u' \rangle + \frac{\partial}{\partial y} \langle u' v' \rangle + \frac{\partial}{\partial z} \langle u' w' \rangle \right).
\end{aligned} \tag{3.10}$$

Likewise, using Equation (3.9) to change Equation (3.7) to:

$$\begin{aligned}
& \frac{\partial \langle v \rangle}{\partial t} + \langle u \rangle \frac{\partial \langle v \rangle}{\partial x} + \langle v \rangle \frac{\partial \langle v \rangle}{\partial y} + \langle w \rangle \frac{\partial \langle v \rangle}{\partial z} = f \langle v \rangle - \frac{1}{\rho} \frac{\partial \langle p \rangle}{\partial y} \\
& - \left( \frac{\partial}{\partial x} \langle u' v' \rangle + \frac{\partial}{\partial y} \langle v' v' \rangle + \frac{\partial}{\partial z} \langle v' w' \rangle \right).
\end{aligned} \tag{3.11}$$

Thus, the averaged continuity and momentum equations are:

$$\frac{\partial \langle u \rangle}{\partial x} + \frac{\partial \langle v \rangle}{\partial y} + \frac{\partial \langle w \rangle}{\partial z} = 0, \quad (3.9)$$

$$\begin{aligned} \frac{\partial \langle u \rangle}{\partial t} + \langle u \rangle \frac{\partial \langle u \rangle}{\partial x} + \langle v \rangle \frac{\partial \langle u \rangle}{\partial y} + \langle w \rangle \frac{\partial \langle u \rangle}{\partial z} = f \langle v \rangle - \frac{1}{\rho} \frac{\partial \langle p \rangle}{\partial x} \\ - \left( \frac{\partial}{\partial x} \langle u'u' \rangle + \frac{\partial}{\partial y} \langle u'v' \rangle + \frac{\partial}{\partial z} \langle u'w' \rangle \right), \end{aligned} \quad (3.10)$$

$$\begin{aligned} \frac{\partial \langle v \rangle}{\partial t} + \langle u \rangle \frac{\partial \langle v \rangle}{\partial x} + \langle v \rangle \frac{\partial \langle v \rangle}{\partial y} + \langle w \rangle \frac{\partial \langle v \rangle}{\partial z} + f \langle v \rangle = -\frac{1}{\rho} \frac{\partial \langle p \rangle}{\partial y} \\ - \left( \frac{\partial}{\partial x} \langle u'v' \rangle + \frac{\partial}{\partial y} \langle v'v' \rangle + \frac{\partial}{\partial z} \langle v'w' \rangle \right). \end{aligned} \quad (3.11)$$

The terms in the brackets on the RHS of Equations (3.13) and (3.14) are known as the eddy stress terms which rely on turbulent functions. According to Prandtl's mixing length theory, these eddy terms are parameterized by expressing them as mean field variables under the hypothesis that the eddy stress is proportional to the gradient of the mean velocity. Moreover, it is important to take into consideration that eddy stresses are much larger than the horizontal gradients and thus, only the vertical gradients can be retained. Therefore, the eddy stress terms  $\langle u'w' \rangle$  and  $\langle v'w' \rangle$  can be written as

$$\begin{aligned} -\rho \langle u'w' \rangle &= \rho A_z \frac{\partial \langle u \rangle}{\partial z} = \tau_x \\ -\rho \langle v'w' \rangle &= \rho A_z \frac{\partial \langle v \rangle}{\partial z} = \tau_y \end{aligned} \quad (3.12)$$

given that  $A_z$  is the eddy exchange coefficient.

Leaving out the brackets for practicality purposes, Equation (3.12) is used to express Equations (3.9)-(3.11) as the basic shallow water equations with averaged velocity components:

$$\frac{\partial u}{\partial x} + \frac{\partial v}{\partial y} + \frac{\partial w}{\partial z} = 0, \quad (3.13)$$

$$\frac{\partial u}{\partial t} + u \frac{\partial u}{\partial x} + v \frac{\partial u}{\partial y} + w \frac{\partial u}{\partial z} - fv = -\frac{1}{\rho} \frac{\partial p}{\partial x} + \frac{1}{\rho} \frac{\partial \tau_x}{\partial z}, \quad (3.14)$$

$$\frac{\partial v}{\partial t} + u \frac{\partial v}{\partial x} + v \frac{\partial v}{\partial y} + w \frac{\partial v}{\partial z} + fu = -\frac{1}{\rho} \frac{\partial p}{\partial y} + \frac{1}{\rho} \frac{\partial \tau_y}{\partial z}. \quad (3.15)$$

where,

$u, v, w$  = Reynold's averaged components of velocity in the  $x, y,$  and  $z$  direction respectively

$t$  = time,

$p$  = pressure,

$\rho$  = density of the seawater assumed to be homogenous and incompressible,

$f$  = Coriolis parameter (as previously mentioned,  $f = 2\Omega \sin \varphi$ ),

$g$  = acceleration due to gravity,

$\tau_x, \tau_y$  =  $x$  and  $y$  components of the fictional stress (Reynolds stress)

### 3.2.2 Water level rise due to air bubble entrainment

During stormy periods, wave breaking along with excessive air bubble entrainment takes place in shallow water regions of the sea (Chanson et al., 2006). The breaking waves produces a disturbance in the air-sea interface by creating a two-phase layer such as the water having air-bubbles and air containing sea-spray droplets (Soloviev and Lukas, 2010). According to Kraus and Businger (1994), this means that the bubbles and spray droplets raise the sea surface area giving rise to a mixed-phase environment that alters the dynamics along with the thermodynamics of the air-sea interaction. In a research on increase in water level due to air bubble entrainment in the surf zone, the results showed that the entrapment of air bubbles leads

to a wave set up that raises water level (Hoque, 2008). Following Hoque and Aoki (2006), the water level rise  $\Delta h$  due to entrained air bubbles above the still water depth can be represented as

$$\Delta h = \int_{h-\Delta h}^0 C(z) dz \quad (3.16)$$

where  $z$  is the vertical elevation positive upwards with  $z = 0$  at the mean surface and  $C(z)$  stands for the time averaged concentration or in more simple terms, it is the vertical distribution of bubble population. The latter idea was first put forward by Wu (1981) where the distribution is represented as

$$C(z) = C_0 \exp(k_1 z) \quad (3.17)$$

$C_0$  is the reference concentration or reference void fraction at the mean water surface  $z = 0$  and  $k_1$  is a decay parameter which indicates the vertical distribution of air bubbles. Following Hoque and Aoki (2006), the latter term can be expressed as

$$k_0 = k_1 \zeta \quad (3.18)$$

In Equation (3.18),  $k_0$  denotes a dimensionless parameter and  $\zeta$  is the local wave height. Then the boundary conditions mentioned below are satisfied when

$$\begin{aligned} C(z) &= C_0 \text{ at the surface } z = 0 \text{ and} \\ C(z) &\rightarrow 0, \text{ for } z \rightarrow -\infty \end{aligned} \quad (3.19)$$

Integration of Equation (3.16) gives

$$\begin{aligned}\Delta h &= \frac{C_0}{k_1} [1 - \exp(-k_1 h - k_1 \Delta h)] \\ &= \frac{C_0}{k} [1 - \exp(-k_1 h) (1 - k_1 \Delta h + O((\Delta h)^2))],\end{aligned}$$

which can be simplified to

$$\Delta h = \frac{C_0}{k} \frac{1 - e^{-k_1 h}}{1 - C_0 e^{-k_1 h}} \quad (3.20)$$

Furthermore, following Hoque and Aoki (2006), simplifications are done in averaged horizontal and vertical velocities, pressure, and density to account for the effect of air bubble entrainment where

$$u = u_w$$

$$v = v_w$$

$$w = w_w + C w_r$$

$$\rho = (1 - C) \rho_w \quad (3.21)$$

The subscript ‘w’ in Equation (3.21) represents water and  $w_r$  is the rising velocity of an air bubble. It is also noteworthy that in times of severe weather events such as tropical storms, the horizontal and vertical velocity fields of the water do not undergo any considerable changes because of air bubble entrainment. However, the density of the air-water mixture in the surface zone becomes much lighter than the water below it. The term  $\rho$  is the density of the air-water mixture,  $\rho_w$  is the density of water and the overall formula has been referred from the study by Hoque and Aoki (2005b) which investigated energy dissipation induced by entrained air bubbles.

$$w = w_w + w_c \quad (3.22)$$

In Equation (3.22),  $w_c$  is the correction term. On top of all the simplifications done so far, finally we have the following set of hydrodynamic equations which also take entrained air bubbles into consideration.

$$\frac{\partial u_w}{\partial x} + \frac{\partial v_w}{\partial y} + \frac{\partial w_w}{\partial z} = 0, \quad (3.23)$$

$$\begin{aligned} \frac{\partial u_w}{\partial t} + u_w \frac{\partial u_w}{\partial x} + v_w \frac{\partial u_w}{\partial y} + w_w \frac{\partial u_w}{\partial z} - f v_w \\ = -\frac{1}{\rho_w(1-C)} \left( \frac{\partial p_w}{\partial x} - \frac{\partial \tau_x}{\partial z} \right), \end{aligned} \quad (3.24)$$

$$\begin{aligned} \frac{\partial v_w}{\partial t} + u_w \frac{\partial v_w}{\partial x} + v_w \frac{\partial v_w}{\partial y} + w_w \frac{\partial v_w}{\partial z} + f u_w \\ = -\frac{1}{\rho_w(1-C)} \left( \frac{\partial p_w}{\partial y} - \frac{\partial \tau_y}{\partial z} \right), \end{aligned} \quad (3.25)$$

The correction term  $w_c$  from Equation (3.22) satisfies the following equation

$$\frac{\partial w_c}{\partial z} - \frac{C_0 k_1 e^{k_1 z}}{1 - C_0 e^{k_1 z}} w_c = \frac{C_0 k_1 e^{k_1 z}}{1 - C_0 e^{k_1 z}} w_w, \quad (3.26)$$

which is subject to the condition that  $w_c \rightarrow 0$  as  $z \rightarrow -h$ .

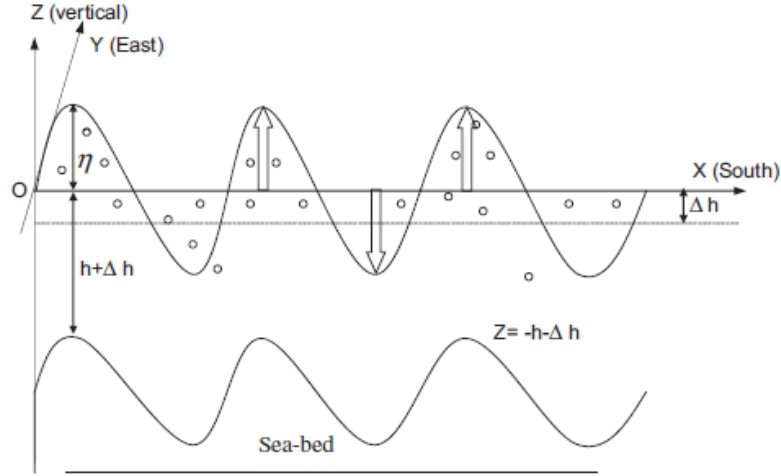
### 3.2.3 Vertically integrated equations

In the process of deriving vertically integrated equations, a system of rectangular Cartesian coordinates is used in which the origin,  $O$ , is in the equilibrium level of the sea surface that acts as the  $xy$  plane.  $O_x$  is directed towards the south,  $O_y$  towards the east, and  $O_z$  points vertically upwards (see Figure 3). The displaced position of the free surface is written as  $z = \xi(x, y, t)$  and

the position of the sea floor is represented by  $z = -h - \Delta h$ . Thus, the total water depth is  $H = h + \Delta h + \zeta$  in which  $\Delta h$  is given by Equation (3.20).

**Figure 3.1**

*Storm surge coordinate system diagram*



*Note.* From “Numerical modeling of storm surges with air bubble effects along the coast of Bangladesh,” by G. C. Paul, and A. I. M. Ismail (2012a). *Ocean Engineering*, 42, 188-194. Copyright 2012 by Elsevier Ltd.

During tropical storms, the upper surface is produced by the circulatory wind of the storm and the bottom stress functions as the dissipation term, also known as bottom friction. The bottom stress and wind stress components are  $(T_x, T_y)$  and  $(F_x, F_y)$ , respectively and the surface pressure is  $P_a$ . The terms  $\tau_x$  and  $\tau_y$  are taken into account to represent vertical turbulent diffusion. Molecular viscosity has been left out in these equations. According to Debsarma (2009), the bottom and surface conditions become,

$$(\tau_x, \tau_y) = (F_x, F_y) \text{ and } u = v = w = 0 \text{ at } z = -h(x, y) - \Delta h, \quad (3.27)$$

$$(\tau_x, \tau_y) = (T_x, T_y), \quad P = P_a, \quad w_w = \frac{\partial \zeta}{\partial t} + u \frac{\partial \zeta}{\partial x} + v \frac{\partial \zeta}{\partial y} \text{ at } z = \zeta(x, y, t) \quad (3.28)$$



The latter condition is the kinematic surface condition and it shows that the free surface is materially following the fluid.

It is also worth highlighting that integrating Equation (3.1) gives

$$\rho = \rho_{atmos} + \rho_w(1 - C)g(\zeta - z) \quad (3.29)$$

The whole process of solving the basic shallow water equations (3.13) - (3.15) is very tedious due to the presence of the vertical coordinate. In contrast to problems regarding the atmosphere, there is a requirement to set up a boundary layer both at the top and the bottom of the domain of integration. However, there is inadequate information available concerning the flow in such boundary layers. To overcome this problem, the best method is to vertically integrate the governing equations. The unknown dependent variables are then (a) the water transport (or mean current) and (b) the surface height. This is a commonly used technique for storm surge computations as the water level is of the utmost priority. The following section discusses the method of integrating each term of the set of hydrodynamic equations (3.13) - (3.15) in the vertical from  $z = -h(x,y)$  to  $z = \zeta(x,y,t)$  and using the bottom and surface conditions stated in Equations (3.27) and (3.28).

Besides the boundary conditions, other tools used are Leibnitz integration rule as stated below

$$\frac{\partial}{\partial x} \int_{-h}^{\zeta} u \, dz = \int_{-h}^{\zeta} \frac{\partial u}{\partial x} \, dz + u \Big|_{\zeta} \frac{\partial \zeta}{\partial x} - u \Big|_{-h} \frac{\partial}{\partial x} (-h).$$

To gain an understanding of what is happening, details of the integration process has been included for Equation (3.10) only.

If the first term is vertically integrated

$$\int_{-h}^{\xi} \frac{\partial u}{\partial x} dz = \frac{\partial}{\partial x} \int_{-h}^{\xi} u dz - u \Big|_{\xi}^{\xi} \frac{\partial \xi}{\partial x} + u \Big|_{-h} \frac{\partial}{\partial x} (-h).$$

But  $u \Big|_{-h} = 0$  and hence

$$\int_{-h}^{\xi} \frac{\partial u}{\partial x} dz = \frac{\partial}{\partial x} \int_{-h}^{\xi} u dz - u \Big|_{\xi} \frac{\partial \xi}{\partial x}. \quad (3.30)$$

Likewise,

$$\int_{-h}^{\xi} \frac{\partial v}{\partial y} dz = \frac{\partial}{\partial y} \int_{-h}^{\xi} v dz - v \Big|_{\xi} \frac{\partial \xi}{\partial y}. \quad (3.31)$$

$$\text{And } \int_{-h}^{\xi} \frac{\partial w}{\partial z} dz = \int_{-h}^{\xi} dw = w \Big|_{-h}^{\xi} = w \Big|_{\xi} - w \Big|_{-h} = \frac{\partial \xi}{\partial t} + u \Big|_{\xi} \frac{\partial \xi}{\partial x} + v \Big|_{\xi} \frac{\partial \xi}{\partial y} \quad (3.32)$$

Then Equation (3.13) is integrated over depth by using Equations (3.30) - (3.32), we get

$$\frac{\partial \xi}{\partial t} + \frac{\partial}{\partial x} \int_{-h}^{\xi} u dz + \frac{\partial}{\partial y} \int_{-h}^{\xi} v dz = 0.$$

If we set  $\bar{u} = \frac{1}{\xi + h} \int_{-h}^{\xi} u dz$  and  $\bar{v} = \frac{1}{\xi + h} \int_{-h}^{\xi} v dz$ , the aforementioned equation is reduced to the following

$$\frac{\partial \xi}{\partial t} + \frac{\partial}{\partial x} [(\xi + h)\bar{u}] + \frac{\partial}{\partial y} [(\xi + h)\bar{v}] = 0. \quad (3.33)$$

Accordingly, Equation (3.10) can be expressed in the following manner

$$\frac{\partial u}{\partial t} + u \frac{\partial u}{\partial x} + v \frac{\partial u}{\partial y} + w \frac{\partial u}{\partial z} - f'v + u \left( \frac{\partial u}{\partial x} + \frac{\partial u}{\partial y} + \frac{\partial u}{\partial z} \right) = -\frac{1}{\rho} \frac{\partial p}{\partial x} + \frac{1}{\rho} \frac{\partial \tau_x}{\partial z}$$

$$\text{or, } \frac{\partial u}{\partial t} + 2u \frac{\partial u}{\partial x} + \left( v \frac{\partial u}{\partial y} + u \frac{\partial v}{\partial y} \right) + \left( w \frac{\partial u}{\partial z} + u \frac{\partial w}{\partial z} \right) - f'v = -\frac{1}{\rho} \frac{\partial p}{\partial x} + \frac{1}{\rho} \frac{\partial \tau_x}{\partial z}$$

$$\text{or, } \frac{\partial u}{\partial t} + \frac{\partial}{\partial x} (u^2) + \frac{\partial}{\partial y} (uv) + \frac{\partial}{\partial z} (uw) - f'v = -\frac{1}{\rho} \frac{\partial p}{\partial x} + \frac{1}{\rho} \frac{\partial \tau_x}{\partial z}. \quad (3.34)$$

Then the result of integrating each term of Equation (3.14) is the same as integrating each term of Equation (3.34). Thus, integration of each term of Equation (3.34) gives

$$\int_{-h}^{\xi} \frac{\partial u}{\partial t} dz = \frac{\partial}{\partial t} \int_{-h}^{\xi} u dz - u \Big|_{z=\xi} \frac{\partial \xi}{\partial t} + u \Big|_{z=-h} \frac{\partial}{\partial t} (-h) = \frac{\partial}{\partial t} \int_{-h}^{\xi} u dz - u \Big|_{z=\xi} \frac{\partial \xi}{\partial t},$$

$$\int_{-h}^{\xi} \frac{\partial}{\partial x} (u^2) dz = \frac{\partial}{\partial x} \int_{-h}^{\xi} u^2 dz - u^2 \Big|_{z=\xi} \frac{\partial \xi}{\partial x} + u^2 \Big|_{z=-h} \frac{\partial}{\partial x} (-h)$$

or,  $\int_{-h}^{\xi} \frac{\partial}{\partial x} (u^2) dz = \frac{\partial}{\partial x} \int_{-h}^{\xi} u^2 dz - u^2 \Big|_{z=\xi} \frac{\partial \xi}{\partial x} - u^2 \Big|_{z=-h} \frac{\partial h}{\partial x},$

$$\int_{-h}^{\xi} \frac{\partial}{\partial y} (uv) dz = \frac{\partial}{\partial y} \int_{-h}^{\xi} uv dz - (uv) \Big|_{z=\xi} \frac{\partial \xi}{\partial y} + (uv) \Big|_{z=-h} \frac{\partial}{\partial y} (-h)$$

or,  $\int_{-h}^{\xi} \frac{\partial}{\partial y} (uv) dz = \frac{\partial}{\partial y} \int_{-h}^{\xi} uv dz - (uv) \Big|_{z=\xi} \frac{\partial \xi}{\partial y} - (uv) \Big|_{z=-h} \frac{\partial h}{\partial y}.$

Then once again,

$$\int_{-h}^{\xi} \frac{\partial}{\partial z} (uv) dz = -(uv) \Big|_{z=\xi} - (uv) \Big|_{z=-h}$$

Then we carry out vertical integration for each term of the hydrostatic equation  $\frac{\partial p}{\partial z} = -\rho g$  where  $\rho$  is taken to be independent of  $z$ ,

$$\int_P^{P_a} \frac{\partial p}{\partial z} dz = -\rho g \int_z^{\xi} dz$$

$$\text{or, } P_a - P = -\rho g (\xi - z)$$

$$\text{or, } P = P_a + \rho g (\xi - z)$$

Thus we get,  $\int_{-h}^{\xi} \frac{\partial P}{\partial x} dz = \frac{1}{\rho} \frac{\partial P_a}{\partial x} \int_{-h}^{\xi} dz = \frac{1}{\rho} \frac{\partial P_a}{\partial x} [\xi + h]$

Hence, if we integrate each term of Equation (3.14)

$$\frac{\partial}{\partial t} \int_{-h}^{\xi} u dz - u \Big|_{z=\xi} \frac{\partial \xi}{\partial t} + \frac{\partial}{\partial x} \int_{-h}^{\xi} u^2 dz - u^2 \Big|_{z=\xi} \frac{\partial \xi}{\partial x} - u^2 \Big|_{z=-h} \frac{\partial h}{\partial x} + \frac{\partial}{\partial y} \int_{-h}^{\xi} uv dz - uv \Big|_{z=\xi} \frac{\partial \xi}{\partial x} - uv \Big|_{z=-h} \frac{\partial h}{\partial x}$$

$$+ uv \Big|_{z=\xi} - uv \Big|_{z=-h} - f \int_{-h}^{\xi} v dz = -\frac{1}{\rho} \frac{\partial P_a}{\partial x} (\xi + h) + \frac{1}{\rho} (T_x - F_x).$$

Defining  $\frac{1}{\xi+h} \int_{-h}^{\xi} u dz = U$ ,  $\frac{1}{\xi+h} \int_{-h}^{\xi} u^2 dz = U^2$  we get

$$\begin{aligned} & \frac{\partial}{\partial t} [U(\xi+h)] + \frac{\partial}{\partial x} [U^2(\xi+h)] + \frac{\partial}{\partial y} [UV(\xi+h)] - u \left[ u \frac{\partial \xi}{\partial x} + v \frac{\partial \xi}{\partial y} - w \right] - u \left[ u \frac{\partial h}{\partial x} + v \frac{\partial h}{\partial y} - w \right] \\ & - u \frac{\partial \xi}{\partial t} = fV(\xi+h) - \frac{1}{\rho} \frac{\partial P_a}{\partial x}(\xi+h) + \frac{1}{\rho} (T_x - F_x) \\ \text{or, } & \frac{\partial}{\partial t} [U(\xi+h)] + \frac{\partial}{\partial x} [U^2(\xi+h)] + \frac{\partial}{\partial y} [UV(\xi+h)] + u \frac{\partial \xi}{\partial t} + u \frac{\partial h}{\partial t} - u \frac{\partial \xi}{\partial t} \\ & = fV(\xi+h) - \frac{1}{\rho} \frac{\partial P_a}{\partial x}(\xi+h) + \frac{1}{\rho} (T_x - F_x) \\ \text{or, } & \frac{\partial}{\partial t} [U(\xi+h)] + \frac{\partial}{\partial x} [U^2(\xi+h)] + \frac{\partial}{\partial y} [UV(\xi+h)] = fV(\xi+h) - \frac{1}{\rho} \frac{\partial P_a}{\partial x}(\xi+h) + \frac{1}{\rho} (T_x - F_x) \end{aligned} \quad (3.35)$$

Similarly, from Equation (3.15)

$$\frac{\partial}{\partial t} [V(\xi+h)] + \frac{\partial}{\partial x} [UV(\xi+h)] + \frac{\partial}{\partial y} [V^2(\xi+h)] = -fU(\xi+h) - \frac{1}{\rho} \frac{\partial P_a}{\partial y}(\xi+h) \quad (3.36)$$

Dropping the bars, Equation (3.33), (3.35), and (3.36) can be written as

$$\frac{\partial \xi}{\partial t} + \frac{\partial}{\partial x} [(\xi+h)u] + \frac{\partial}{\partial y} [(\xi+h)v] = 0, \quad (3.37)$$

$$\begin{aligned} \text{or, } & \frac{\partial}{\partial t} [u(\xi+h)] + \frac{\partial}{\partial x} [uu(\xi+h)] + \frac{\partial}{\partial y} [uv(\xi+h)] = f_v(\xi+h) - \frac{1}{\rho} \frac{\partial P_a}{\partial x}(\xi+h) \\ & + \frac{1}{\rho} (T_x - F_x), \end{aligned} \quad (3.38)$$

$$\begin{aligned} \text{or, } & \frac{\partial}{\partial t} [v(\xi+h)] + \frac{\partial}{\partial x} [uv(\xi+h)] + \frac{\partial}{\partial y} [vv(\xi+h)] = -f_u(\xi+h) - \frac{1}{\rho} \frac{\partial P_a}{\partial y}(\xi+h) \\ & + \frac{1}{\rho} (T_y - F_y). \end{aligned} \quad (3.39)$$

It can be observed from Equations (3.38) and (3.39) that the local variation of the averaged velocity components are governed by forcing terms such as the Coriolis force, wind stress, surface pressure and gravitational force. Given that the latitudinal position of the area of study has been determined the Coriolis force can be easily found. Additionally, given that  $g$  is known,

then the gravitational force can also be found. Also, to reiterate once more, the stress due to powerful circulatory winds is the driving force behind the surge amplitude during severe tropical storms. As for the remaining forcing terms, bottom stress can be expressed in terms of the depth-averaged current and in such cases, the conventional quadratic law is used:

$$F_x = \rho C_f u \sqrt{u^2 + v^2} \quad (3.40)$$

$$F_y = \rho C_f v \sqrt{u^2 + v^2}$$

where  $C_f = 2.6 \times 10^{-3}$  is an empirical bottom friction coefficient. Considering the forcing terms and the approximations made above, the vertically integrated form of  $x$  and  $y$  components of momentum equations, namely Equations (3.34)-(3.35), respectively, can be expressed in the flux form as:

$$\begin{aligned} \frac{\partial}{\partial t} [u(\xi + h)] + \frac{\partial}{\partial x} [uu(\xi + h)] + \frac{\partial}{\partial y} [uv(\xi + h)] = f_v(\xi + h) - \frac{1}{\rho} \frac{\partial P_a}{\partial x}(\xi + h) \\ + \frac{T_x}{\rho(\xi + h)} - \frac{C_f u \sqrt{u^2 + v^2}}{(\xi + h)} \end{aligned} \quad (3.41)$$

$$\begin{aligned} \frac{\partial}{\partial t} [v(\xi + h)] + \frac{\partial}{\partial x} [uv(\xi + h)] + \frac{\partial}{\partial y} [vv(\xi + h)] = -f_u(\xi + h) - \frac{1}{\rho} \frac{\partial P_a}{\partial y}(\xi + h) + \frac{T_y}{\rho} \\ - \frac{C_f v \sqrt{u^2 + v^2}}{(\xi + h)} \end{aligned} \quad (3.42)$$

For convenience, Equations (3.33), (3.38), and (3.39) can be written as

$$\frac{\partial \xi}{\partial t} + \frac{\partial \tilde{u}}{\partial x} + \frac{\partial \tilde{v}}{\partial y} = 0 \quad (3.43)$$

$$\frac{\partial \tilde{u}}{\partial t} + \frac{\partial}{\partial x}(u\tilde{u}) + \frac{\partial}{\partial y}(v\tilde{u}) = f\tilde{v} - \frac{1}{\rho} \frac{\partial P_a}{\partial x}(\xi + h) + \frac{T_x}{\rho} - \frac{\rho c_f}{\xi + h} u (u^2 + v^2)^{\frac{1}{2}} \quad (3.44)$$

$$\text{and } \frac{\partial \tilde{v}}{\partial t} + \frac{\partial}{\partial x}(u\tilde{v}) + \frac{\partial}{\partial y}(v\tilde{v}) = -f\tilde{u}v - \frac{1}{\rho} \frac{\partial P_a}{\partial y}(\xi + h) + \frac{T_y}{\rho} - \frac{\rho c_f}{\xi + h} \tilde{v} (u^2 + v^2)^{\frac{1}{2}} \quad (3.45)$$

where  $u(\xi + h) = \tilde{u}$  and  $v(\xi + h) = \tilde{v}$  are new prognostic variables and  $(\xi + h)$  represents the total depth of the basin.

Hence, the three basic equations of the numerical model consist of the equation of continuity (3.43) and the two equations of momentum (3.44) and (3.45). These three coupled equations have the unknowns, namely  $\tilde{u}$ ,  $\tilde{v}$ , and  $\xi$ . The forcing terms in these equations are a result of the Coriolis terms, the inverted barometric effect which are  $\frac{\partial P_a}{\partial x}$  and  $\frac{\partial P_a}{\partial y}$  due to fall in atmospheric pressure, the component of wind stress ( $T_x$ ,  $T_y$ ) in Equations (3.44) and (3.45), and the bottom stress component ( $F_x$ ,  $F_y$ ). Debsarma (2009) explained that if the above forcing terms could be described by meteorological data and the geometry of the continental shelf then the problem would be resolved by numerical integration. Then the response in the sea at any instant  $t > 0$  can give the surge heights. In the following section, more relevant information considering wind stress generation is discussed for this thesis.

### 3.2.4 Wind Stress Generation

As discussed earlier, the forcing terms in Equations (3.43)-(3.45) are the Coriolis force, the surface pressure, wind stress and bottom friction. The surge occurs due to an idealised cyclone of constant strength, tracking across the analysis area with constant speed. In regards to the wind

stress forcing associated with storm surge, the inverse barometric effect can be left out in surge forecasting models as previously mentioned. Moreover, the Coriolis force can be found given that the latitudinal location for the area of interest and as already seen the bottom stress can be parameterized in terms of depth averaged currents using a quadratic law. Now we have to only compute the surface winds and the wind stresses.

There has been no solid theory until now on which computation of surface winds can be based. Some numerical models for storm surge have applied wind speed that has bearing on the pressure gradient. The pressure field can be described as:

$$p(r) = p(\infty) - \frac{\Delta p}{[1 + (r/R)^2]^{1/2}} \quad (\text{Isozaki, 1970}) \quad (3.46)$$

$$p(r) = 1010 - \frac{\Delta p}{[1 + (r/R)^2]} \quad (\text{Das et al., 1972}) \quad (3.47)$$

$$p(r) = p(\infty) - \Delta p \exp(-r/R) \quad (\text{Johns \& Ali, 1980}) \quad (3.48)$$

where  $p(r)$  and  $p(\infty)$  show sea level pressure at  $r$  and at the cyclone periphery,  $R$  is the radius of maximum winds and  $\Delta p$  indicates the pressure drop. Then the wind generated by the cyclone is calculated using the gradient wind formula. This can require wind information such as maximum sustained wind velocity, the corresponding radial distance from the eye of the storm, and the difference of the atmospheric pressure between the eye and the periphery which can be collected from the Bangladesh Meteorological Department (BMD). Keeping these parameters in mind, several empirical formulae can generate the necessary wind field and some have been discussed below. If we consider Equation (3.47), we can find its correlating gradient wind formula which is

$$V^2 = 4 V_m^2 [\mu^2 \div (1 + \mu^2)^2] \quad (3.49)$$

In the above equation,  $\mu = r/R$  and  $V_m$  is the maximum sustained wind at the radial distance  $R$  and  $r$  is the radial distance at which the wind field is wanted. The link between maximum wind (knots) and the pressure drop (hPa) can be shown by

$$V_m = C(\Delta p)^{1/2} \quad (3.50)$$

where C represents a numerical constant.

Furthermore, the gradient wind formula related to Equation (3.49) can be found by (see Johns and Ali, 1980)

$$V = -\frac{fr}{2} + \left[ \frac{f^2 r^2}{4} + \frac{r}{\rho_a} \frac{\partial p}{\partial r} \right]^{1/2} \quad (3.51)$$

where  $\rho_a$  considered as  $1.293 \text{ kg m}^{-3}$  is the density of air.

The most commonly used formula for computation of the wind field along with the ones applied for the Bay of Bengal region (Jelesnianski, 1965) are given below:

$$V = V_m \left( \frac{r}{R} \right)^{3/2}, \quad 0 \leq r \leq R, \quad (\text{Jelesnianski, 1965}) \quad (3.52)$$

$$V = V_m \left( \frac{R}{r} \right)^{1/2}, \quad r > R, \quad (3.53)$$

$$V = V_m \left( \frac{2Rr}{R^2 + r^2} \right), \quad (\text{Jelesnianski, 1972}) \quad (3.54)$$

Then the wind stress terms in Equations (3.44) and (3.45) can be parameterized in terms of the wind field related to the cyclone. It can be expressed by the conventional quadratic law as (Roy, 1995)

$$(T_x, T_y) = \rho_a c_D (u_a^2 + v_a^2)^{1/2} (u_a, v_a), \quad (3.55)$$

Otherwise, it can be further simplified into

$$T_x = C_D \rho_a u_a (u_a^2 + v_a^2)^{1/2} \quad \text{and} \quad T_y = C_D \rho_a v_a (u_a^2 + v_a^2)^{1/2}, \quad (3.56)$$

where  $u_a$  and  $v_a$  represent the x and y components of sur

face wind,  $C_D$  represents the drag coefficient and studies have proposed that wind speed and drag coefficient can be associated in the following way

$$C_D = (1.00 + 0.07v_{10}) \times 10^{-3} \quad (3.57)$$



where  $v_{10}$  gives the wind speed at 10m from the mean sea level. This relation is applicable for wind speed less than  $14 \text{ m sec}^{-1}$ .  $C_D$  is between  $2 \times 10^{-3}$  to  $3 \times 10^{-3}$  for wind speeds fluctuating from 10 and  $30 \text{ m sec}^{-1}$ . without any considerable dependence on wind speed. The most commonly used uniform value of  $C_D$  is  $2.8 \times 10^{-3}$ .

### 3.2.5 Boundary and initial conditions

The surface and bottom conditions have already been given by Equations (3.27) and (3.28), respectively. Furthermore, the appropriate conditions have to be also satisfied along the lateral boundaries of the part of the sea under consideration at all times. Theoretically, the only boundary condition required in the vertically integrated system is that the normal component of the depth averaged velocity vanishes at the coast, i.e. it is zero at closed boundaries which can be shown as

$$u \cos \alpha + v \sin \alpha = 0 \text{ for all } t \geq 0 \quad (3.58)$$

where  $\alpha$  indicates the inclination of the outward direction normal to the  $x$ -axis. Therefore,  $u=0$  along the  $y$ -directed boundaries and  $v=0$  along the  $x$ -directed boundaries. Otherwise, it is a condition of no flow across the model coastline and island boundaries. Zero condition closed boundaries are also not appropriate for flood models. However, at the open sea boundary, the normal component of the depth averaged velocity cannot disappear and different open boundaries can apply depending on the data at hand and the type of modelling being implemented. One option is that at the open-sea boundary, the normal currents across the boundary may be assigned, giving a condition similar to the one stated in Equation (3.58) modified by a non-zero term on the right hand side of the equation. On the other hand, Heaps (1973) suggested a radiation type of boundary condition, a very commonly applied boundary condition for the Bay of Bengal region, which takes the form

$$u\cos\alpha + v\sin\alpha + (g/h)^{1/2}\zeta = 0 \quad \text{for all } t \geq 0 \quad (3.59)$$

This radiation type of condition allows the outward propagation of internally generated disturbances (energy) from the area under consideration in the form of simple progressive waves and communicates with the tides of the Bay of Bengal approaching the coast of Bangladesh. It can also get rid of the transient response with ease due to the frictional dissipation in the system. By using a radiation type of condition in the numerical model, unrealistically large currents and grid scale oscillations can be eliminated in the domain of the open boundary may happen by using conventional open-sea boundary condition, i.e.,  $\zeta=0$  at  $y=0$ . Other forms of radiation type of condition that are widely used can be found in the literature (Arnold, 1987; Bills & Noye, 1987; Hubbert et al. 1990; Tang & Grimshaw, 1996).

In case of the initial condition, it is typically assumed that the motion in the sea is produced from an initial state of rest where  $\zeta = u = v = 0$  everywhere for  $t \geq 0$ . In the coarse mesh scheme (CMS) there are three open sea boundaries at south (15°N), west (85°E) and east (95°E). The western and eastern open sea boundaries are parallel to the x-axis and the southern open sea boundary is parallel to the y-axis. Following Johns et al. (1981), the radiation boundary conditions are then written as

$$\text{the west boundary: } v + \left(\frac{g}{h}\right)^{1/2} \xi = 0, \quad (3.60)$$

$$\text{the east boundary: } v - \left(\frac{g}{h}\right)^{1/2} \xi = 0, \quad (3.61)$$

$$\text{the south boundary: } u - \left(\frac{g}{h}\right)^{1/2} \xi = -2 \left(\frac{g}{h}\right)^{1/2} a \sin\left(\frac{2\pi t}{T} + \varphi\right). \quad (3.62)$$

where  $a$  and  $\varphi$  are the prescribed amplitude and phase of the tidal forcing, respectively. This is the period of the tidal constituent being taken into account.

Along the northern boundary of the VFMS, an open boundary segment is taken between longitudes 90.46°E to 90.61°E with the breadth of it extending for approximately 16 km. This shows the Meghna river located between Ramdaspur and Noakhali mainland along 23°N latitude. Along this north-west corner of the model the river discharge effect is taken into account by (Roy, 1995)

$$u_b = u + \frac{Q}{(\xi + h)B}, \quad (3.63)$$

where Q denotes fresh water discharge through the river, and B is the breadth of the river in m.

## **Chapter 4**

### **Numerical Procedure**

#### **4.1 General**

This chapter entails the numerical solution process of the set of vertically integrated shallow water equations discussed in Chapter 3. The two dimensional hydrodynamic model has been specifically developed for the coastal region of Bangladesh. The model is set up in Cartesian coordinate system to investigate the air bubble entrainment effect on water level associated with a tropical storm and is solved by semi implicit finite difference schemes. Firstly, nested schemes are employed to include the coastal complexities of the area of interest and the offshore islands accurately. Nested schemes enable specification of high resolution for the study domain of this thesis while also allowing lower resolution elsewhere. At the innermost northeast corner of the model, the Meghna river discharge is taken into account. Tidal forcing is implemented along the southern open boundary of the parent model to ensure that there is an appropriate stable tidal condition over the model domain. This tidal regime is established as the initial state of the sea for nonlinear interaction of tide and surge. The coastal and island boundaries are approximated through proper stair steps and the computational method for solving the model equations uses a rectangular grid structure. This model is used to simulate water levels due to tide and surge interaction including air bubble effects associated with the April 1991 cyclone at various coastal and island locations along the Bangladesh coastline. The results obtained after running the model have been discussed in the analysis subsection of this chapter.

## 4.2 Set up of nested schemes

In this section, we examine the physical domain of this research and the details of the numerical schemes applied in our vertically integrated shallow water model. In order to properly include the aspect of coastline bending and offshore islands, the mesh size or the the distance between two consecutive grid points is required to be small near the coast and it can be larger away from the coast (Roy et al., 1999). Thus, nested schemes are utilized here as they give specification of high resolution for the specific region of this study. By using nesting schemes we can see considerable increase in accuracy as there is improved spatial resolution, great reduction in the number of computational grids and fall in overall cost. This helps to counter the issues surrounding the application of an improved mesh size over the whole study domain. The size of the area of our focus is also taken to be large enough so that the storm can pass over the area for a minimum of 3 days before making landfall. The main reason for doing is because there is already a significant surge response near the coastline even before the storm approaches the coast. Taking the aforementioned facts into account, a high-resolution fine mesh scheme (FMS) is nested into a coarse mesh scheme (CMS). Then a very fine mesh scheme (VFMS) is nested again into the FMS. The CMS or the physical domain extends the area from latitudes 15°N to 23°N and longitudes 85°E to 95°E. The grid spacing along north-south (along the x-axis) and east-west (along the y axis) directions are 15.08 km and 17.52 km, respectively. There are 60 × 61 grid points in the xy-plane of the model. The fine grid model is concerned with the inclusion of the curvature of the coastline and the offshore islands as finer resolution is needed in this regard. So the FMS covering the area between latitudes 21°15'N to 23°N and longitudes 89°E to 92°E is placed into the CMS. This fine grid model also consists the study region for this thesis. The mesh size for FMS along north-south direction is 2.15 km and along the east-west direction

is 3.29 km. There are 92 x 95 grid points for the FMS. According to Ali and Choudhury (2014), it is noteworthy that the coastline of Bangladesh is highly complex with the Meghna estuarine part being significantly complex as it is quite flat and facilitates surge amplification. Meghna estuarine region is also densely populated with low lying islands of different sizes between Barisal and Chittagong and as mentioned earlier it has a complex coastal geometry. Taking these two factors into consideration, we use a VFMS for this region only by extending from latitudes 21.77°N to 23°N and longitudes 90.40°E to 92°E, nested into the FMS. The mesh size along north-south direction is 720.73m and along east-west direction is 1142.39m and the computational grid points for VFMS in the xy-plane are 190 x 145. Figure 4.1 portray the boundaries of the CMS, FMS, and VFMS domains utilized in this model. Given that the computational method uses a rectangular grid, the coastline and the island boundaries have been approximated following the grid lines applying stair step representation.

All of the three schemes have the same hydrodynamic Equations (3.43)-(3.45) but have different boundary conditions. Coupling of the schemes is critical. It should be noted that the CMS is independent and it uses the boundary conditions given by Equations (3.60)-(3.62). Then according to Roy (1995), along the open boundaries of the FMS, the parameters  $\zeta$ ,  $u$ , and  $v$  are passed from those obtained in CMS in each time step of the solution process. It needs to be highlighted that the values of the parameters  $\zeta$ ,  $u$ , and  $v$  attained from the CMS were interpolated with the help of weighted interpolation to get a set of boundary conditions for the FMS. Likewise, for the VFMS, the parameters  $\zeta$ ,  $u$ , and  $v$  are prescribed from those found in FMS along the open boundaries of the VFMS in each time step of the solution process. This method is necessary since the resolution of the schemes are different from one another.

Furthermore, as it can be seen in Figure 4.1, the Meghna river is covering the area between the

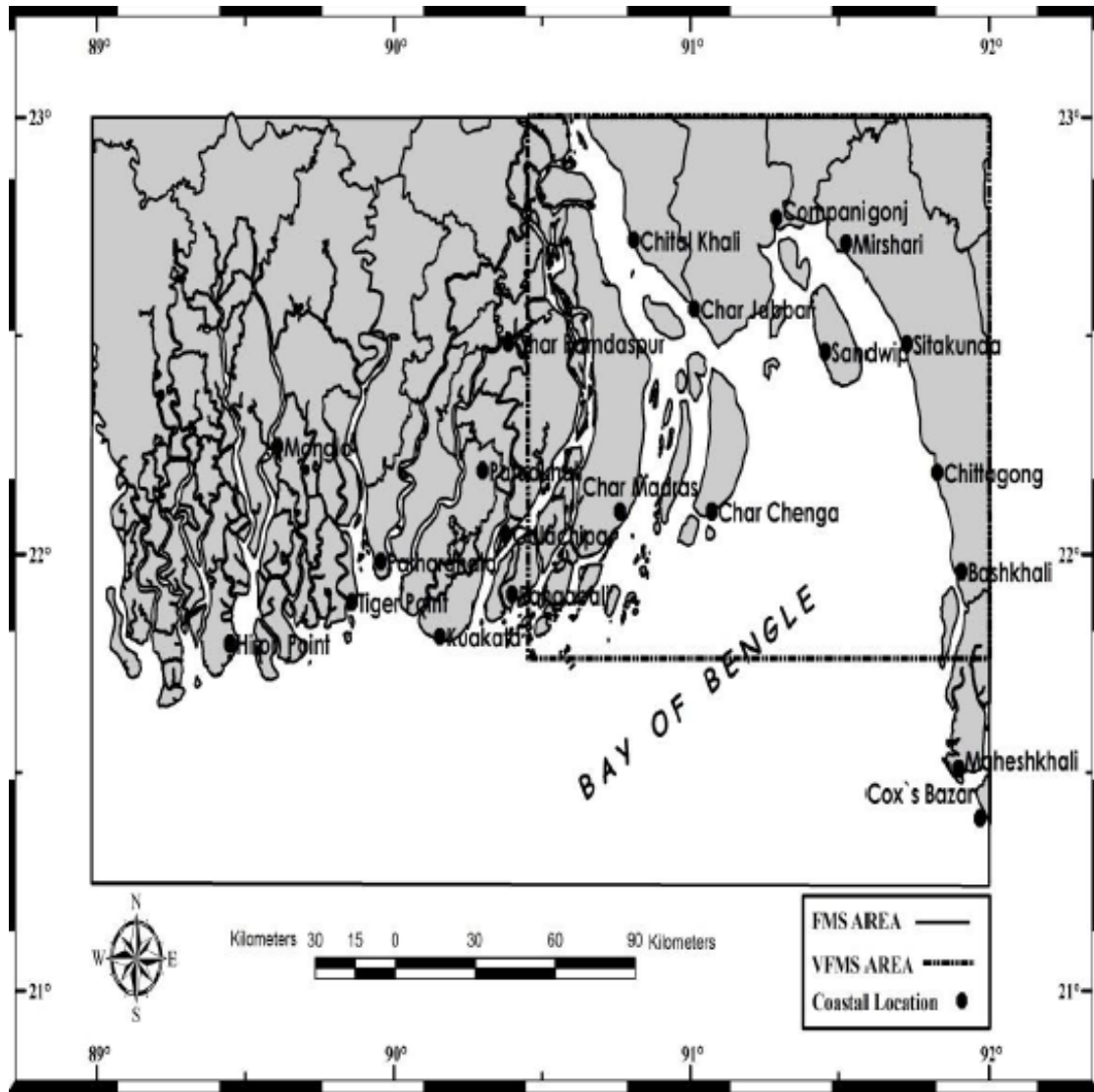
longitudes 90.4 and 90.6 along the north-east part of the VFMS and as mentioned in Chapter 3, the discharge of the river is incorporated through (see Roy, 1995)

$$u_b = u + \frac{Q}{(\xi + h)B},$$

where  $Q$  is the river discharge and  $B$  is the breadth of the river. According to Jain et al. (2007), the prescribed value for  $Q$  in calculations is  $Q = 5100.0 \text{ m}^3/\text{s}$ . Even though Bangladesh has numerous rivers that discharge into the Bay of Bengal, we consider only Meghna estuary as our area of interest as it is part of the GBM river system that forms the third largest freshwater outlet in the world's oceans. Thus, discharge of Meghna is more important than other rivers in the country and we take into account the discharge through Meghna estuary only.

**Figure 4.1**

*Domains of the different schemes (CMS, FMS, VFMS) with the positions of some coastal areas and their water levels*



*Note.* Adapted from “Contribution of offshore islands in the prediction of water levels due to tide–surge interaction for the coastal region of Bangladesh” by G. C., & Ismail and A. I. M. Ismail, 2012, *Natural Hazards*, 65(1), 13-25. Copyright 2012 by Springer Science+Business Media B.V.



## 4.3 Numerical Procedure

### 4.3.1 Grid Generation and Stair Step Representation

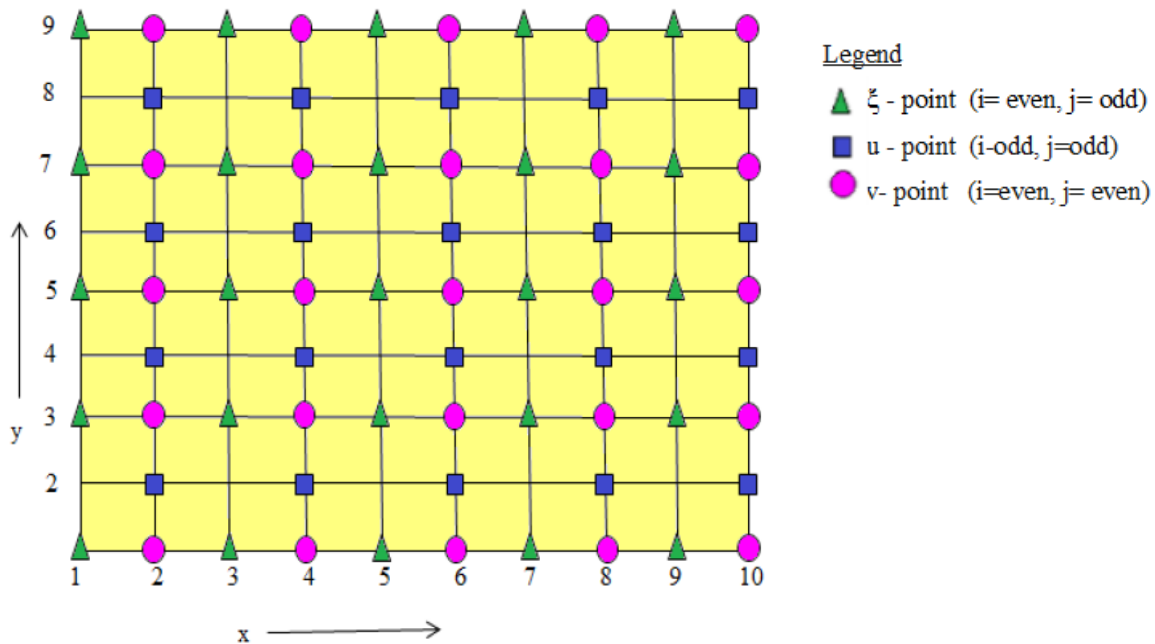
Grids can be described as tiny shapes created from discretization of the geometric region. They are found to be both 2-dimensional and 3-dimensional with widespread applications in disciplines such as geography, computational fluid dynamics (CFD) and others. This type of model set-up is useful for saving time, cost, and producing better results in CFD-related work. In this case, the study domain is covered by a 2-dimensional mesh of rectangular grids. There are mainly three kinds of grids such as i) structured or staggered grid, (ii) unstructured grid, and (iii) hybrid grid. A staggered grid is applied when multiple functions need to be solved. It provides the benefit of defining the functions at different regions on the grid. When working with finite difference equations, it makes the finite-difference approximations far less complicated and more consistent with the physics being represented. This type of grid is associated with regular connectivity and is also capable of connecting many different nodal points found in different geometrical locations. Alternatively, unstructured grids are useful in case of complex geometries when it becomes necessary to have larger number of grids. Each single cell is handled as a block and the grid does not give any structure of coordinate lines. Otherwise, an unstructured grid has random connectedness and it is not easy to express as a 2-dimensional or 3-dimensional array in computer memory. According to Ali (1979), it cannot deal with high frequency waves, namely two grid waves. In this research paper, a staggered grid system is more than adequate and an example of how it looks in  $(x, y)$  plane is displayed in Figure 4.2 (a). The grid lines lie parallel to the co-ordinate axes and form a homogenous, rectangular mesh with length  $\Delta\zeta$  in the  $\zeta$ -direction and  $\Delta y$  in the  $y$  direction. The system has 3 types of computational points. The point  $\zeta$  (denoted by a circle) is calculated at each grid point when  $i$  is even and  $j$  is odd. If  $i$  and  $j$  are both odd

then a  $u$ -point (denoted by a triangle) is computed. Lastly, if  $i$  and  $j$  are both even then the computed point is a  $v$ -point (denoted by a square). If  $m \times n$  are the number of grid points in the computational area,  $m$  is taken to be even and  $n$  is taken as odd. Taking the aforementioned conditions into account, the southern boundary contains  $\zeta$  and  $v$  points and both the western and eastern boundaries contain  $\zeta$  and  $u$  points.

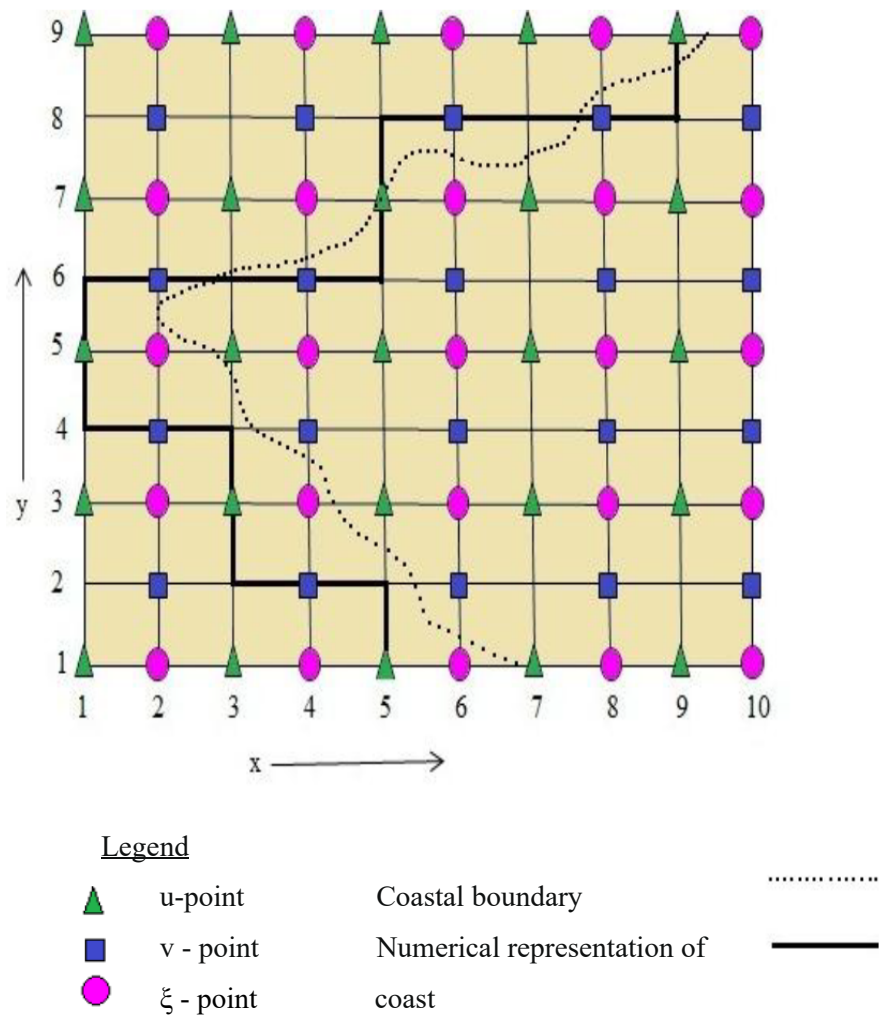
The lateral boundaries of the finite difference grid are approximated along the nearest odd  $y$ -directed grid lines, otherwise  $i$  is odd, resulting in only  $u$ -points for this part of the boundary or along the nearest even  $x$ -directed grid lines, otherwise when  $j$  is even, giving  $v$ -points for this part. Therefore, the boundaries are defined by a stair step method where at each section there lies only that component of velocity found to be normal to the section (see, Figure 4.2b). The purpose of this is to make sure of the vanishing of the normal component of the velocity at the boundary in this scheme.

**Figure 4.2**

*(a) A structured grid system*



(b) Example of a coastal boundary and its numerical representation



*Note.* Adapted from “Impact Assessment of a Major River Basin in Bangladesh on Storm Surge Simulation” by M. A. Al Mohit, M. Yamashiro, N. Hashimoto, M. B. Mia, Y. Ide, and M. Kodama, 2018, *Journal of Marine Science and Engineering*, 6(3), 99. Copyright 2018 by MDPI.

### 4.3.2 Computational Procedure: Discretization of the governing equations

The governing equations given by (3.43)-(3.45) as well as the boundary conditions (3.42)-(3.44) are discretized by finite difference scheme which is forward in time and central in space and the equations are solved by a conditionally stable semi-implicit method using a staggered grid method as shown in details in Section 4.3.1. Taking into account the discrete coordinate points in the  $xy$ -plane are given by

$$x_i = (i-1)\Delta x, \quad i = 1, 2, 3, \dots, m \text{ (even),}$$

$$y_j = (j-1)\Delta y, \quad j = 1, 2, 3, \dots, n \text{ (odd),}$$

with  $\Delta x$  and  $\Delta y$  being the grid increments. A sequence of time instants is given by

$$t_k = k\Delta t, \quad k = 1, 2, 3, \dots,$$

where  $\Delta t$  is the time increment.

Any variable  $\zeta$  at a grid point  $(i, j)$  at time  $t_k$  is written as:

$$\zeta(x_i, y_j, t_k) = \zeta_{i,j}^k.$$

Finite difference operators can be written as:

$$\frac{\partial \zeta}{\partial t} = \frac{\zeta_{i,j}^{k+1} - \zeta_{i,j}^k}{\Delta t},$$

$$\frac{\partial \zeta}{\partial x} = \frac{\zeta_{i+1,j}^k - \zeta_{i-1,j}^k}{2\Delta x},$$

$$\frac{\partial \zeta}{\partial y} = \frac{\zeta_{i,j+1}^k - \zeta_{i,j-1}^k}{2\Delta y}.$$

Averaging operators for variables such as  $U$  can be expressed as:

$$\overline{U_{i,j}^k}^x = \frac{U_{i+1,j}^k + U_{i-1,j}^k}{2}, \quad \overline{U_{i,j}^k}^y = \frac{U_{i,j+1}^k + U_{i,j-1}^k}{2}, \quad \text{and} \quad \overline{U_{i,j}^k}^{xy} = \overline{\overline{U_{i,j}^k}^x}^y.$$

Furthermore, the last term on the RHS of (3.44) and (3.45) are discretized in such a way so that schemes turn out to be semi-implicit. For instance, the term  $\tilde{u}\sqrt{(u^2+v^2)}$  from (3.44) is discretized in the following manner

$$\tilde{u}^{k+1}\sqrt{(u^{k^2}+v^{k^2})},$$

with  $k+1$  subscript denoting that  $\tilde{u}$  is to be assessed at the advanced time level. Therefore, the finite difference form of (3.43) after its implementation is

$$\xi_{i,j}^{k+1} = \xi_{i,j}^k - \Delta t[TL1 + TL2], \quad (4.1)$$

given that  $TL1 = \left( \frac{\tilde{u}_{i+1,j}^k - \tilde{u}_{i-1,j}^k}{2\Delta x} \right)$  and  $TL2 = \left( \frac{\tilde{v}_{i,j+1}^k - \tilde{v}_{i,j-1}^k}{2\Delta y} \right)$ .

The term  $\xi_{i,j}^{k+1}$  in (4.1) is calculated at  $i = 1, 2, 3, \dots, m-2$  and  $j = 3, 5, 7, \dots, n-2$ .

Likewise, (3.44) takes the following form

$$\tilde{u}_{i,j}^{k+1} = \frac{\tilde{u}_{i,j}^k - \Delta t(TL1 + TL2 + TL3) + \Delta t(TR1 + TR2)}{(1 + \Delta t.FR3)}, \quad (4.2)$$

with

$$TL1 = \left( \frac{\tilde{u}_{i+2,j}^k U_{i+2,j}^k - \tilde{u}_{i-2,j}^k U_{i-2,j}^k}{4\Delta x} \right),$$

$$TL2 = \left( \frac{\overline{\tilde{u}_{i,j+1}^k V_{i,j+1}^k}^x - \overline{\tilde{u}_{i,j-1}^k V_{i,j-1}^k}^x}{2\Delta y} \right),$$

$$TL3 = -f_i \overline{\tilde{v}_{i,j}^k}^{xy},$$

$$TR1 = -g(\xi_{i,j}^{k+1} - h_{i,j}) \frac{\xi_{i+1,j}^{k+1} - \xi_{i-1,j}^{k+1}}{2\Delta x},$$

$$TR2 = \frac{\tau_x}{\rho},$$

$$\text{and, } FR3 = \frac{C_f \sqrt{U_{i,j}^{k^2} + \left( \overline{V_{i,j}^k}^{xy} \right)^2}}{\xi_{i,j}^{k+1} + h_{i,j}}.$$

The term  $\tilde{u}_{i,j}^{k+1}$  is similarly calculated at  $i = 1, 2, 3, \dots, m-2$  and  $j = 3, 5, 7, \dots, n-2$ .

Additionally, (3.38) transforms to

$$\tilde{v}_{i,j}^{k+1} = \frac{\tilde{v}_{i,j}^k - \Delta t.(TL1 + TL2 + TL3) + \Delta t.(TR1 + TR2)}{(1 + \Delta t.FR3)}, \quad (4.3)$$

$$\text{with } TL1 = \left( \frac{\overline{U_{i+1,j}^k \tilde{v}_{i+1,j}^k}^x - \overline{U_{i-1,j}^k \tilde{v}_{i-1,j}^k}^x}{2\Delta x} \right),$$

$$TL2 = \left( \frac{V_{i,j+2}^k \tilde{v}_{i,j+2}^k - V_{i,j-2}^k \tilde{v}_{i,j-2}^k}{4\Delta y} \right),$$

$$TL3 = f_i \overline{\tilde{u}_{i,j}^{k+1}}^{xy},$$

$$TR1 = -g(\xi_{i,j}^{k+1} + h_{i,j}) \frac{\xi_{i,j+1}^{k+1} - \xi_{i,j-1}^{k+1}}{2\Delta y},$$

$$TR2 = \frac{\tau_y}{\rho},$$

$$\text{and, } FR3 = \frac{C_f \sqrt{\left( \overline{U_{i,j}^k} \right)^2 + V_{i,j}^k}}{\xi_{i,j}^{k+1} + h_{i,j}}.$$

The term  $\tilde{v}_{i,j}^{k+1}$  in (4.3) is calculated at  $i = 2, 4, 6, \dots, m-2$  and  $j = 2, 4, 6, \dots, n-1$ .

Taking the boundary conditions in (3.42) - (3.44), the elevations at  $j = 1, j = n$  and  $i = m$  are calculated, respectively as stated below.

$$\xi_{i,1}^{k+1} = -\xi_{i,3}^{k+1} - 2\sqrt{(h_{i,2} / g)} V_{i,2}^k, \quad (4.4)$$

$$\xi_{i,n}^{k+1} = -\xi_{i,n-2}^{k+1} + 2\sqrt{(h_{i,n-1} / g)} V_{i,n-1}^k, \quad (4.5)$$

$$\xi_{M,j}^{k+1} = -\xi_{M-2,j}^{k+1} + 2\sqrt{(h_{M-1,j} / g)} U_{M-1,j}^k + 4a \sin\left(\frac{2\pi k \Delta t}{T} + \varphi\right), \quad (4.6)$$

with  $i = 2, 6, 8, \dots, m-2$  and  $j = 1, 3, 5, \dots, n-1$ .

Along the northeast edge of the VFMS, the river discharge through the Meghna river is considered as shown in Fig. 4.1. In consideration of this river discharge, the velocity component  $U_b$  at a grid point  $(i,j)$  is calculated using the equation given in section 4.2 by:

$$(U_b)_{1,j}^{k+1} = U_{3,j}^{k+1} + \frac{Q}{(\xi_{1,j}^{k+1} + h_{1,j})B}, \quad \text{where } j = 7, 9, 11, \dots, 19. \quad (4.7)$$

### 4.3.3 The Data Sources and Numerical Values

This study involves many inputs such as meteorological, oceanographic, hydrological, and geographical data. Additionally, the study also uses a lot of parameters. The chosen values are examined and anything else takes their standard values from the diagram displayed by Fig. 4.3.3 used in the research paper by Johns et al. (1985). The data concerning the bathymetry for the grid points is from Figure 4.3. The meteorological inputs include storm path, central pressure, maximum sustained wind speed, and radius of the maximum win. Many of these input data have

already been discussed thoroughly in “The Cyclone 1991” and “Wind Speed and Surge Height” subsections of Chapter 2. The wind distribution was produced with the help of the data available at Bangladesh Meteorological Department (BMD), and empirical formula from Jelesnianski (1965). The storm track observations of the April 1991 cyclonic storm was collected from Paul and Ismail (2013) and has been displayed by Figure 2.8 in Chapter 2. In this thesis, two important geometric factors like the coastal geometry and the islands are also considered. The map for the study domain was produced using Google My Maps through ArcGIS software. This resulted in the formulation of the three schemes: CMS, FMS, and VFMS. They were computerized in keeping with their resolutions via a MATLAB routine and the approximations of the coastal and island boundaries were made through stair step method in MATLAB. The water depth input for the grid points of the schemes was collected using inverse square distance weighted interpolation. The water level data and tidal data was collected from Bangladesh Inland Water Transportation Association (BIWTA). In addition, during extreme weather events like cyclonic storms there is wave breaking with large-scale air bubble entrainment taking place in the shallow water areas. According to the findings of Chanson (1994) and Lin and Hwung (1992), there can be pervasive entrained bubbles caused by plunging breaking waves. Moreover, Hwung et al. (1992) mentions that plunging breakers have far more potential than other breakers for entrainment of air bubbles. This is the reason for choosing a plunging breaker type for the study. Further assumptions include air bubbles covering the entire study domain. The decay parameter for the void fraction distribution in the surface zone,  $k_1$ , was decided by observing how the theoretical curve fit the experimental data. It was taken to be  $k_1 = 0.9\text{m}^{-1}$  for the best fitted curve. Despite the fact a specific value of  $k_1$  is being used, it was found that other probable values of the parameter were also in good agreement with the ones displayed in diagrammatic



forms of the thesis. The simulations were carried out for  $0 \leq C_0 \leq 0.7$  given that  $C_0$  denotes the model results without the presence of air bubbles. The reason for  $C_0 \leq 0.7$  is because of the pseudo free surface threshold criterion (Paul & Ismail, 2012b). It is worth mentioning that based on the experimental findings of Hoque and Aoki (2006),  $C_0 = 0.3$  for plunging breakers and  $C_0 = 0.2$  for a spilling breaker but these values may vary on the horizontal distance from the point of breaking. Based on the research by Roy et al. (1999), the values of the friction and drag coefficients are  $C_f = 0.0026$  and  $C_D = 0.0028$  respectively and are considered to be uniform throughout our area of study. The initial values of  $\zeta$ ,  $u$ , and  $v$  are considered to be zero to act as the initial condition of static equilibrium and given this state, there can be a stable tidal cycle produced which has been elaborated in the subsection 4.3.4. As mentioned by Roy et al. (1999), these pure tidal oscillations give the initial condition of the sea for the tide-surge interaction occurrence. The time step used is 60 seconds to meet the Courant-Friedrichs-Levy (CFL) criterion of stability.

#### **4.3.4 Tide Generation for the Study Domain**

The process of generation of tide corresponds to the methods followed by Paul and Ismail (2012) and Roy (1995). Based on the work of McCammon and Wunsch (1977), the initial values of  $a$  and  $\phi$  are run through Eq. (4.6) along the southern open boundary of the CMS. The period of the tidal oscillation is taken to be  $T = 12.4$  h since the average period is about 12.4 h every time and it's of the  $M_2$  tidal constituent. As stated by Paul and Ismail (2013) this is the most energetic tidal constituent for our study domain. It is worth mentioning that the period of tidal oscillation in the area under consideration is not entirely periodic and  $M_2$  and  $S_2$  constituents are predominant in that area. Following Roy (1995), given that there is no wind field, a stable tidal regime is obtained from the cold start after four cycles of integration. There still remains the matter of

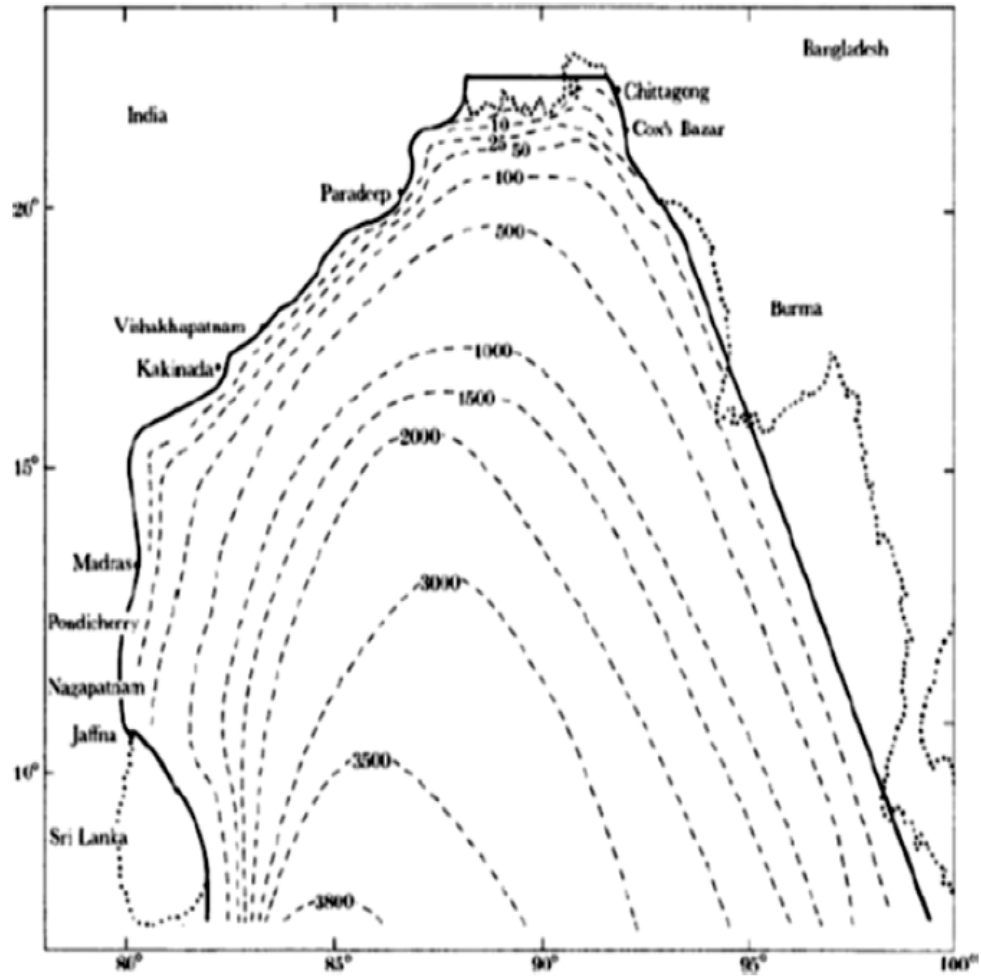
producing a pure tidal oscillation with the exact values of  $a$  and  $\phi$  in the Bay of Bengal relating to the tidal constituent with period  $T$ . This can be solved by using the methods proposed by Roy (1995) and Paul and Ismail (2012) to get the required values for  $a$  and  $\phi$ . To determine the overall water levels, the tidal oscillation produced is used as the initial condition at  $t = 0$ .

#### **4.3.5 The Numerical Experiment**

In the subsection 4.3.3, it has been mentioned that the initial values of  $\zeta$ ,  $u$  and  $v$  are set as 0. During the initial state of rest, a stable tidal regime was produced for the area under consideration by prescribing the tidal constituent  $M_2$  along the southern open boundary in the absence of a wind field. The procedure of the tidal generation has been elaborated in the previous subsection 4.3.4. In the case of nonlinear interaction of tide and surge, this tidal regime gave the initial condition of the sea. The necessary input data have all been mentioned in subsection 4.3.3 have been collected from BIWTA and BMD. The time step used was 60 seconds to achieve the CFL stability criterion.

Figure 4.3

*Input data for depth collected from the diagram shown*



*Note.* From “ Numerical modelling of tide-surge interaction in the Bay of Bengal,” by B. Johns, A. D. Rao, Z. Dubinsky, & P. C. Sinha, 1985, *Philosophical Transactions of the Royal Society of London. Series A, Mathematical and Physical Sciences*, 313(1526), 507-535. Copyright 2017 by Royal Society.

## **Chapter 5**

### **Data Analysis and Conclusion**

#### **5.1 Summary**

This chapter discusses the model outcomes along with the comparisons made of the simulated results with the observed data. The computations have been carried out for ten regions along the Bangladesh coastline which have been shown in Figure 4.1. The model results compared well with the observations which further confirms the validation of the model. However, it should also be noted that on many occasions in-depth comparisons could not be made of the computed time series of water level with the observations due to lack of actual observed time series data. Lastly, in the final section of this chapter, conclusion and future improvements have been discussed.

#### **5.2 Discussion of results and model validation**

The results are calculated for the April 1991 cyclone for a period of 80 hours which starts from 26 April 1800 UTC up to 30 April 0200 UTC. The output in each case is only shown for the last 48 hours in the selected locations which include Chittagong, Companigonj, Char Chenga, Char Jabbar, Char Madras, Rangabali, Kuakata, Tiger Point, and Hiron Point (see, Figure 4.1). The computation results have been displayed via diagrams (Figures 5.1-5.3) over a range of  $C_0$  values. As mentioned earlier, comprehensive comparisons of the simulated time series of water levels to reported ones are difficult to make due to lack of adequate and valid observed time series data. While collecting relevant data such as the hourly height of water from Bangladesh Inland Water Transport Authority (BIWTA), limited data was available due to equipment or

technical problems during the period of severe cyclonic storm. The cyclonic time history and each phase of the storm have been elaborated in Section 2.5.

Figure 5.1 represents the estimated water levels caused by tide during the cyclonic storm with the tidal data collected from BIWTA at Chittagong and Hiron Point. These locations were selected as the data was accessible for these two regions. The results are found to compare well with the observations from BIWTA and the findings of Flather(1994). Figure 5.2(a) show the maximum estimated water level elevations due to surge during April 1991 cyclone without the absence of air bubbles and Figure 5.2(b) display the maximum estimated water level due to surge at  $C_0 = 0.5$ . The peak surge levels display the computed time series of water levels during the April 1991 storm for  $C_0 = 0$  ranged from 3.01 to 5.89 m whereas the peak levels for  $C_0 = 0.5$  were found to be 3.08 - 6.08 m. Based on the BMD data, the surge height was found in the range of 3.5-6.1m for the locations bordering the coastline. Furthermore, Figures 5.2(a) and (b) show that the locations between Chittagong and Char Jabbar are very susceptible to powerful incoming surges. According to research by Roy et al.(1999), there was 0.70-5.45m water level elevations due to surge along the coastline of Bangladesh; Khalil(1993) found surge levels to be 4–9 m high for these regions while Paul and Ismail(2012b) estimated surge levels being 2.69–6.98 m. Therefore, the computed water levels due to surge during the April 1991 are in strong agreement with the findings in different research work. However, the estimated results for Hiron Point do not compare well with the findings in Roy et al.(1999) due to the approximation of the coastal geometry. Figure 5.2(c) represent the water levels simulated during the cyclonic storm as a result of combined factors such as tide, surge, and their interaction when the value of the reference void concentration, i.e.  $C_0$  is 0 at Chittagong. The peak water levels caused by tide, surge and the interaction between the two were estimated to be 1.85m, 5.15m and 5.95m. Figure

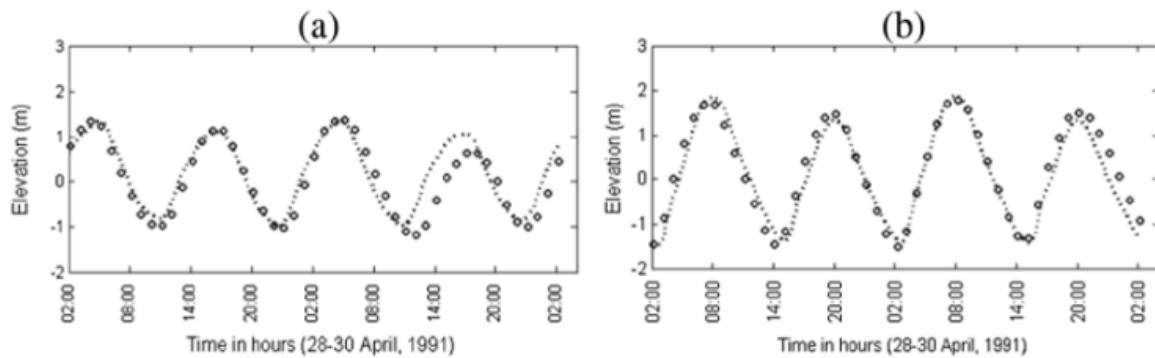
5.2(d) shows water levels with respect to the mean sea level when there is 50% reference void fraction ( $C_0 = 0.5$ ) as a result of the aforementioned factors. In this case, the peak computed water levels were found to be 1.85m, 5.31m, and 6.07m. Based on the data collected by BMD, the water level rise induced by the surge was 5.5m at Chittagong. More simulations for the time series of total water levels caused by the tide-surge interaction for 20% reference void fraction during the April 1991 cyclone is represented by Figure 5.2(e) and (f). The maximum computed water levels by the model was found to be in the 3.32 - 7.26 m range. The calculated results compare quite well with the findings of Flather(1994); Roy et al.(1999); Paul and Ismail (2012b, 2013) and Paul et al.(2014). Taking into account the aforementioned results represented in Figures 5.1 and 5.2(d)-(f), the maximum water levels keep rising as the storm advances towards the coast due to the factors discussed earlier such as surge and tide-surge interaction in the different regions. This is foreseeable due to the strong circulatory winds achieving maximum intensity. Then recession takes place which can be observed to occur earlier at the western coastal locations than at the eastern coastal locations. At each location, the maximum water level elevation happens before the landfall. The latter observation is also noticeable in the diagrammatic representations of our results.

In Figure 5.3, we compare the simulated time series of water levels associated with the storm at Hiron Point, Char Chenga (Hatiya), and Chittagong against the BIWTA data. As it can be seen that the computed results are in close accordance with the observed data. The major underlying

problem that is preventing a more comprehensive study over more locations is due to not having adequate data. Thus, it is not possible to compare the overall computed water level rise with the observed ones for the rest of the locations.

**Figure 5.1**

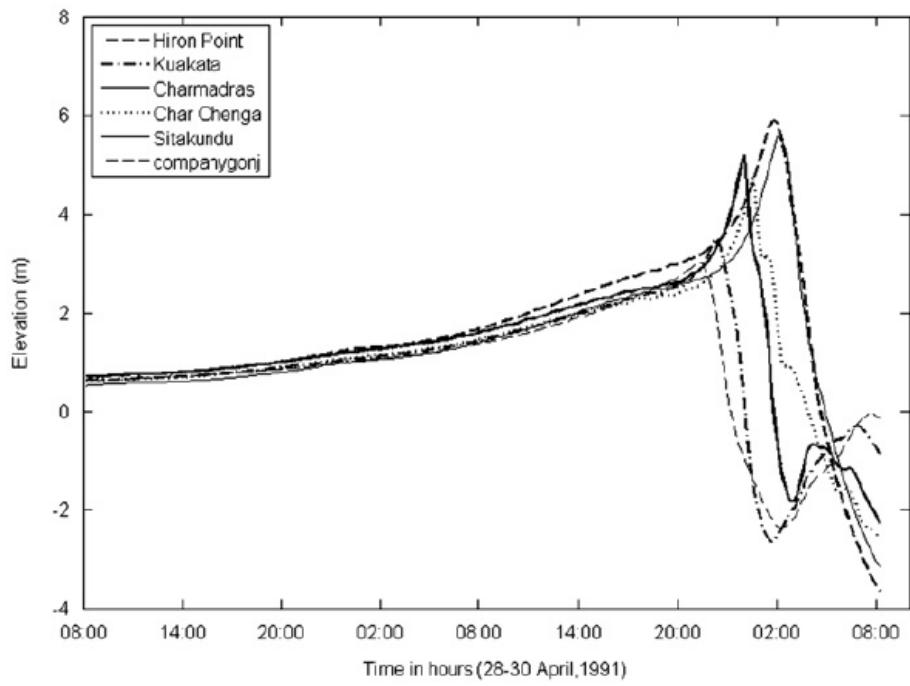
*Estimated water levels due to tide in April 1991 Cyclone*



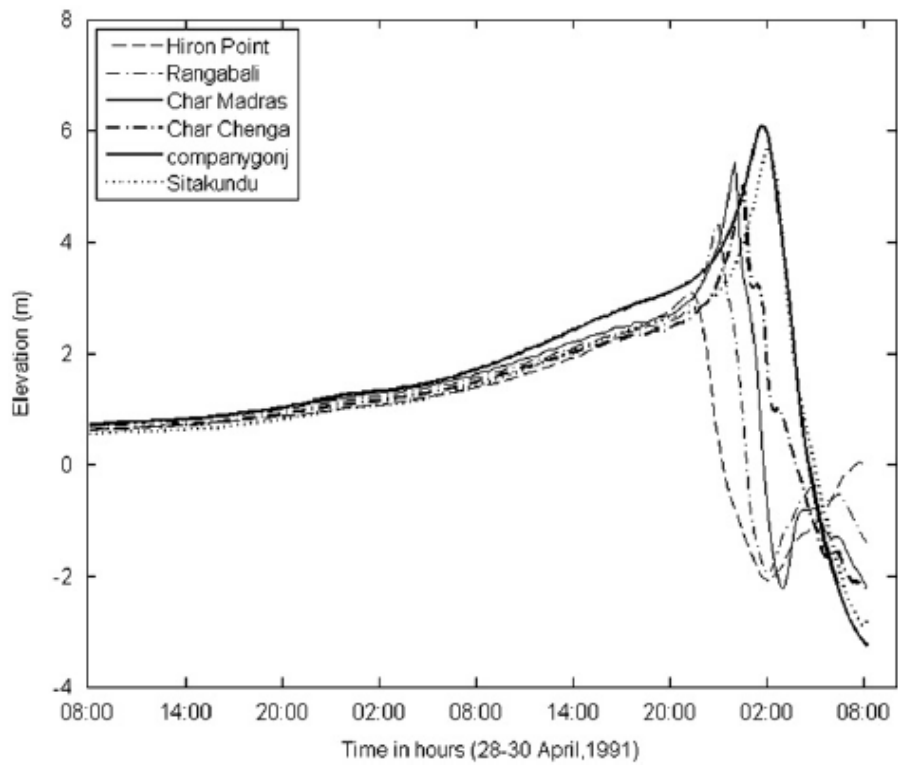
*Note.* Comparison of the simulated results at  $C_0=0$  for tide with the BIWTA tidal data during the April 1991 cyclone for the given time-period. The regions shown are Hiron Point and Chittagong. In these figures, the circle gives the observations and the curve shows the simulation of the tidal levels. From “Development of Tide-Surge Interaction Model for the Coastal Region of Bangladesh,” by G. C. Paul, A. I. M. Ismail, A. Rahman, M. F. Karim, and A. Hoque, 2016, *Estuaries and coasts*, 39(6), 1582-1599. Copyright 2016 by Coastal and Estuarine Federation.

**Figure 5.2**

*(a) Maximum water level elevation without air bubbles caused by surge*

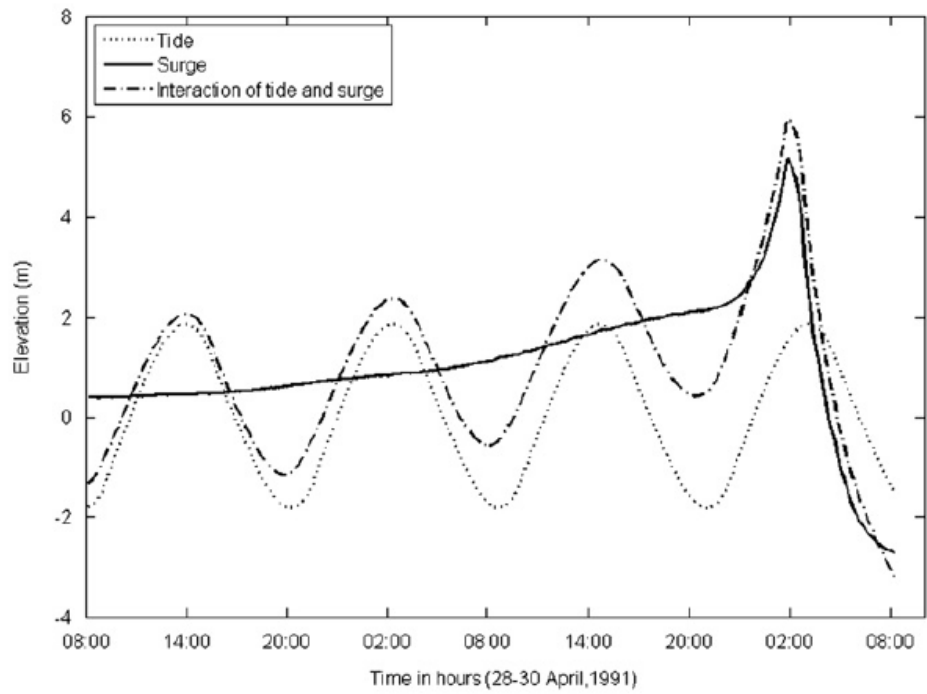


*(b) Maximum water level elevation with air bubbles caused by surge*

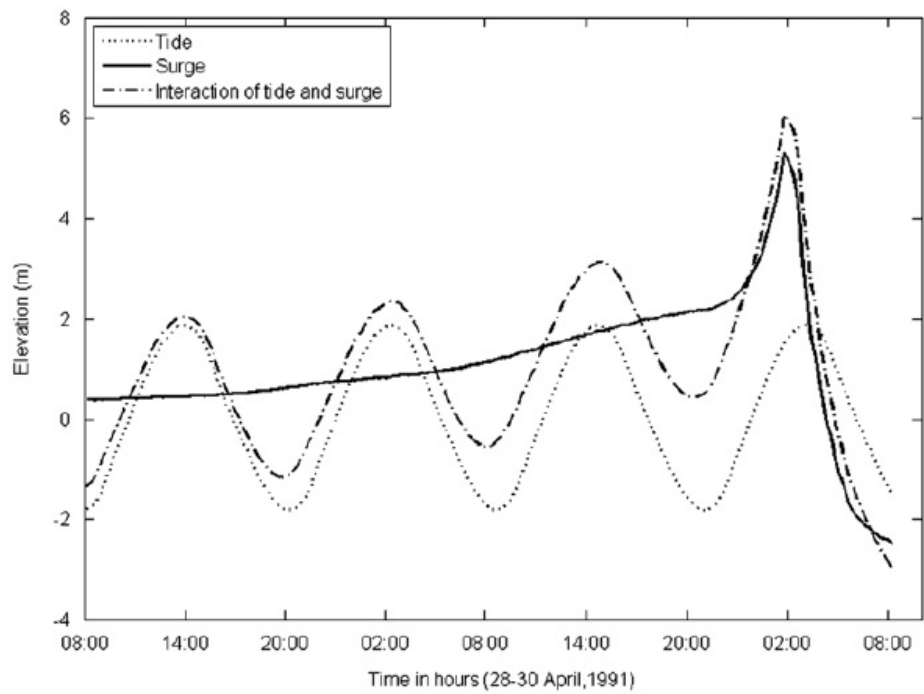




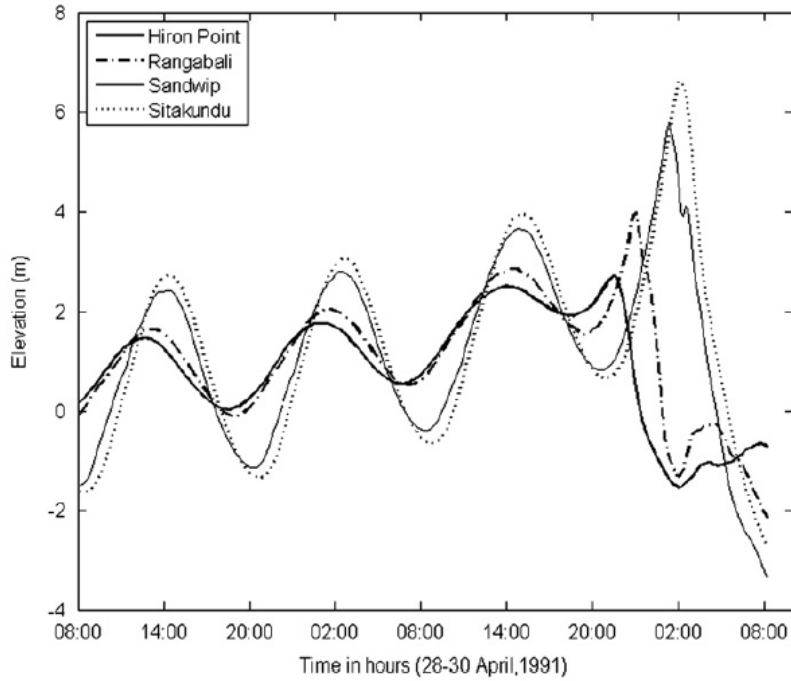
(c) Simulated water level elevation due to tide, surge and the interaction between the two at  $C_0=0$ .



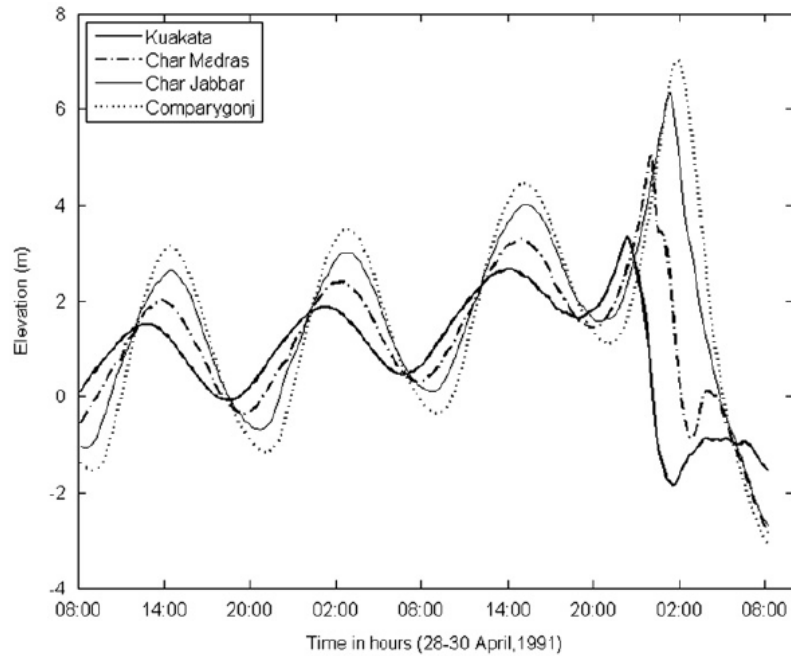
(d) Simulated water level elevation due to tide, surge and the interaction between the two at  $C_0=0.5$ .



(e) Simulated water level elevation caused by tide, surge and the interaction between the two at  $C_0=0.2$



(f) Simulated water level elevation caused by tide, surge and the interaction between the two at  $C_0=0.2$

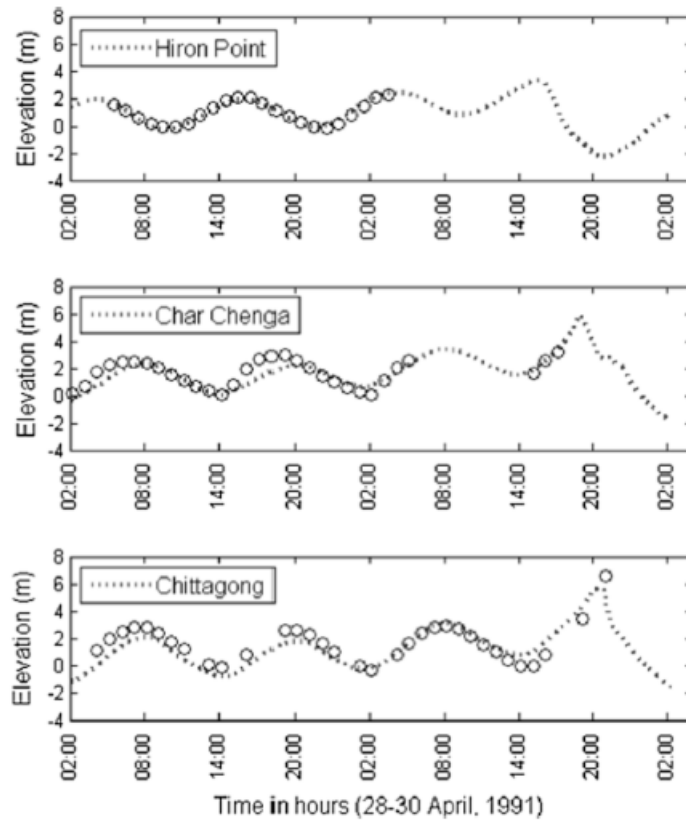


*Note.* (a) Simulated water level elevations ( $C_0=0$ ) with respect to the mean sea level (MSL) caused by surge at some regions near the coastline during the cyclonic storm of April 1991 in Bangladesh, (b) Simulated water level elevations ( $C_0=0.5$ ) with respect to the mean sea level (MSL) caused by surge at some regions near the coastline during the April 1991 cyclonic storm, (c) Simulated water level rise (w.r.t

MSL) with ( $C_0=0$ ) caused by tide, surge and the interaction of the two at Chittagong during the April 1991 cyclone, **(d)** Simulated water level rise (w.r.t MSL) with ( $C_0=0.5$ ) caused by tide, surge and the interaction of the two at Chittagong during the April 1991 cyclone, **(e)** and **(f)** Simulated water level elevations (w.r.t MSL) with  $C_0=0.2$  caused by tide, surge and the interaction of the two at certain regions during the April 1991 cyclone. From “Tide-surge interaction model including air bubble effects for the coast of Bangladesh,” by G.C.Paul, A.I.M.Ismail, 2012, *Journal of the Franklin Institute*, 349(8), 2530-2546. Copyright 2012 by The Franklin Institute.

**Figure 5.3**

*Comparison of simulated overall water levels with observed data*



*Note.* Simulated overall water levels in contrast to the observed data taken from BIWTA. In the figures, the curves show the computed results and the circles show the BIWTA data. From “Development of Tide-Surge Interaction Model for the Coastal Region of Bangladesh,” by G.C.Paul, A.I.M.Ismail, A.Rahman, M.F.Karim, A.Hoque, 2016, *Estuaries and coasts*, 39(6), 1582-1599. Copyright 2016 by Coastal and Estuarine Federation.

In case of other values of the void concentration fraction in relation to the time series of sea surface elevation, it can be seen that these estimated values yield results which are in good agreement with the overall features of Figures 5.2 (e)-(f) and 5.3. The model computations reveal that the overall peak water levels compare well once again with the findings of other such similar research. Some noticeable observations from our results are that there were higher water levels around Chittagong in comparison to the western coastal areas. This follows up with the cyclonic history of the April 1991 storm as its track was almost over Chittagong and the maximum surge strongly corresponded with the high tide. This observation is also discernible in Figures 5.2(b) and (c). Furthermore, the peak surge level as well as the peak total sea surface elevation were computed to be at Companiganj which is an upazila of Noakhali located to the north of Sandwip. This may have happened because the storm navigated the coast north of Chittagong with Sandwip to the left. The highest. According to Flather(1994), the maximum overall water level for April 1991 cyclone was 7.21m near the coast of Noakhali whereas the model estimated overall water level was 7.13m. Hence, the computed result is in good agreement with the results found by Flather(1994). Based on the computations and observations so far, it is apparent that model computations can yield greater water level elevations due to the air bubble effect for the locations marking the coastline. Otherwise, it can compute greater water level for bigger values of the reference void fraction.

### 5.3 Conclusion and future recommendations

In this thesis, cyclone induced storm surges have been produced with the inclusion of the air bubble effect during the wave breaking stage of the storm. The formulation of the storm surge model takes into account the tide-surge phenomenon as well as air bubble entrainment in order to estimate the water level elevations for the coastal regions of Bangladesh. The model used nested finite difference method along with stair step representation. The computed results of the model were in good agreement with the observed results and various other research work, otherwise, it found that air bubbles can cause higher water levels in our study domain. The results were computed for a range of values where  $C_0 \leq 0.7$ . Based on the discussion in Section 5.1, certain regions such as Chittagong and Companiganj recorded higher water level rise in the presence of air bubbles. Based on the literature review of storm surge, it has also been deduced that factors such as bottom geometry can influence water levels as a result of air bubbles. There is a requirement for more investigative work employing factors such as bottom geometry which can help to identify which areas are comparatively more impacted by air bubble entrainment causing higher water levels.

In this study, bottom geometry was not analyzed during the cyclonic storm. Another problem in regards to storm surge research for the Bay of Bengal region is the lack of available data for carrying out thorough analysis of different factors on sea surface elevation at coastal stations. Furthermore, grid resolution could be more refined as this is another factor which is significant for proper implementation of islands of different sizes in the Meghna estuarine area along with the bending of the coastal belt. A standard prediction model needs to simulate water levels with precision and not waste computing time and memory. Given the grid resolutions used in our model and the results produced, it can be seen that they compare quite well with the actual

observations and other existing studies. Therefore, the model is suitable for including air bubbles and the curvature of the coastline and island boundaries with accuracy. Hence, the findings of this study can contribute to a warning system for storm surge forecasting in the coastal areas of Bangladesh.

## References

- Abrol, V. (1987). Application of a linear surge model for the evaluation of storm surges along the coastal waters of Kalpakkam, East Coast of India. *Indian Journal of Marine Sciences*, 16, 1-4.
- Ahmed, H. (2019). Bangladesh Coastal Zone Management Status and Future. *Journal of Coastal Management*, 22(1), 6.
- Ali, A. (1999). *Storm Surges in the Bay of Bengal and Some Related Problems* (Doctoral dissertation, University of Reading).
- Ali, A. (1999). Climate change impacts and adaptation assessment in Bangladesh. *Climate Research*, 12(2-3), 109-116.
- Ali, A., Rahman, H., & Chowdhury, S. S. H. (1997a). River discharge, storm surges and tidal interactions in the Meghna river mouth in Bangladesh. *Mausam*, 48(4), 531-540.
- Ali, A., & Choudhury, G. A. (2014). Storm surges in Bangladesh: An introduction to CEGIS storm surge model. *University Press Limited*.
- Ali, A., Rahman, H., Chowdhury, S. S. H., & Begum, Q. N. (1997). Back water effect of tides and storm surges on fresh water discharge through the Meghna estuary. *J Remote Sensing Environ*, 1, 85-95.
- Allison, M. A., Khan, S. R., Goodbred Jr, S. L., & Kuehl, S. A. (2003). Stratigraphic evolution of the late Holocene Ganges–Brahmaputra lower delta plain. *Sedimentary Geology*, 155(3-4), 317-342.
- Antony, C., Testut, L., & Unnikrishnan, A. S. (2014). Observing storm surges in the Bay of Bengal from satellite altimetry. *Estuarine, Coastal and Shelf Science*, 151, 131-140.
- Arnold, R. J. (1987). An improved open boundary condition for a tidal model of Bass Strait. *North-Holland Mathematics Studies*, 145, 45-158.
- As-Salek J. A. (1997). Negative surges in the Meghna estuary in Bangladesh. *Monthly Weather Review*, 125, 1638–1648.
- As-Salek, J. A. (1998). Coastal trapping and funneling effects on storm surges in the Meghna estuary in relation to cyclones hitting Noakhali–Cox’s Bazar coast of Bangladesh. *Journal of Physical Oceanography*, 28(2), 227-249.

- As-Salek, J. A., & Yasuda, T. (2001). Tide–surge interaction in the Meghna estuary: Most severe conditions. *Journal of Physical Oceanography*, 31(10), 3059-3072.
- Bangladesh University of Engineering and Technology & Bangladesh Institute of Development Studies. (1993). *Multipurpose cyclone shelter programme: Final report*.
- Bangladesh Bureau of Statistics. (2003). *Population Census 2000: National Report (Provisional)*.
- Bills, P., & Noye, J. (1987). An investigation of open boundary conditions for tidal models of shallow seas. *North-Holland Mathematics Studies*, 145, 159-194.
- Bresch, D., & Noble, P. (2007). Mathematical justification of a shallow water model. *Methods and applications of analysis*, 14(2), 87-118.
- Chanson, H. (1994). Drag reduction in open channel flow by aeration and suspended load. *Journal of Hydraulic Research*, 32(1), 87-101.
- Chanson, H., Aoki, S., & Hoque, A. (2006). Bubble entrainment and dispersion in plunging jet flows: Freshwater vs. seawater. *Journal of Coastal Research*, 22(3), 664-677.
- Community Development Library. (1992). *The April disaster: Study on cyclone affected region in Bangladesh*.
- Coleman, J. M. (1969). Brahmaputra River: channel processes and sedimentation. *Sedimentary geology*, 3(2-3), 129-239.
- Condon, A. J., & Peter Sheng, Y. (2012). Evaluation of coastal inundation hazard for present and future climates. *Natural Hazards*, 62(2), 345-373. <https://doi.org/10.1007/s11069-011-9996-0>
- Das, P. K. (1972). Prediction model for storm surges in the Bay of Bengal. *Nature*, 239(5369), 211-213.
- Das, P. K., Sinha, M. C., & Balasubramanyam, V. (1974). Storm surges in the Bay of Bengal. *Quarterly Journal of the Royal Meteorological Society*, 100(425), 437-449.
- Dasgupta, S., Huq, M., Khan, Z. H., Ahmed, M. M. Z., Mukherjee, N., Khan, M., & Pandey, K. D. (2010). Vulnerability of Bangladesh to cyclones in a changing climate: Potential damages and adaptation cost. *World Bank Policy Research Working Paper*, (5280).
- Debsarma, S. K. (2009). Simulations of storm surges in the Bay of Bengal. *Marine Geodesy*, 32(2), 178-198.



- Debsarma, S. K., Rahman, M., & Nessa, F. F. (2014). *Monitoring and prediction of tropical cyclones in the Indian Ocean and Climate Change*. Springer.
- Dietrich, J. C., Dawson, C. N., Proft, J. M., Howard, M. T., Wells, G., Fleming, J. G., ... & Atkinson, J. H. (2013). *Computational challenges in the geosciences*. Springer.
- Dube, S. K., Chittibabu, P., Sinha, P. C., Rao, A. D., & Murty, T. S. (2004). Numerical modelling of storm surge in the head Bay of Bengal using location specific model. *Natural Hazards*, 31(2), 437-453.
- Dube, S. K., Rao, A. D., Sinha, P. C., Murty, T. S., & Bahulayan, N. (1997). Storm surge in the Bay of Bengal and Arabian Sea: the problem and its prediction. *Mausam*, 48(2), 283-304.
- Dube, S. K., Sinha, P. C., & Rao, A. D. (1982). The effect of coastal geometry on the location of peak surge. *Mausam*, 33(4), 445-450.
- Dube, S. K., Sinha, P. C., & Roy, G. D. (1985). The numerical simulation of storm surges along the Bangladesh coast. *Dynamics of atmospheres and oceans*, 9(2), 121-133.
- Dube, S. K., Sinha, P. C., & Roy, G. D. (1986). Numerical simulation of storm surges in Bangladesh using a bay-river coupled model. *Coastal Engineering*, 10(1), 85-101
- Dube, S. K., Sinha, P. C., Rao, A. D., Jain, I., & Agnihotri, N. (2005). Effect of the Mahanadi River on the development of storm surge along the Orissa coast of India: A numerical study. *pure and applied geophysics*, 162(8), 1673-1688.
- ESCAP, U. (1987). *Coastal environmental management plan for Bangladesh*. ST/ESCAP/618, 2.
- Falconer, R. A. (1993). An introduction to nearly horizontal flows. In *Coastal, Estuarial and Harbour Engineers' Reference Book* (p. 27-36). E. & F.N. Spon Ltd.
- Flather, R. A. (1994). A storm surge prediction model for the northern Bay of Bengal with application to the cyclone disaster in April 1991. *Journal of Physical Oceanography*, 24(1), 172-190.
- Flather, R. A., & Heaps, N. S. (1975). Tidal computations for Morecambe Bay. *Geophysical Journal International*, 42(2), 489-517.
- Flather, R. A., & Khandker, H. (1993). *The storm surge problem and possible effects of sea level changes on coastal flooding in the Bay of Bengal*. Cambridge University Press.
- Flierl, G. R., & Robinson, A. R. (1972). Deadly surges in the Bay of Bengal: Dynamics and storm-tide tables. *Nature*, 239(5369), 213-215.

Frank, N. L. (1971). The deadliest tropical cyclone in history?. *Bulletin of the American Meteorological Society*, 52(6), 438-444.

GoB. (2008). *Cyclone Sidr in Bangladesh: Damage, loss, and needs assessment for disaster recovery and reconstruction*. MoFDM.

Gönnert, G., Dube, S. K., Murty, T. S., & Seifert, W. (2001). Global storm surges: Theory, observations and applications. *German Coastal Engineering Research Council*, 623.

Ghosh, S. K., Dewan, B. N., & Singh, B. V. (1983). Numerical simulation of storm surge envelopes associated with the recent severe cyclones impinging on the east and west coasts of India. *Mausam*, 34(4), 399-404.

Glahn, B., Taylor, A., Kurkowski, N., & Shaffer, W. A. (2009). The role of the SLOSH model in National Weather Service storm surge forecasting. *National Weather Digest*, 33(1), 3-14.

Haider, R., Rahman, A. A., & Huq, S. (Eds.). (1991). *Cyclone '91: An environmental and perceptual study*. Bangladesh Centre for Advanced Studies.

Heaps, N. S. (1973). Three-dimensional numerical model of the Irish Sea. *Geophysical Journal International*, 35(1-3), 99-120.

Hebenstreit, G. T., Gonzalez, F. I., & Morris, A. F. (1985). Nearshore tsunami simulation of Valparaiso Harbor, Chile. *Proc. Int. Tsunami Symp., TS Murty and WJ Rapatz (eds.), Inst. Ocean Sciences, Sidney, BC*.

Henry, R. F., Duncalf, D. S., Walters, R. S., Osborne, M. J., & Murty, T. S. (1997). A study of tides and storm surges in offshore waters of the Meghna estuary using a finite element model. *Mausam*, 48(4), 519-530.

Hibberd, S., & Peregrine, D. H. (1979). Surf and run-up on a beach: a uniform bore. *Journal of Fluid Mechanics*, 95(2), 323-345.

Holland, G. J. (1980). An analytic model of the wind and pressure profiles in hurricanes. *Monthly Weather Review*. 108(8), 1212-1218.

Holthuijsen, L. H. (2010). *Waves in oceanic and coastal waters*. Cambridge University Press.

Hoque, A. (2008). Studies of water level rise by entrained air in the surf zone. *Experimental thermal and fluid science*, 32(4), 973-979.

Hoque, A., & Aoki, S. I. (2005b). A quantitative analysis of energy dissipation among three typical air entrainment phenomena. *Environmental Fluid Mechanics*, 5(4), 325-340.

- Hoque, A., & Aoki, S. I. (2006). Air entrainment by breaking waves: A theoretical study. *CSIR-NIScPR*, 35(1), 17-23.
- Hoque, M. M. (1991). Field study and investigations on the damage caused by cyclones in Bangladesh: A report on the 29 April 1991 cyclone. *Cyclone Damage in Bangladesh*, 75.
- Hubbert, G. D., Leslie, L. M., & Manton, M. J. (1990). A storm surge model for the Australian region. *Quarterly Journal of the Royal Meteorological Society*, 116(494), 1005-1020.
- Hwung, H. H., Chyan, J. M., & Chung, Y. C. (1992). Energy dissipation and air bubbles mixing inside surf zone. *Coastal Engineering Proceedings*, (23).
- Isozaki, I. (1970). An investigation on the variations of sea level due to meteorological disturbances on the coast of the Japanese Islands (V). *Pap. Meteor. Geophys*, 21, 1-32.
- Islam, M. R. (2004). *Where land meets the sea: A profile of the coastal zone of Bangladesh*. University Press.
- Islam, M. S. (2001). *Sea-level changes in Bangladesh: The last ten thousand years*. Asiatic Society of Bangladesh.
- Islam, M. S. (2003). Perspectives of the coastal and marine fisheries of the Bay of Bengal, Bangladesh. *Ocean & Coastal Management*, 46(8), 763-796.
- Islam, T., & Peterson, R. E. (2009). Climatology of landfalling tropical cyclones in Bangladesh 1877–2003. *Natural Hazards*, 48(1), 115-135.
- IWM. (2009). *Preparation of inundation map considering the decay factors for land use, geomorphology and slope*. Comprehensive Disaster Management Programme, Ministry of FOOD and Disaster Management, GoB.
- IWM. (2002). *Second coastal embankment rehabilitation projects*. Dhaka
- Jain, S. K., Agarwal, P. K., & Singh, V. P. (2007). *Hydrology and water resources of India*. Springer Science & Business Media.
- Jakobsen, F., Azam, M. H., Ahmed, M. M. Z., & Mahboob-ul-Kabir, M. (2006). Cyclone storm surge levels along the Bangladeshi coastline in 1876 and 1960–2000. *Coastal Engineering Journal*, 48(3), 295-307.
- Jelesnianski, C. P. (1965). A numerical calculation of storm tides induced by a tropical storm impinging on a continental shelf. *Monthly Weather Review*, 93(6), 343-358.

Jelesnianski, C. P. (1972). *SPLASH:(Special Program to List Amplitudes of Surges from Hurricanes); Part I: Landfall storms*. National Weather Service,

Jelesnianski, C. P. (1992). *SLOSH: Sea, lake, and overland surges from hurricanes*. U. S. Department of Commerce, National Oceanic and Atmospheric Administration, National Weather Service.

Jelesnianski, C. P., & Taylor, A. D. (1973). NOAA technical memorandum, ERL, WMPO-3. Washington.

Johns, B., & Ali, M. A. (1980). The numerical modelling of storm surges in the Bay of Bengal. *Quarterly Journal of the Royal Meteorological Society*, 106(447), 1-18.

Johns, B., Dube, S. K., Mohanty, U. C., & Sinha, P. C. (1981). Numerical simulation of the surge generated by the 1977 Andhra cyclone. *Quarterly Journal of the Royal Meteorological Society*, 107(454), 919-934.

Johns, B., Rao, A. D., Dubinsky, Z., & Sinha, P. C. (1985). Numerical modelling of tide-surge interaction in the Bay of Bengal. *Philosophical Transactions of the Royal Society of London. Series A, Mathematical and Physical Sciences*, 313(1526), 507-535.

Johns, B., Sinha, P. C., Dube, S. K., Mohanty, U. C., & Rao, A. D. (1983a). On the effect of bathymetry in numerical storm surge simulation experiments. *Computers & Fluids*, 11(3), 161-174.

Joseph, A., Prabhudesai, R. G., Mehra, P., Sanil Kumar, V., Radhakrishnan, K. V., Kumar, V., Ashok Kumar, K., Agarwadekar, Y., Bhat, U.G., Luis, R., Rivankar, P., & Viegas, B. (2011). Response of west Indian coastal regions and Kavaratti lagoon to the November-2009 tropical cyclone Phyan. *Natural Hazards*, 57(2), 293-312.

Karim, M. F., & Mimura, N. (2008). Impacts of climate change and sea-level rise on cyclonic storm surge floods in Bangladesh. *Global environmental change*, 18(3), 490-500.

Katsura, J. (1992). Storm surge and severe wind disasters caused by the 1991 cyclone in Bangladesh. *Kyoto Daigaku Bōsai Kenkyūjo nenpō*, (35), 119-159.

Kay, S., Caesar, J., Wolf, J., Bricheno, L., Nicholls, R. J., Islam, A. S., Haque, A., Pardaens, A., & Lowe, J. A. (2015). Modelling the increased frequency of extreme sea levels in the Ganges–Brahmaputra–Meghna delta due to sea level rise and other effects of climate change. *Environmental Science: Processes & Impacts*, 17(7), 1311-1322.

Khalil, G. M. (1993). The catastrophic cyclone of April 1991: Its impact on the economy of Bangladesh. *Natural hazards*, 8(3), 263-281.

- Khan, M. H., & Awal, M. A. (2009). Global warming and sea level rising: Impact on Bangladesh agriculture and food security.
- Kowalik, Z., & Bang, I. (1987). Numerical computation of tsunami run-up by the upstream derivative method. *Science of Tsunami Hazards*, 5(2), 77-84.
- Kraus, E. B., & Businger, J. A. (1994). *Atmosphere-ocean interaction* (2nd ed.). Oxford University Press.
- Lewis, M., Bates, P., Horsburgh, K., Neal, J., & Schumann, G. (2013). A storm surge inundation model of the northern Bay of Bengal using publicly available data. *Quarterly Journal of the Royal Meteorological Society*, 139(671), 358-369.
- Lewis, M., Horsburgh, K., & Bates, P. (2014). Bay of Bengal cyclone extreme water level estimate uncertainty. *Natural Hazards*, 72(2), 983-996.
- Lin, C., & Hwung, H. H. (1992). External and internal flow fields of plunging breakers. *Experiments in Fluids*, 12(4), 229-237.
- McCammon, C., & Wunsch, C. (1977). Tidal charts of the Indian Ocean north of 15° S. *Journal of Geophysical Research*, 82(37), 5993-5998.
- Miyan, M. A. (2005). Cyclone disaster mitigation in Bangladesh. In *Proceeding of the second Regional Technical Conference on Tropical Cyclones, Storm Surges and Floods*. Secretariat of the World Metrological Organization, Geneva.
- Milliman, J. D. (1991). Flux and fate of fluvial sediment and water in coastal seas. *RFC Mantoura*, 69-89.
- Mohit, M. A. A., Yamashiro, M., Hashimoto, N., Mia, M. B., Ide, Y., & Kodama, M. (2018). Impact assessment of a major river basin in Bangladesh on storm surge simulation. *Journal of Marine Science and Engineering*, 6(3), 99.
- Mohiuddin Sakib, F. N., Haque, A., Rahman, M., Jisan, M. A., Noor, S., Akter, R., ... & Omar, T. Storm Surge Flooding due to SIDR-AILA and SIDR-AILA-LIKE Cyclones along the Bangladesh Coast.
- MoWR. (1999). Integrated coastal zone management: Concepts and issues; A Government of Bangladesh Policy Note. Ministry of Water Resources.
- Murty, T. S. (1984). Storm surges-meteorological ocean tides. *Canadian Bulletin of Fisheries and Aquatic Sciences*, Canadian Department of Fisheries and Oceans, 212, 897.

Murty, T. S., Flather, R. A., & Henry, R. F. (1986). The storm surge problem in the Bay of Bengal. *Progress in Oceanography*, 16(4), 195-233.

Murty, T. S., & Henry, R. F. (1983). Tides in the Bay of Bengal. *Journal of Geophysical Research: Oceans*, 88(C10), 6069-6076.

National Geographic Society. (2012, October 9). *Coast*. <https://www.nationalgeographic.org/encyclopedia/coast/>

Nelson. (2018). *Coastal zones*. Tulane University. [https://www2.tulane.edu/~sanelson/Natural\\_Disasters/coastalzones.htm](https://www2.tulane.edu/~sanelson/Natural_Disasters/coastalzones.htm)

NHC, & CPHC. (n.d.). *Storm surge overview*. National Hurricane Center. <https://www.nhc.noaa.gov/surge/>

NHC, & CPHC. (n.d.). *Storm Surge vs. Storm Tide [Diagram]*. <https://www.nhc.noaa.gov/surge/>

Overland, J. E. (1975). *Estimation of hurricane storm surge in Apalachicola Bay, Florida*. Office of Hydrology, National Weather Service.

Patullo, J., Munk, W., W. H., Revelle, R., & Strong, E. S. (1989). The seasonal oscillation in sea level. *Journal of Marine Research*, 14, 88-156.

Paul, G. C., & Ismail, A. I. M. (2012a). Numerical modeling of storm surges with air bubble effects along the coast of Bangladesh. *Ocean Engineering*, 42, 188-194.

Paul, G. C., & Ismail, A. I. M. (2012b). Tide–surge interaction model including air bubble effects for the coast of Bangladesh. *Journal of the Franklin Institute*, 349(8), 2530-2546.

Paul, G. C., & Ismail, A. I. M. (2012). Contribution of offshore islands in the prediction of water levels due to tide–surge interaction for the coastal region of Bangladesh. *Natural Hazards*, 65(1), 13-25.

Paul, G. C., Ismail, A. I. M., Rahman, A., Karim, M. D., & Hoque, A. (2016). Development of tide–surge interaction model for the coastal region of Bangladesh. *Estuaries and coasts*, 39(6), 1582-1599.

PDO-ICZMP. (2001). *Inception report-The preparatory phase for sustainable development of the coastal zone of Bangladesh*. Ministry of Water Resources, Program Development Office for Integrated Coastal Zone Management Plan.

Pramanik, M. A. H. (1988). Role of remote sensing technology in flood studies in Bangladesh. In *Flood in Bangladesh* (p. 224-234). Dhaka, Bangladesh: Community Development Library.

- Proudman, J. (1955). The effect of friction on a progressive wave of tide and surge in an estuary. *Proceedings of the Royal Society of London. Series A. Mathematical and Physical Sciences*, 233(1194), 407-418.
- Qayyum, M. F. (1983). Prediction of storm surges for Bangladesh coasts by empirical method: Results and discussions. *WMO-ESCAP Panel on Tropical Cyclones, Dhaka*, 22-29.
- Rahman, M. M., Haque, A., Nicholls, R. J., Jisan, M. A., Nihal, F., Ahmed, I., & Lázár, A. N. (2015, June). Storm Surge Flooding in the Ganges-Brahmaputra-Meghna Delta: Present and Future Scenarios. In *E-proceedings of the 36th IAHR World Congress* (Vol. 28).
- Rahman, S. M. N., Gafoor, A., & Hossain, T. I. M. T. (1993, August). Coastal zone monitoring using remote sensing techniques. In *Proceedings of IGARSS'93-IEEE International Geoscience and Remote Sensing Symposium* (pp. 706-709). IEEE.
- Rao, A. D., Dash, S., Babu, S. V., & Jain, I. (2007). Numerical Modeling of Cyclone's Impact on the Ocean—A Case Study of the Orissa Super Cyclone. *Journal of Coastal Research*, 23(5), 1245-1250.
- Reid, R. O., & Bodine, B. R. (1968). Numerical model for storm surges in Galveston Bay. *Journal of the Waterways and harbors Division*, 94(1), 33-57.
- Rezaie, A. M., Ferreira, C. M., & Rahman, M. R. (2019). Storm surge and sea level rise: Threat to the coastal areas of Bangladesh. In *Extreme Hydroclimatic Events and Multivariate Hazards in a Changing Environment* (pp. 317-342). Elsevier.
- Roy, G. D. (1985). Some aspects of storm surges along the coast of Bangladesh. *Ganith (J. Bangladesh Math. Soc.)*, 6(1), 1-8.
- Roy, G. D. (1995). Estimation of expected maximum possible water level along the Meghna estuary using a tide and surge interaction model. *Environment International*, 21(5), 671-677.
- Roy, G. D. (1999a). Inclusion of off-shore islands in a transformed coordinates shallow water model along the coast of Bangladesh. *Environment international*, 25(1), 67-74.
- Roy, G. D., & Hussain, F. (2001). *A nearly orthogonal 2D grid system in solving the shallow water equations in the head Bay of Bengal (IC--2001/162)*. International Atomic Energy Agency.
- Roy, G. D., Kabir, A. H., Mandal, M. M., & Haque, M. Z. (1999). Polar coordinates shallow water storm surge model for the coast of Bangladesh. *Dynamics of Atmospheres and Oceans*, 29(2-4), 397-413.

Shahadat, F., Ahmed, M. M. Z., Saha, B. C., & Jakobsen, F. (2000). Numerical Investigation of 1876 Cyclone Surge. *Disaster: Issues and Gender Perspectives, 23-24 June 2000, Dhaka*.

SDNP. (2004). *Climate Change & Bangladesh: Sea level rise*. Sustainable Development Networking Programme.

[http://www.bdix.net/sdnbd\\_org/world\\_env\\_day/2004/bangladesh/climate\\_change\\_sealevel.htm](http://www.bdix.net/sdnbd_org/world_env_day/2004/bangladesh/climate_change_sealevel.htm)

Sevenhuysen, G. P. (1991). *Report on cyclone disaster response in Bangladesh*. Disaster Research Unit, University of Manitoba.

Sielecki, A., & Wurtele, M. G. (1970). The numerical integration of the nonlinear shallow-water equations with sloping boundaries. *Journal of Computational Physics, 6*(2), 219-236.

Singh, O. P., Khan, T. M., & Rahman, S. (2000). *The vulnerability assessment of the SAARC coastal region due to sea level rise: Bangladesh case*. SAARC Meteorological Research Centre (SMRC).

Sinha, P. C., Dube, S. K., Roy, G. D., & Jaggi, S. (1986). Numerical simulation of storm surges in Bangladesh using a multi-level model. *International journal for numerical methods in fluids, 6*(5), 305-311.

Sinha, P. C., Dube, S. K., Rao, A. D., & Rao, G. S. (1984). Numerical simulation of the surge generated by the November 1982 Gujrat cyclone. *Vayu Mandal, 14*, 31-33.

Sinha, P. C., Jain, I., Bhardwaj, N., Rao, A. D., & Dube, S. K. (2008). Numerical modeling of tide-surge interaction along Orissa coast of India. *Natural Hazards, 45*(3), 413-427.

Sinha, P. C., Rao, Y. R., Dube, S. K., & Murty, T. S. (1997). Effect of sea level rise on tidal circulation in the Hooghly Estuary, Bay of Bengal. *Marine Geodesy, 20*(4), 341-366.

Sinha, P. C., Rao, Y. R., Dube, S. K., Rao, A. D., & Chatterjee, A. K. (1996). Numerical investigation of tide-surge interaction in Hooghly Estuary, India. *Marine Geodesy, 19*(3), 235-255.

SMRC. (1998). The impact of tropical cyclones on the coastal regions of SAARC countries and their influence in the region. *SAARC Meteorological Research Centre Report No. 1*, 329.

Soloviev, A., & Lukas, R. (2010). Effects of bubbles and sea spray on air-sea exchange in hurricane conditions. *Boundary-layer meteorology, 136*(3), 365-376.

Talukder, J. (1992). *Living with cyclone: Study on storm surge prediction and disaster preparedness*. Community Development Library.



- Tang, Y., & Grimshaw, R. (1996). Radiation boundary conditions in barotropic coastal ocean numerical models. *Journal of Computational Physics*, 123(1), 96-110.
- Thacker, W. C. (1977). Irregular grid finite-difference techniques: simulations of oscillations in shallow circular basins. *Journal of Physical Oceanography*, 7(2), 284-292.
- Thacker, W. C. (1979). Irregular-grid finite-difference techniques for storm surge calculations for curving coastlines. In *Elsevier Oceanography Series* (Vol. 25, pp. 261-283). Elsevier.
- Treves, T. (2018). United Nations Convention on the Law of the Sea-Montego Bay, 10 December 1982.". *United Nations: Office of Legal Affairs*.
- Uddin, A. M. K., & Kaudstaal, R. (2003). *Delineation of the coastal zone*. Program Development Office for Integrated Coastal Zone Management Plan (PDO-ICZMP), Dhaka, 1-42.
- UNEP. (2008). Protocol on integrated coastal zone management in the Mediterranean.
- Unnikrishnan, A. S., Sundar, D., & Blackman, D. (2004). Analysis of extreme sea level along the east coast of India. *Journal of Geophysical Research: Oceans*, 109(C6).
- U. S. Congress. (1972). *Coastal Zone Management Act of 1972 (Public Law 92-583)*.
- WARPO. (2004). *National Water Management Plan*. Ministry of Water Resources.
- WMO. (2001). *Operational plan for the Bay of Bengal and the Arabian Sea*. WMO/TD- No.84; TCP- No. 21. Geneva.
- Wu, Q., Kim, S., Ishii, M., & Beus, S. G. (1998). One-group interfacial area transport in vertical bubbly flow. *International Journal of Heat and Mass Transfer*, 41(8-9), 1103-1112.